Louisiana Transportation Research Center

Final Report 603

Accelerated Load Testing of Geosynthetic Base Reinforced/Stabilized Unpaved and Pavement Test Sections

by

Murad Y. Abu-Farsakh, Ph.D., P.E.
Qiming Chen, Ph.D., P.E.
Shadi Hanandeh, Ph.D.

LTRC

4101 Gourrier Avenue | Baton Rouge, Louisiana 70808
(225) 767-9131 | (225) 767-9108 fax | www.ltrc.lsu.edu

TECHNICAL REPORT STANDARD PAGE

1. Report No.	2. Government Accession No.	3. Recipient's Catalog No.
FHWA/LA. 18/603		

4. Title and Subtitle	5. Report Date
Accelerated Load Testing of Geosynthetic Base Reinforced/Stabilized Unpaved and Pavement Test Sections	August 2019
	6. Performing Organization Code **LTRC Project Number: 11-3GT** **State Project Number: 736-99-1735**
7. Author(s) **Murad Y. Abu-Farsakh, Ph.D., P.E., Qiming Chen, Ph.D., P.E., and Shadi Hanandeh, Ph.D.**	8. Performing Organization Report No.
9. Performing Organization Name and Address **Louisiana Transportation Research Center** **4101 Gourrier Avenue** **Baton Rouge, LA 70808**	10. Work Unit No.
	11. Contract or Grant No. **LTRC Number: 11-3GT** **State Project Number: 736-99-1735**
12. Sponsoring Agency Name and Address **Louisiana Transportation Research Center** **4101 Gourrier Avenue** **Baton Rouge, LA 70808**	13. Type of Report and Period Covered **Final Report** **Dec 2010 - June 2018**
	14. Sponsoring Agency Code

15. Supplementary Notes
Conducted in Cooperation with the U.S. Department of Transportation, Federal Highway Administration

16. Abstract

This research study aims at evaluating the benefits of using geosynthetics to reinforce/stabilize base aggregate layer/subgrade in pavements under repeated loading test conditions. For this purpose, a total of six 80-ft. long and 13 ft. wide full-scale test lane sections were constructed, among which two sections were reinforced by one or two layers of triaxial geogrids, two sections were reinforced by one layer of high strength woven geotextile with different base layer thickness, and the remaining two sections were the control sections. The field test sections were instrumented by a variety of sensors to measure the load- and environment-associated pavement response and performance. Two series of tests, moving wheel load tests and cyclic plate load tests, were conducted to investigate the field performance of geosynthetic reinforced/stabilized paved roads and to identify the differences in pavement response to moving wheel and cyclic plate loads. In addition, six similar test sections were constructed inside a 6.5-ft. × 6.5-ft. × 5.5-ft. test box. The test box sections were also instrumented by a variety of sensors to measure the load-associated pavement response and performance. Laboratory cyclic plate load tests were then conducted.

The results of accelerated load testing on the pavement test sections demonstrate the benefits of using geosynthetics in reducing the permanent deformation in the pavement structure. The adjusted traffic benefit ratio (TBR_{adj}) associated with geosynthetic reinforcement can be increased up to 2.12 at a rut depth of 0.75 in. for pavement constructed using 18 in. thick base layer on top of weak subgrade soil using two layers of geogrid reinforcement. The inclusion of geosynthetics results in redistributing the applied load to a wider area, thus reducing the accumulated permanent deformation within the subgrade. The benefit of geosynthetics on reducing the maximum stress on top of subgrade is more appreciable at higher load levels. It was also found that the geosynthetics placed at the base-subgrade interface was able to improve the performance of both subgrade and base layers; by placing an additional layer of geogrid at the upper one-third of the base layer, the performance of the base layer was further enhanced. While geosynthetics showed appreciable benefit on reducing the permanent deformation of the subgrade layer, it showed less effect on the resilient properties of the subgrade layer. Drainage of the base layer has important effect on the performance of pavement structures for both unreinforced and reinforced lane sections.

The life-cycle cost analysis (LCCA) demonstrated the cost savings of using geosynthetics in pavement as compared to the unreinforced/untreated sections. However, compared to the 12-in. cement/lime treated subgrade with the cement stabilized base pavement section, the LCCA showed it is more cost effective to use geosynthetics for base thickness less than 12 in. (or < 15 in. of unreinforced aggregate base). The cost benefit becomes close for base thickness > 12 in. between using a single geosynthetic layer and a 12-in. cement/lime treated subgrade with a cement stabilized base. Moreover, the cost benefit of using double geogrid layers exceeds the cost savings of a 12-in. treated subgrade with a cement stabilized base.

17. Key Words	18. Distribution Statement
	Unrestricted. This document is available through the National Technical Information Service, Springfield, VA 21161.

19. Security Classif. (of this report)	20. Security Classif. (of this page)	21. No. of Pages	22. Price
Unclassified	**Unclassified**	109	

Accelerated Load Testing of Geosynthetic Base Reinforced Unpaved and Pavement Test Sections

by

Murad Y. Abu-Farsakh, Ph.D., P.E.
Qiming Chen, Ph.D., P.E.
Shadi Hanandeh, Ph.D.

Louisiana Transportation Research Center
4101 Gourrier Avenue
Baton Rouge, LA 70808

LTRC Project No. 11-3GT
State Project No. 736-99-1735

conducted for

Louisiana Department of Transportation and Development
Louisiana Transportation Research Center

August 2019

Project Review Committee

Each research project will have an advisory committee appointed by the LTRC Director. The Project Review Committee is responsible for assisting the LTRC Administrator or Manager in the development of acceptable research problem statements, requests for proposals, review of research proposals, oversight of approved research projects, and implementation of findings.

LTRC appreciates the dedication of the following Project Review Committee Members in guiding this research study to fruition.

LTRC Administrator

Zhongjie "Doc" Zhang, Ph.D., P.E.
Pavement and Geotechnical Research Administrator

Members

Jeff Lambert, DOTD
Francisco Gudiel, DOTD
Mark Ordogne, DOTD
Xingwei Chen, DOTD
Jason Lacombe, DOTD
Mark Wayne, Tensar Corp.
Bruce Lacina, TenCate Geosynthetics
Jayhyun Kwon, Kennesaw State University
Scott Nelson, FHWA

Directorate Implementation Sponsor

Christopher P. Knotts, P.E.
DOTD Chief Engineer

ABSTRACT

This research study aims at evaluating the benefits of using geosynthetics to reinforce/ stabilize base aggregate layer/subgrade in pavements under repeated loading test conditions. For this purpose, a total of six 80-ft. long and 13-ft. wide full-scale test lane sections were constructed, among which two sections were reinforced by one or two layers of triaxial geogrids, two sections were reinforced by one layer of high strength woven geotextile with different base layer thickness, and the remaining two sections were the control sections. The field test sections were instrumented by a variety of sensors to measure the load- and environment-associated pavement response and performance. Two series of tests, moving wheel load tests and cyclic plate load tests, were conducted to investigate the field performance of geosynthetic reinforced/stabilized paved roads and to identify the differences in pavement response to moving wheel and cyclic plate loads. In addition, six similar test sections were constructed inside a 6.5-ft. × 6.5-ft. × 5.5-ft. test box. The test box sections were also instrumented by a variety of sensors to measure the load-associated pavement response and performance. Laboratory cyclic plate load tests were then conducted.

The results of accelerated load testing on the pavement test sections demonstrate the benefits of using geosynthetics in reducing the permanent deformation in the pavement structure. The adjusted traffic benefit ratio (TBR_{adj}) associated with geosynthetic reinforcement can be increased up to 2.12 at a rut depth of 0.75 in. for pavement constructed using 18 in. thick base layer on top of weak subgrade soil using two layers of geogrid reinforcement. The inclusion of geosynthetics results in redistributing the applied load to a wider area, thus reducing the accumulated permanent deformation within the subgrade. The benefit of geosynthetics on reducing the maximum stress on top of subgrade is more appreciable at higher load levels. It was also found that the geosynthetics placed at the base-subgrade interface was able to improve the performance of both subgrade and base layers; by placing an additional layer of geogrid at the upper one-third of the base layer, the performance of the base layer was further enhanced. While geosynthetics showed appreciable benefit on reducing the permanent deformation of the subgrade layer, it showed less effect on the resilient properties of the subgrade layer. Drainage of the base layer has important effect on the performance of pavement structures for both unreinforced and reinforced lane sections.

The life-cycle cost analysis (LCCA) demonstrated the cost savings of using geosynthetics in pavement as compared to the unreinforced/untreated sections. However, compared to the 12-in. cement/lime treated subgrade with cement stabilized base pavement section, the LCCA showed it is more cost effective to use geosynthetics for base thickness less than 12 in. (or <

15 in. of unreinforced aggregate base). The cost benefit becomes close for base thickness > 12 in. between using a single geosynthetic layer and 12-in. cement/lime treated subgrade with cement stabilized base. Moreover, the cost benefit of using double geogrid layers exceeds the cost savings of 12-in. treated subgrade with cement stabilized base.

ACKNOWLEDGMENTS

The authors would like to acknowledge the financial support provided by the Louisiana Department of Transportation and Development (DOTD), Tensar International., and TenCate Geosynthetics, America. The comments and suggestions of. Zhongjie (Doc) Zhang, Ph.D., pavement and geotechnical administrator, and Gavin Gautreau, geotechnical engineering manager, of LTRC are gratefully acknowledged. The help from the pavement research section and Accelerated Load Facilities (ALF) personnel is greatly appreciated. The authors also wish to thank the graduate students at LTRC who helped with installing instruments and in-situ testing.

IMPLEMENTATION STATEMENT

The results of this study demonstrated the potential benefits of using geosynthetic reinforcement (both triaxial geogrid and high strength woven geotextile) in flexible pavements through the improvement of the strength/stiffness of the base course material and stabilizing the subgrade layer, thus reducing the pavement's permanent deformation (rutting) under cyclic loading.

The findings of this research study can be implemented in the design of flexible pavements built over weak subgrade soils with resilient modulus $M_r < 4500$ psi (or CBR < 3) by stabilizing the subgrade/base aggregate layers with one layer of geosynthetics or two layers of geogrids. This is important especially in cases where it is difficult to stabilize/treat the weak subgrade soil with cement or lime. The use of woven reinforcement geotextiles, or geogrids with a Class C nonwoven separator with elastic tensile strength at 2 percent strain, T2% ≥ 250 lb/ft, is recommended.

- For the design of geosynthetic reinforced flexibile pavements built over weak subgrade soil using the PavementME, it is recommended to use the α values presented in Table 26 for a single geosynthetic layer and double geogrid layers to estimate the effective base course resilient modulus, as an input parameter for use in pavement design.
- When considering the long-term benefits of geosynthetics, the values of traffic benefit ratio, TBR, presented in Table 27 for a single geosynthetic layer and double geogrid layers are recommended to estimate the extended service life of geosynthetics reinforced flexibile pavements built over weak subgrade soils.
- When considering the short-term benefits of geosynthetics, the base course reduction, BCR, factors presented in Table 28 for a single geosynthetic layer and double geogrid layers are recommended to estimate the reduced base course layer thickness for geosynthetics reinforced flexibile pavements built over weak subgrade soils.
- To optimize the benefits of using geosynthetics in pavements with thick base course layers (> 12 in.) build over weak subgrade soils, it is recommended to install one geosythetic (geogrid or geotextile) layer at the base subgrade interface, and a second geogrid layer at the upper one third of the base thickness. Usually the two layers are geogrids. However, using one geotextile layer at the base subgrade interface and one geogrid layer at upper one third of the base thickness is also possible that needs to be tested.

TABLE OF CONTENTS

LIST OF TABLES

LIST OF FIGURES

INTRODUCTION

Background

In the state of Louisiana, roads often have to be built over weak subgrade soils due to the soft nature of Louisiana soils and the presence of high ground water tables, which create many design and construction challenges. Traditional solutions to this problem include replacement of part of the subgrade, appropriate sizing of pavement and base course layers thicknesses, and/or stabilization/treatment of weak subgrade soils with cementatious materials. A common practice in Louisiana is to stabilize/treat the upper part of subgrade with cement or lime, depending on soil type, to create a working platform through improving the engineering strength/stiffness properties of the subgrade. This practice can help reduce the risks of excessive permanent deformations (rutting) by spreading the tire pressure into a wider influence area, thus reducing the vertical pressure acting on top of the untreated subgrade layer. However, the difficulty of stabilizing/treating very weak subgrade soil with cement or lime in certain conditions calls for an alternative solution. The use of geosynthetics (mainly geogrids and geotexitles) to reinforce the base aggregate layer and/or stabilize the subgrade layer within the pavement structure can offer a cost-effective alternative solution to this problem.

The concept of using geosynthetics (geogrids and geotextiles) as reinforcement in roadway construction started in the 1970s. Since then, numerous studies have revealed that using geosynthetic reinforcement layers (mainly geogrids) in pavement structures can either extend the pavement service life and/or reduce the base course layer thickness *[1-11]*. The geosynthetic type, the geometry/interlocking of geogrids, the location/layers of geosynthetics, the base thickness, and the subgrade strength have significant effect on the performance of geosynthetic reinforced flexible pavement *[5, 12, 13]*. With the benefits of geosynthetics in pavement performance improvement being widely recognized, much research of geosynthetic reinforced flexible pavement has centered on understanding the mechanism of geosynthetic (mainly geogrids) reinforcement *[13-17]*. However, no method or specification for design of flexible pavements with geosynthetic reinforcement is universally agreed upon, and a universal design/analysis of such structures is still being investigated.

The literature reveals considerable research aimed at developing design guidelines, empirical relationships, or/and design methods for certain reinforcement-pavement conditions and design requirements. Currently, most design approaches are based on the 1993 AASHTO pavement design guide with certain assumptions. With pavement design and analysis moving toward Mechanistic-Empirical based methods, quantifying the benefits of geosynthetics and

incorporating these benefits into Mechanistic-Empirical Pavement Design Guide (MEPDG) has recently received a lot of attention *[4, 18]*. Nevertheless, a lack of understanding the mechanisms of geosynthetic reinforcement, especially rigorously quantifying the geosynthetic benefits, has limited the effectiveness of attempts to change the engineering design practice. These limitations provide a motive for continual research on geosynthetic reinforced pavements to better understand geosynthetic reinforcement benefits and their incorporation into future pavement designs within mechanistic-empirical pavement design methods.

Literature Review

Geosynthetics in Pavement

The use of reinforcing inclusions to improve the mechanical properties of soils dates to ancient times. However, only within the last 30 years or so, have analytical and experimental studies led to contemporary soil reinforcement techniques; one of these techniques is the use of geosynthetic materials in roadways. The most commonly used types of geosynthetics in pavement applications are geogrids and geotextiles.

Geogrids are characterized by large openings made by either coating woven or knitted geosynthetics to form a grid (polyester geogrids), welding oriented strands to form a grid (polyester geogrids), or punching holes in flat sheets then drawing them to align the polymer molecules (polypropylene and polyethylene geogrids). The polyester geogrids are flexible, while the polypropylene and polyethylene geogrids are more rigid. Granular soil particles can partially penetrate the apertures of geogrids, thus creating a strong interlocking action (Figure 1).

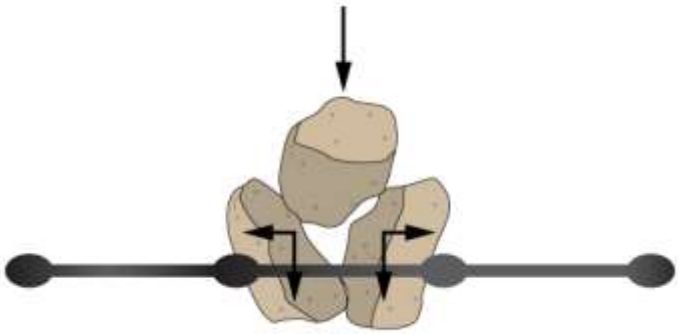

Figure 1
Geogrid apertures improving aggregate interlocking

Geotextiles are permeable textile structures made of polymeric materials. The polymers are

formed into geotextiles using either woven, knitted or non-woven methods. Each has its own unique applications and benefits. In general, woven geotextiles exhibit high tensile, high modulus and low elongation, and knitted and nonwovens geotextiles exhibit lower tensile, higher elongation and higher flow rates. As a continuous sheet, geotextiles can prevent intermixing of aggregate base and the subgrade materials, called separation, thus allowing a stiff material placed on a soft subgrade to maintain its full thickness throughout the life of the pavement (Figure 2).

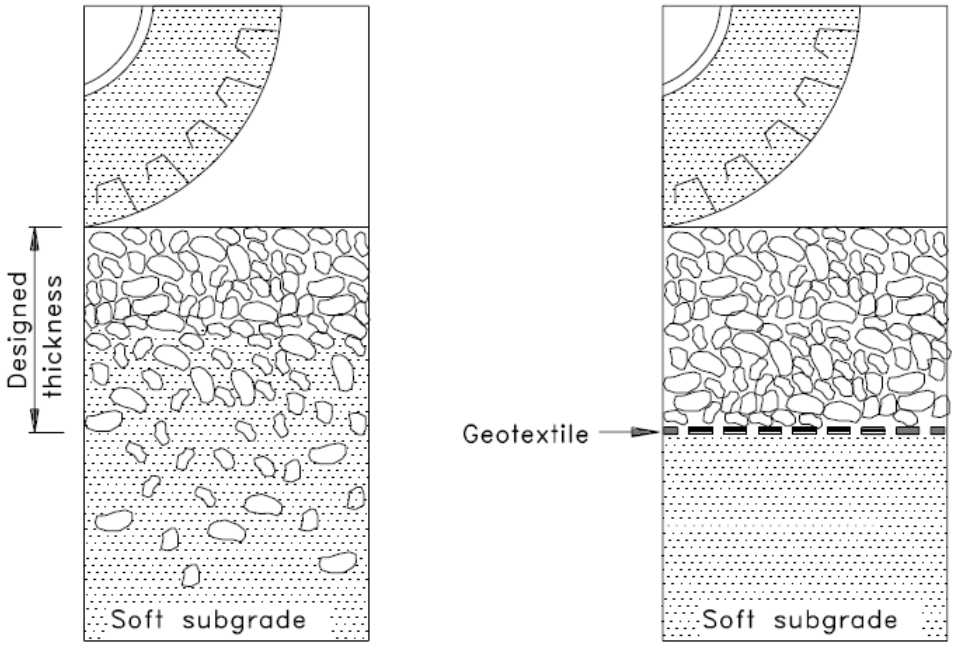

Figure 2
Intermixing of base course and subgrade materials without a geotextile (a), and Separation of these materials using a geotextile (b) *[19]*

Reinforcement Mechanism of Geosynthetics in Pavement

Depending on the type of interaction, the properties of the soil and reinforcement, and the desired types and levels of improvement, whether design service, reducing rutting, or reducing layer thickness, four improvement mechanisms (reinforcement functions) can be distinguished: (1) improved bearing capacity, (2) lateral restraint, (3) tensioned membrane, and (4) stabilization function. These functions are illustrated in Figures 3, 4 and 5.

Improved bearing capacity (

Figure 3). The reinforcement contributes to an increase in bearing capacity by significantly changing the geometry of the potential collapse pattern, preventing the most adverse mechanisms from occurring.

Confinement effect (lateral restraint effect) (Figure 4). The confinement effect is mainly due to interlocking between geogrid apertures and granular materials, and the interface friction between geogrids or geotextiles and granular materials. The aperture size and geometry, rib shape, junction shape of geogrids all contribute to the interlock behavior and hence the interface load transfer. When the base aggregate layer is subjected to traffic loading, the aggregate tends to move laterally. Due to relative displacement between aggregate and reinforcement, interface friction force is induced at the base aggregate-reinforcement interface. The developed interface shear resistance between the base aggregate and the geosynthetic transfers shear load from the base layer to a tensile load in the geosynthetic. Consequently, lateral deformation or potential tensile strain in the base layer is restrained. As a result, vertical deformation of the pavement surface is reduced. Since base aggregates are stress-dependent materials, improved lateral confinement can also increase the modulus/compressive strength of base course aggregates.

Membrane effect (Figure 5). With the traffic loading, the pavement layer materials beneath the wheel move downward; the reinforcement is deformed and tensioned. Due to its stiffness, the curved reinforcement develops an upward force to support the wheel load and reduce the vertical stress acting on the subgrade. A certain amount of rut depth is needed to mobilize the tensioned membrane effect. The reinforcement should have enough width and stiffness to prevent it from failing by pull-out and tension.

Stabilization function. whereby the particles interlocking with the geogrid are confined within the geogrid apertures and/or interface friction (geogrids and geotextiles) resulting in reduced particle movement and rotation. The particles restrained in this way, then influence particles adjacent to them and confer a degree of confinement to them, resulting in a stabilized granular layer.

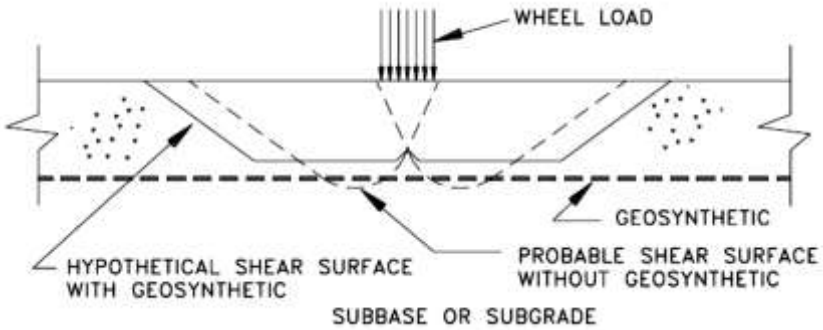

Figure 3
Improved bearing capacity caused by base reinforcement *[19]*

Factors Affecting the Benefits of Geosynthetics in Pavement

The benefits of using geosynthetic reinforcement for base course and subgrade layers of flexible reinforcement have been addressed by many researchers for more than two decades *[20-27]*. Documented literature indicated that the base course thickness for a given flexible pavement can be reduced when geosynthetic reinforcement is included in the design *[210-26, 28, 29]*. This reduction is usually defined by the Base Course Reduction (BCR) factor, which is defined as the ratio of the thickness of the reinforced base course layer to that of the unreinforced base course that will have the same service life under the same traffic level. Many studies have indicated that geogrids and geotextiles have successfully been used to provide a platform for construction over soft subgrades *[20, 22, 25- 31]*. Numerous research programs have also reported extended service lives for pavement sections with geosynthetics compared to similar sections without geosynthetics *[20-26, 28, 29]*. The influence of geosynthetic reinforcement on the rutting behavior or the service life of the flexible pavement has been most commonly defined by the Traffic Benefit Ratio (TBR). TBR has been defined as the ratio of the number of cycles needed to achieve a particular rut depth in a reinforced section to that of an unreinforced section with identical layers' thicknesses, material properties, and loading characteristics.

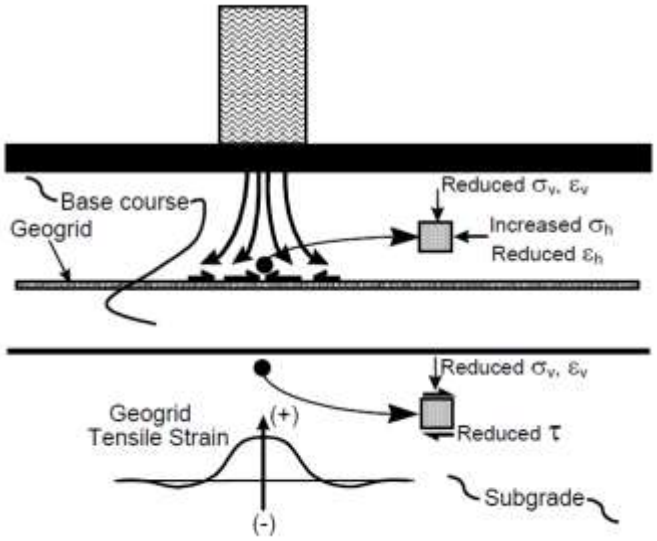

Figure 4
Lateral restraint mechanisms *[12]*

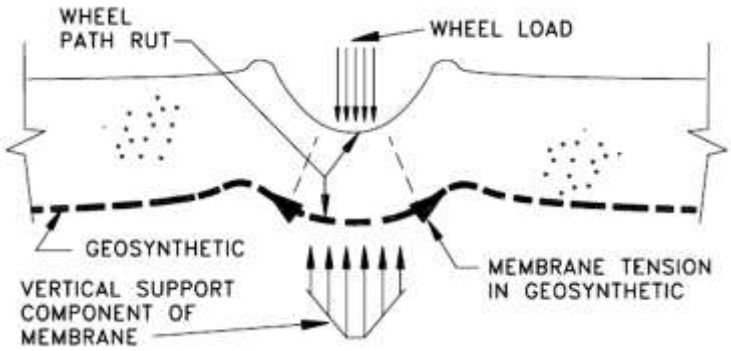

Figure 5
Tension membrane mechanisms *[19]*

The amount of improvement in pavement performance with the inclusion of geosynthetics depends on many factors, including the strength of the subgrade, properties of geosynthetic reinforcement material, location of the reinforcement in pavement, the thickness of base layer, etc. Previous studies have shown that the weaker the subgrade, the greater the improvement geosynthetics provided and there was little improvement obtained for subgrades with high California Bearing Ratio (CBR) *[12, 23, 32]*. Another factor that plays an important role in the performance of geosynthetic reinforced pavement is the thickness of base course. The benefit of geosynthetics generally decreases with an increase in the thickness of the base course and becomes insignificant if the base course is very thick *[26, 33]*. Although geosynthetics may provide significant benefits for low volume roads, its benefits would diminish as the thickness of AC layer increases; hence its advantages for applications in high volume roads is still being determined *[3, 34]*.

The improved performance of geosynthetic reinforced pavement also depends on the properties of geosynthetic(s), such as the type and tensile modulus of geosynthetics, flexural stiffness of geogrid, aperture stability modulus of geogrid, junction strength of geogrid, aperture size of geogrid, frictional capacity with fill materials, and filtration capabilities for geotextiles. While the overall geosynthetic benefits are will realized, the effect of each of these parameters in isolation on the pavement performance is not quantified *[19]*. Appropriate selection of geosynthetics is therefore compromised by the difficulty in associating their relevant properties to pavement performance. Some of the properties currently used in specifications may be unnecessary, resulting in increased costs of application. The properties needed to meet the reinforcement requirements should be evaluated, and tests should be developed if needed *[34]*. The majority of the work indicated better performance for higher tensile modulus geosynthetics (geogrids and geotextiles) than lower tensile modulus geosynthetics *[5, 20-22, 25, 26]*. Occasionally, geogrids with lower tensile modulus were reported to be more effective than geogrids with higher tensile modulus

[25]. Meanwhile, Giroud and Han selected the aperture stability modulus of punched and drawn biaxial geogrids instead of low-strain tensile modulus of geogrid to develop their design method for unpaved reinforced roads *[35]*. The inconsistent relationship between geosynthetic properties and performance can be understood by considering large number of variables that exist in pavement design. Under different conditions, the relative importance of different geosynthetic properties may vary. The properties that are important for one product may not be for another. There are no nationally accepted specifications for properties of geosynthetics under confined conditions (within pavement), which need to be further investigation. As one of such attempts, Zornberg et al. suggested a new test method to quantify the confined stress-strain properties of the geogrids for their application to the pavements *[36]*. It is very clear that a definitive method of analysis relating specific geosynthetic performance properties to reinforced pavement performance has to be developed to move the design of geosynthetic reinforced flexible pavement from pure empirical to mechanistic-empirical.

The location of the geosynthetric reinforcement/stabilization relative to the base course layer may be distinguished as one of the most important factors contributing to the success of the design of flexible pavements with reinforced bases. Many studies had suggested that geogrid reinforcement benefits are dependent upon the placement depth of the reinforcement layer. Generally, the location of geogrid depends on the subgrade strength, the thickness of the base course layer, and the magnitude of applied load *[29]*. Moghaddas-Nejad and Small suggested that for small loads and thin base course layer thickness of (40 mm), a geogrid's optimal location will be in the middle of the base layer *[37]*. For moderate loads, studies indicated that the placing a geogrid in the middle position of an 8-in. thick base layer resulted in better rutting performance than when placed at the bottom *[29]*. In the case of heavier loads, Haas et al. suggested that the optimal location of geogrids was at the bottom of base layers up to 10 in. in thickness *[22]*. However, Haas et al. and Perkins indicated that, for heavy loads and bases thicker than 10 in, the optimal location was at the middle of the base layer *[12, 22]*. For very heavy loads, Perkins and Ismeik indicated that the bottom of a 12-in. thick base was better than the middle *[29]*. Haas et al. showed that for the case of weak subgrade underlying a thick base course layer, optimal results were obtained when the geogrid reinforcement was placed within the subgrade *[22]*. They also suggested that for optimal effects, the geogrid reinforcement of flexible pavement should be placed in the zone of moderate elastic tensile strain of 0.05 to 0.2 percent beneath the center of load application. Al-Qadi et al. concluded, from their accelerated testing on full-scale pavement sections with base thickness of 8, 12, and 18 in., that for a thin base course layer, placing geogrid at the subgrade/base course interface gives better performance and that the geogrid should be placed at the upper third of the base course layer for a thicker base course layer (≥ 12 in.)

[13]. Abu-Farsakh and Chen conducted a series of cyclic plate load testing on pavement sections with 12-in. thick base. In their study, better performance was observed when the geogrid layer was placed at the upper one third of base layer than that when the geogrid was placed at the base-subgrade interface or at the middle of base layer *[5]*.

Separation between layers is another important consideration in the design of flexible pavements when a weak subgrade is encountered. It is a time-dependent process, in which the base course layer thickness decreases with time due to the intrusion of granular base aggregate into weak fine subgrades, and or the movement/pumping of subgrade fines into granular base layer, as illustrated in Figure 2. Chapter 5 The FHWA NHI 07-092 *Geosynthetics Design and Construction Reference Manual* recommends using a separation geotextile in the application for soft and/or wet subgrades (CBR < 3), and for firmer subgrades (3 < CBR < 7) when they have a significant fines content and/or will be exposed to water. Mixing between the base course and the subgrade layers reduces the as-design thickness, permeability and shear strength of the base course layer. Factors influencing the particle migration are the size of the base course particle size and gradation, the thickness of the pavement layers above the subgrade, the subgrade strength (subgrade reaction or CBR), high fines content and their plasticity, and the traffic load and intensity. Due to the large aperture size associated with most commercial geogrids, they may not be considered as typical separation geosynthetics, although geogrids may be effective in separating base course with a grain size that is compatible with the size of geogrid apertures. For example well-graded granular material when confined by a geogrid can perform as an effective separator. Better results, in terms of layer separation, were obtained using the geotextiles especially when weak, wet and/or high fines content subgrades are encountered *[29, 30, 38, 39]*.

Design Approaches for Geosynthetic Reinforcement in Pavement

The literature now contains considerable research aimed at developing design guidelines, empirical relationships, or/and design methods for certain geosynthetic reinforced pavement conditions and design requirements. However, currently, no method or specification for design of flexible pavements with geosynthetic reinforcement is universally agreed upon, and the design/analysis of such structures is still being investigated. This is mainly attributed to the complexity of the problem delineated by the number of influential variables, and the nature of interaction mechanisms.

The design of flexible pavements with geosynthetic reinforcement involves a number of variables and their interactions that need further investigation. Those variables are (i) the

pavement thicknesses [asphalt concrete (AC) and base course layers], (ii) the strength of the subgrade material, (iii) mechanical properties of the reinforcement (i.e., modulus, creep, relaxation modulus, etc.), (iv) physical properties of the reinforcement (i.e., rib thickness and aperture size/geometry for geogrids compared to the base material, flow rate of geotextiles), (v) the location of the reinforcement layer within the base course, (vi) the mixing of the base course with the subgrade material due to particle migration, and (vii) construction specifications. A successful design should assure the capability of the reinforcement to develop the required interactions with the pavement layer materials necessary to maintain the permanent deformations within tolerable limits under the anticipated traffic loading throughout the service life of the structure.

Available pavement design methods incorporating geosynthetic reinforcement generally target a reduction of base course thickness (BCR) or extension of service life of the pavement (TBR). Some methods have been based on the use of a specific geosynthetic, others have been established for generic types of geosynthetic reinforcement, and some have been generically established for almost any type of geosynthetic reinforcement *[19]*. Usually, the 1993 AASHTO flexible pavement design method is followed *[19, 21, 40]*.

Designing for an extension of service life of the pavement,

$$W_{18(R)} = W_{18(UNR)} \times TBR \quad (1)$$

where, $W_{18(UNR)}$ and $W_{18(R)}$ are the predicted numbers of 18-kip equivalent single axle load applications for the unreinforced and reinforced pavement, respectively.

Designing for a reduction in base course thickness,

$$D_{2(R)} = D_{2(UNR)} \times (1 - BCR) \quad (2)$$

where, $D_{2(UNR)}$ is the base thickness for the unreinforced pavement; $D_{2(R)}$ is the geosynthetic reinforced base thickness for the reinforced pavement such that the service life identical to the unreinforced pavement is obtained.

or

$$D_{2(R)} = \frac{SN_{UNR} - a_1 D_1}{a_{2(R)} m_2} \quad (3)$$

where, SN_{UNR} is the structure number of the unreinforced pavement; $a_{2(R)}$ is the increased base layer coefficient, which can be estimated by substituting $W_{18(R)}$ obtained from Equation (1) into the 1993 AASHTO design equation.

A combination of benefits, i.e., combination of some extension of service life and some

reduction of base thickness, can be achieved by specifying a desired BCR or a desired TBR, or both *[19, 40]*.

While the benefits of geosynthetics in pavement performance improvement are widely recognized, a large range of TBR values is reported in the literature. This creates a dilemma for pavement design engineers because while they may realize the benefit of geosynthetics, they may not know the appropriate TBR values for their design(s), which are not constants for a specific geosynthetic. In fact, the TBR and BCR values for a specific geosynthetic varies with the base layer thickness, material properties, subgrade strength, etc. They are specific to a set of conditions and pavement layer thickness.

With pavement design moving toward Mechanistic-Empirical based methods, Perkins et al. proposed a methodology to incorporate the benefits of geosynthetics in flexible pavements by introducing enhanced input parameters to the traditional (unchanged) M-E design method *[4]*. While the traditional components of mechanistic-empirical models for unreinforced pavement were included, new enhanced input parameters for the reinforcement were added into their model. These new parameters include structural elements for geosynthetic reinforcement, a material model for the reinforcement, a model for reinforcement–aggregate shear interaction, additional response modelling steps that account for the influence of the reinforcement on lateral confinement of the base aggregate during construction and subsequent traffic loading, and a modified permanent deformation damage model used for aggregate within the influence zone of the reinforcement. However, a major effort and/or collaboration will be required to add the components described in their papers into current Pavement ME design software and manuals.

OBJECTIVE

The main objective of this research was to evaluate the benefits of using triaxial geogrid and high strength woven geotextile to reinforce/stabilize base course aggregate layer and/or stabilize weak subgrade soils in flexible pavement applications. This was achieved through conducting both field and laboratory accelerated load testing on geosynthetic reinforced unpaved and flexible pavement test sections. Different types and configurations of geosynthetics were considered for reinforcements. A variety of sensors was installed for each section to measure the load-associated pavement response and performance. Another objective was to quantify the benefits of using geosynthetics within the framework of the 1993 AASHTO pavement design guide and the AASHTO Pavement ME, and incorporating them into the design.

SCOPE

The stated objectives of this research study were achieved through conducting an extensive experimental testing program. The testing program includes: (1) field moving wheel accelerated load testing on instrumented geosynthetic-reinforced pavement test lane sections built over weak subgrade soil at the LTRC - Pavement Research Facility (PRF) site; (2) full-scale cyclic plate load testing on the same field pavement test lane sections constructed for moving wheel accelerated load testing; and (3) laboratory large-scale in-box cyclic plate load testing on instrumented geosynthetic-reinforced pavement test sections constructed inside a 6.5-ft. × 6.5-ft. × 5.5-ft. test box. The load-associated responses and performance of the different test sections were monitored during testing using various instrumented sensors.

The results of field and laboratory experiment tests were carefully analyzed and evaluated. The benefits of using geosynthetics (triaxial geogrid and high strength woven geotedxtile) in flexible pavement were quantified within the framework of the 1993 AASHTO pavement design guide and the AASHTO Pavement ME design. Based on the results of this study, typical design parameters were recommended for the design of geosynthetics reinforced flexible pavement built over weak subgrade soils (CBR = 0.5-3). Additionally, the economic benefits of using geosynthetics in flexible pavement were demonstrated by a direct comparison with the unreinforced flexible pavement and the 12-in. cement/lime treated subgrade through a group of base thickness design scenarios and life-cycle cost analyses.

METHODOLOGY

In this study, field and laboratory accelerated loading tests were conducted to evaluate the performance of geosynthetic reinforced/stabilized unpaved/paved roads under cyclic moving traffic wheel and cyclic plate loads.

Field Pavement Test Sections

Six test lane sections with different reinforcement configurations were constructed over native soft soil at an outdoor site located at the LTRC Pavement Research Facility (PRF) of the Louisiana Department of Transportation and Development (DOTD) in Port Allen, LA. Two series of tests, moving wheel load tests and cyclic plate load tests, were conducted to investigate the field performance of geosynthetic reinforced/stabilized unpaved/paved roads and to identify the differences in pavement response to moving wheel and cyclic plate loads.

Field Pavement Test Sections and Instrumentation

Test Sections. Six test lane sections were constructed over native soft soil. Test sections were 80 ft. long and 13 ft. wide. Figure 6a depicts the schematic of the site while the cross sections of the six test lanes is depicted in Figure 6b and also summarized in Table 1. Section 1 and Section 4 are the control sections that were constructed without geosynthetic reinforcements; of which Section 1 was constructed over 1 ft. thick sand embankment wrapped by nonwoven geotextile as a common practice in Southern Louisiana. Section 4 is a typical control section constructed using nonwoven geotextile for separation and filtration. Section 2 and Section 3 were reinforced/stabilized by a triaxial geogrid, GG, placed at the aggregate base - subgrade interface, which are underlain by nonwoven geotextile for separation and filtration. An additional layer of geogrid, GG, reinforcement was also installed at the upper one-third of the aggregate base layer thickness in Section 2. A high strength geotextile, GT, was used to reinforce/stabilize Section 5 and Section 6 with different aggregate layer thicknesses. A 3-in. HMA surface course was later constructed over the test lane sections, after completion of pre-rut phase testing that was performed to simulate the possible prestressing and mobilization of the geosynthetics due to construction traffic.

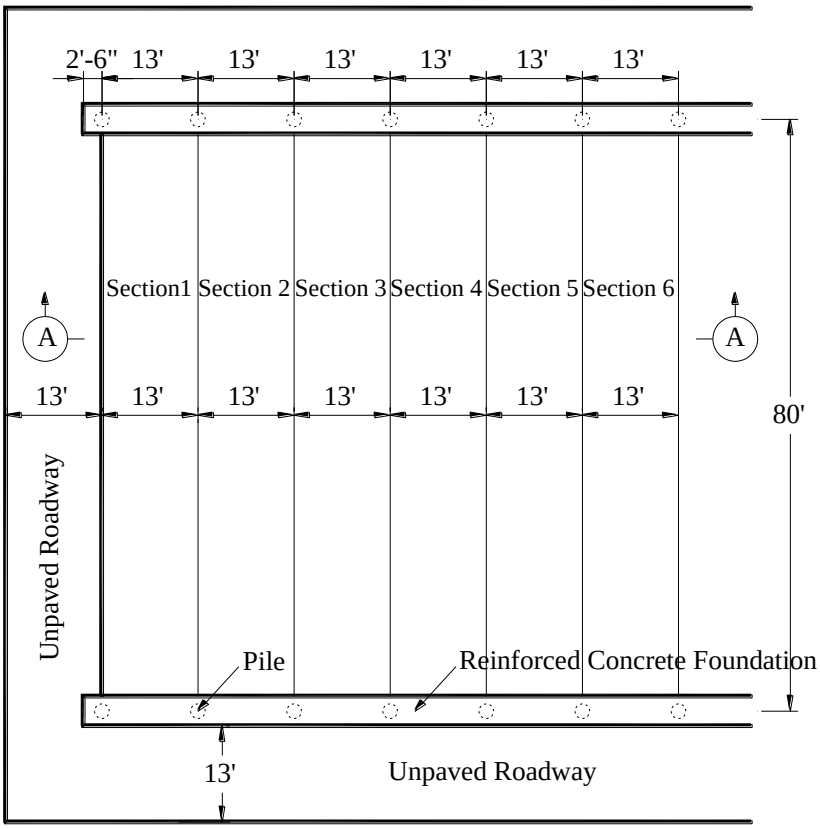

(a) Plan view

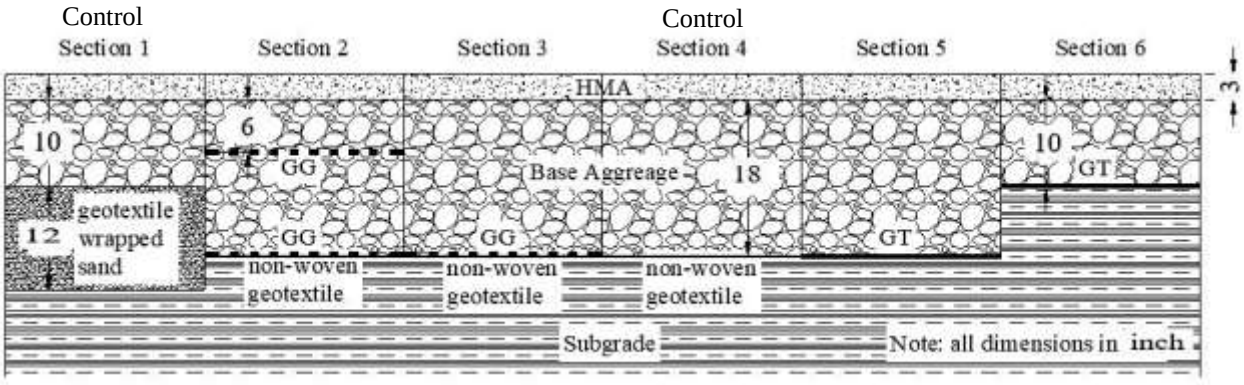

(b) Cross section of the test sections (section A-A)

Figure 6
Plan layout and cross section of ALF test sections

Table 1

ALF geosynthetic-reinforced test sections

Section	Description	Geosynthetic Location	Base	HMA	Testing Phase criterion	
					Pre-rut Phase	Loading Phase
Section 1	—	12” compacted nonwoven geotextile-wrapped sand layer	10”	3”	1” pre-rut or 2000 passes	¾” rut
Section 2	Double TX 5 geogrid reinforced section	One layer of geogrid placed on nonwoven geotextile @ base-subgrade interface and one layer at the upper 1/3 rd	18”	3”		
Section 3	TX 5 geogrid reinforced section	One layer of geogrid placed on nonwoven geotextile @ base-subgrade interface	18”	3”		
Section 4	Control section	LA DOTD Class D nonwoven geotextile on subgrade surface	18”	3”		
Section 5	RS580i high strength woven geotextile reinforced section	One layer @ base-subgrade interface	18”	3”		
Section 6	RS580i high strength woven geotextile reinforced section	One layer @ base-subgrade interface	10”	3”		

Instrumentation. The test sections were instrumented using a variety of instruments to measure the load – and environment – associated pavement responses and performance. Figure 7 depicts a typical layout of instrumentations used in this study.

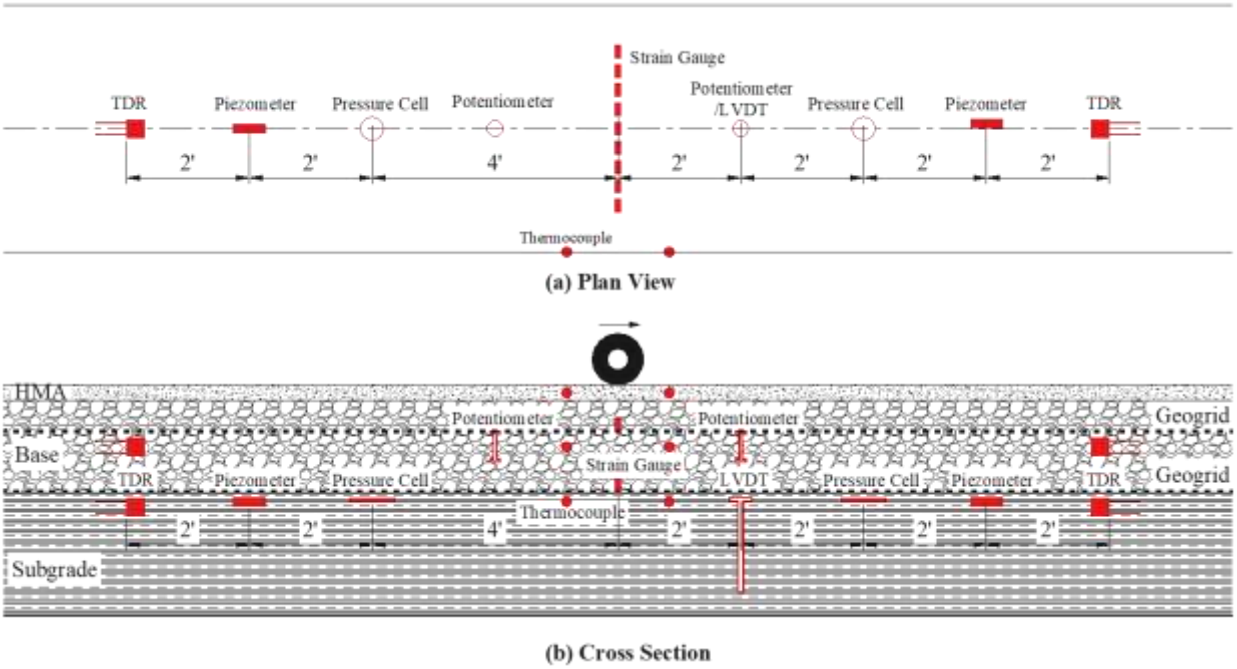

Figure 7
Instrumentation plan for test section 2

For each test section, two earth pressure cells (Geokon Model 3500) were installed at the top of the subgrade to measure the total vertical stresses. Piezometers (Geokon Model 3400) were installed next to the pressure cells to measure possible excess pore water pressure generated by the cyclic wheel load (Figure 7). Both the pressure cells and Piezometers were installed at a depth of about 1 in. below the subgrade surface.

Spring-loaded LVDTs (RDP DCTH2000A) were customized and attached to a 3 ft. long steel rod that was driven into the subgrade soil. A thin, rigid disk with a diameter of 2 in. was attached onto the contact tip of the spring-loaded LVDT to provide sufficient contact area with the soil. The LVDT measured the total deformation of the subgrade, since the end of each LVDT was fixed with respect to the depth of the subgrade. Potentiometers (Honeywell MLT-38000201) were customized to measure the strain at the mid-height of the aggregate layer. The potentiometer has a maximum travel distance of 1 in. Two circular end plates with diameters of 2 in. were attached onto the potentiometer. The customized potentiometers were installed and affixed at the mid-height of the aggregate layer without fixing one end of the potentiometer. The potentiometer measures relative distance between the two circular plates. Measurements from potentiometer can help separate the contribution of aggregate layer to the total rut depth of pavement sections.

Pavement Layer Materials

Subgrade. The native subgrade soil consisted of a high plasticity clay, having a liquid limit of 88 and a plastic index of 53 with 96.6 % passing # 200. It is classified as CH per Unified Soil Classification System (USCS) or A-7-6 according to the American Association of State Highway and Transportation Officials (AASHTO) classification system. The clay has an optimum moisture content of 35% and a maximum dry density of 78.1 pcf according to the standard Procter test (ASTM D698).

Base Course Material. Crushed limestone was used in the base course layer for all test sections. The crushed limestone had 1.56% passing No. 200 opening sieve, an effective particle size (D_{10}) of 0.015 in., a mean particle size (D_{50}) of 0.123 in., a D_{85} of 0.75 in., a uniformity coefficient (C_u) of 37, and a coefficient of curvature (C_c) of 3. This crushed limestone is classified as GW and A-1-a according to the USCS and the AASHTO classification systems, respectively. The maximum dry density, as determined by the modified Proctor test (ASTM D1557) is 129 pcf at an optimum moisture content of 9.4%.

HMA Concrete. The HMA used in the construction is a wearing course. It is a 0.5 in. design level 1 Superpave mixture. The asphalt binder was classified as PG 76-22M according to the Performance Grade (PG) specification. The optimum asphalt binder content is 4.1%. The theoretical maximum density of HMA is 154.8 pcf.

Geosynthetics. Two types of reinforcement geosynthetics and one DOTD Class C geotextile were used in this research, a triaxial geogrid, GG, and a high-strength woven geotextile, GT. The triaxial geogrid was made by means of punching and drawing polypropylene (PP) sheets. The geotextile was made from high-tenacity polypropylene filaments that are woven into a sheet. The physical and mechanical properties of these geosynthetics as reported by the manufacture are presented in Table 2. Index properties of the DOTD Class C nonwoven geotextile used in Sections 1 through 4 were not tested. However, the particular product was chosen to meet the requirements of Class C geotextile according to the DOTD's standard specifications for this type of application (Louisiana Department of Transportation and Development, 2006). Class C geotextile has the following minimum values of index properties: grab tensile strength of 3.3 lb/in, elongation of 50% at failure, and burst strength of 5.3 lb/in. Although the Class C geotextile's strength is much lower than the geogrid's and its primary functions were separation and filtration, whether the nonwoven geotextile had any reinforcing effects on the pavement's performance is not known.

Table 2
Physical and mechanical properties of geosynthetics

Reinforcement	Polymer Type	T, lb/in		J, lb/in		Aperture Size, in
		MD[a]	CD[b]	MD[a]	CD[b]	
GG	Polypropylene	7.71[c]		1541[d]		1.57×1.57×1.57
GT	Polypropylene	39.9[e]	150[e]	2000[f]	7450[f]	0.0167[g]

[a]Machine direction, [b]Cross machine direction, [c]Tensile strength at 0.5% strain in radial direction, [d]Tensile modulus at 0.5% strain in the radial direction, [e]Tensile strength at 2% strain, [f]Tensile modulus at 2% strain, [g]Apparent opening size (AOS)

Construction of Test Lanes

The first step in this research study required preparation of the new location for the proposed test sections at the PRF site, located south of the current test site (Figure 8a). This included constructing two reinforced concrete pile-supported foundations to carry the ALF testing facility, as shown in Figure 8b. The piles were cut to levels of 6 inches above the excavated grade level (i.e., to elevations of -7.35 ft. for the south side and -7.75 ft. for the north side). An 18-in. thick reinforced concrete pile cap was constructed as detailed in the construction plan. The final elevations of top pile cap foundation was +4.65 ft. for the south side and +4.25 ft. for the north side from a specified survey reference point. The natural soil for seven lanes between the north and south pile cap (78 ft. × 78.5 ft.) was excavated to the elevations specified by the attached construction plan. For test section 1: the elevations from a specified survey reference point were -19.35 ft. at the south side to -19.75 ft. at the north side; for test sections 2 to 5: the elevations were -13.35 ft. at the south side to -13.75 ft. at the north side; while for test section 6: the elevations were -7.35 ft. at the south side to -7.75 ft. at the north side. Lane 7 was constructed to host and practice the ALF machine prior to testing the instrumented lanes 1 to 6. Light construction equipment was used for excavation to minimize subgrade disturbance and the subgrade was leveled after excavation. A nuclear density gauge, Geogauge (Gg), light falling weight deflectometer (LFWD), dynamic cone penetrometer (DCP), and Vane Shear Testing Apparatus were deployed after the subgrade surface was prepared to measure the in-place properties of subgrade (Figure 9).

(a) Site preparation

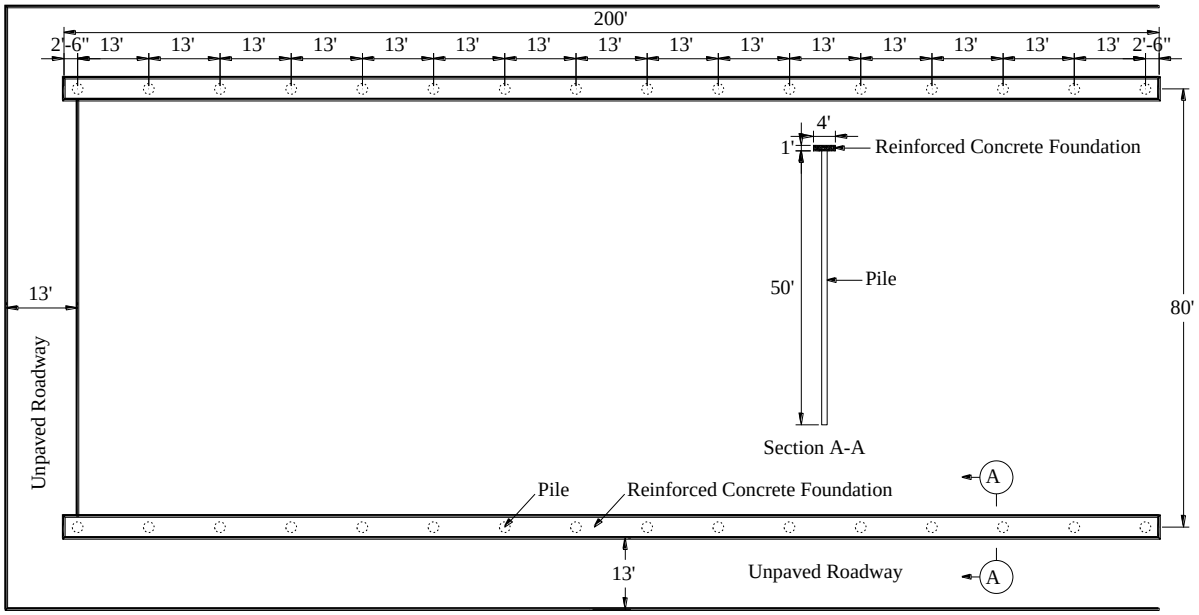

(b) Site layout

Figure 8
Site preparation and layout

(a) Nuclear density gauge

(b) Geogauge

(c) LFWD

(d) DCP

(e) Vane Shear

Figure 9
In-situ tests

After the completion of subgrade preparation, the instrumentation was installed. When installing the customized LVDTs, 3 ft.-long steel rods were driven deep into the subgrade soil using a hammer. The LVDTs were then vertically attached to these steel rods (Figure 10). The clay subgrade soil was then was backfilled and compacted with a small rod around the LVDTs.

Figure 10
Placement of LVDTs

To install the piezometers, short trenches were first excavated to a predetermined depth with a hand trowel (Figure 11). Horizontal holes with a slightly larger diameter than the piezometer were excavated at the end of each trench. The previously saturated piezometers were then inserted in the holes and covered immediately with saturated subgrade soil.

Figure 11
Placement of piezometers

When installing pressure cells, holes with the same shape but slightly larger than the pressure cell were excavated to a predetermined depth with a hand trowel. The bottom of each hole

was flattened gently with a compaction hammer. The pressure cells were then placed into the holes and adjusted until level with the assistance of a small bubble level placed on the pressure cell (Figure 12). The subgrade soil was backfilled and compacted over the pressure cells. To minimize over-registration/under-registration of pressure due to over-compaction/under-compaction, a tight control of the backfill compaction was made to ensure that the density of backfill was close to that of the surrounding soil.

Figure 12
Placement of pressure cells

To install the time-domain reflectometers (TDR), short trenches were first excavated to the predetermined depth with a hand trowel (Figure 13). The TDRs were then inserted horizontally into the subgrade and covered immediately with subgrade soil.

Figure 13
Placement of TDRs

After instrumentation installation, the geogrids/geotextiles with installed strain gauges were placed on the top of the subgrade of test sections 2, 3, 5, and 6 (Figure 14). To protect the strain gauges from damage during the compaction of the base course layer, the gauges were

covered with a small amount of subgrade soil and gently compacted by hand before the base course was spread over the geogrids/geotextiles.

Figure 14
Placement of geogrids with strain gauges

After the installation of the reinforcement geosynthetics, a 12-in. compacted geotextile-wrapped sand layer was constructed on test section 1, following the typical procedures and specifications as described by the DOTD design manual; while 12 in. of compacted class II base coarse material (Mexican limestone) was constructed on test sections 2 to 5, by placing 14 in. of loose material, mixing with desired water and then compacting it using a smooth static roller to 12 in. thickness. The DOTD specifications were followed for constructing the base layer, i.e., the in-place density ≥ 95% of maximum dry density ($\gamma_{d\text{-}max}$) and moisture content = ± 2% of optimum moisture content (w_{opt}) as determined by the modified Proctor test (ASTM D1557). The nuclear density gauge was used to measure the in-place dry density and moisture content for construction control.

Once the first lift of the base layer met compaction requirement, the second geogrid layer of test section 2 with strain gauges was installed. After that, 6 in. of compacted class II base coarse material was constructed on test sections 2 to 5, by placing 7 in. of loose aggregate material and compacting it to 6 in. thickness; and 10 in. of compacted class II base coarse material was constructed on test sections 1 and 6, by placing 11.7 in. of loose aggregate material and compacting it 10 in. thickness. Again, the nuclear density gauge was used to measure the in-place dry density and moisture content for construction control. The Geogauge (Gg), LFWD, and DCP were then utilized to measure the in-place material properties of base and subgrade layers.

After the completion of base course construction, researchers installed potentiometers. To install potentiometers, round holes were excavated to the predertermined depth with a hand trowel. The potentiometers were placed vertically into the hole (Figure 15). The finer portion of base course material (passing No. 4 sieve) was backfilled and compacted with a screwdriver handle around the potentiometers.

Figure 15
Placement of potentiometers

When installing the TDRs, short trenches were first excavated to a predetermined depth with a hand trowel. The TDRs were then buried horizontally. To protect the TDRs from damage during the compaction and testing, the TDRs were covered with a small amount of finer portion of base material (passing No. 4 sieve) and gently compacted by hand before the remaining base course material was backfilled and compacted.

Prior to paving the hot mix asphalt (HMA), all sections were pre-rutted using the moving wheel accelerated load facility (ALF) until reaching a maximum surface rut depth of 1 in. or 2000 passes, whichever came first. The purpose from pre-rut testing was to simulate the possible prestressing and mobilization of the geosynthetics due to construction traffic. Please note that pre-rutting of test sections is not a normal testing practice that might affect the outcome of geosymthetic benefits. After pre-rutting, the base course material was remixed and re-compacted. A 3 in. thick Superpave level 1 (well-performing) hot mix asphalt (PG76-22M) was then constructed over the entire repaired base coarse layers of six test lane sections (86.5 ft. × 78 ft.). The falling weight deflectometer (FWD), Geogauge (Gg), LFWD, DCP, and PSPA were then used to measure the in-place material properties of pavement layers.

Test Facilities

Moving Wheel Load Tests. A full-scale accelerated load facility (ALF) was used to apply cyclic moving wheel loads on test lane sections and pre-rut. Figure 16 shows a picture of the ALF with an insert of the dual-wheel assembly. ALF is a testing device that applies unidirectional trafficking to the test sections with a nominal speed of 16.8 km/h (10.5 mph) or 350 passes per hour. ALF has a dual-tire axle consisting of two Michelin XZE-model truck tires. The load is adjustable from 9,750 lb. (43.4 kN) to 18,950 lb. (84.4 kN). With a computer-controlled load trolley, the weight and movement of traffic is simulated in one direction at a speed of 10.5 mph (16.8 km/h). The wheel path length generated by ALF is about 12 m (40 ft.) long. Lateral wander that can be normally distributed over a width of 30 in. (762 mm) [15 in. (381 mm) at each side of the pavement centerline] was utilized in this experiment.

Testing was conducted in two phases for all sections: (1) pre-rut loading phase, prior to construction of HMA layer and (2) main loading phase, after HMA construction. During the pre-rut phase, the applied load was 9,750 lb. The base course surface was pre-rutted to a maximum rut depth of 1 in. or 2000 passes, whichever came first, prior to HMA paving. The base course layer surface was then remixed and re-compacted before the construction of the 3 in. HMA layer. During the HMA surfaced loading phase, the sections were loaded to maximum ¾ in. rut depth. The starting load was 9,750 lb. (43.4 kN). The load was increased to 12,050 lb. (53.6 kN) after 110,000 cycles (151,510 ESALs), and then to 14,350 lb. (63.8 kN) after 210,000 cycles (472,860 ESALs). The tire pressure was set to 105 psi (724 kPa).

Figure 16
Moving wheel load testing facility

Cyclic Plate Load Tests. A hydraulic actuator, with a force rating of 22 kips (100 kN) and a dynamic stroke of 6 in. (152.4 mm), was placed between two I-beams supporting the crosshead. Figure 17 presents a photo of the in-field cyclic plate loading test setup. The cyclic load was applied through a steel rod that fits into a concave-shaped hole on the loading plate that sits on the surface of the HMA (hot mix asphalt) layer. The loading plate was a 1-in. (25 mm) thick steel plate, 12 in. (305 mm) in diameter. The maximum applied load in

tests was 9,000 lb. (40 kN), which results in a loading pressure of 80 psi (550 kPa) and simulates dual wheels under an equivalent 18,000 lb. (80 kN) single axle load. The load pulse, as shown in Figure 18, has a linear load increase from 500 lb. (2.2 kN) to 9,000 lb. (40 kN) in 0.3 second, followed by a 0.2-second period where the load is held constant at 9,000 lb. (40 kN), followed by a linear load decrease to 500 lb. (2.2 kN) over a 0.3-second period, then followed by a 0.5-second period of 500 lb. (2.2 kN) (rest period), before the next loading cycle is applied. This load pulse results in a frequency of 0.77 Hz.

Figure 17
In-field cyclic plate load testing facility

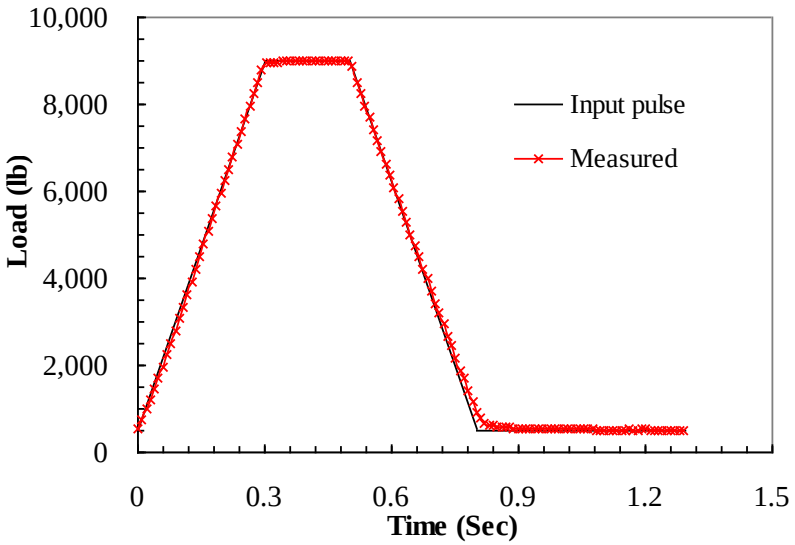

Figure 18
Load pulse applied in the test

Laboratory Pavement Test Sections and Instrumentation

Test Sections. Six test sections were constructed in LTRC green steel test box with inside dimensions of 2.0 m (length) × 2.0 m (width) × 1.7 m (height). Figure 19 shows a typical box pavement test section with the geometric dimensions and layout of instrumentations used in this study.

Each test section was constructed with 1.06 m of very wet high plasticity clay to represent the weak natural subgrade soil. A 305 mm thick non-woven geotextile–wrapped sand embankment was then constructed for Section 1. Sections 2 and 3, which have same base layer thickness of 457 mm, were reinforced by triaxial geogrid. While both Sections 2 and 3 have one geogrid layer placed above a nonwoven geotextile at the base-subgrade interface, there is an additional geogrid layer installed at the upper one-third of the base layer for Section 2. Section 4 is a control section with a 457-mm thick base layer and a layer of non-woven geotextile at the base-subgrade interface, a typical practice in Louisiana. The high-strength woven geotextile, placed at the base–subgrade interface, was used to reinforce Sections 5 and 6, which have a base layer thickness of 457 mm and 254 mm, respectively. The preparation details of test sections can be found in Abu-Farsakh and Chen (2011). The summary of configurations of each test section is shown in Figure 6b.

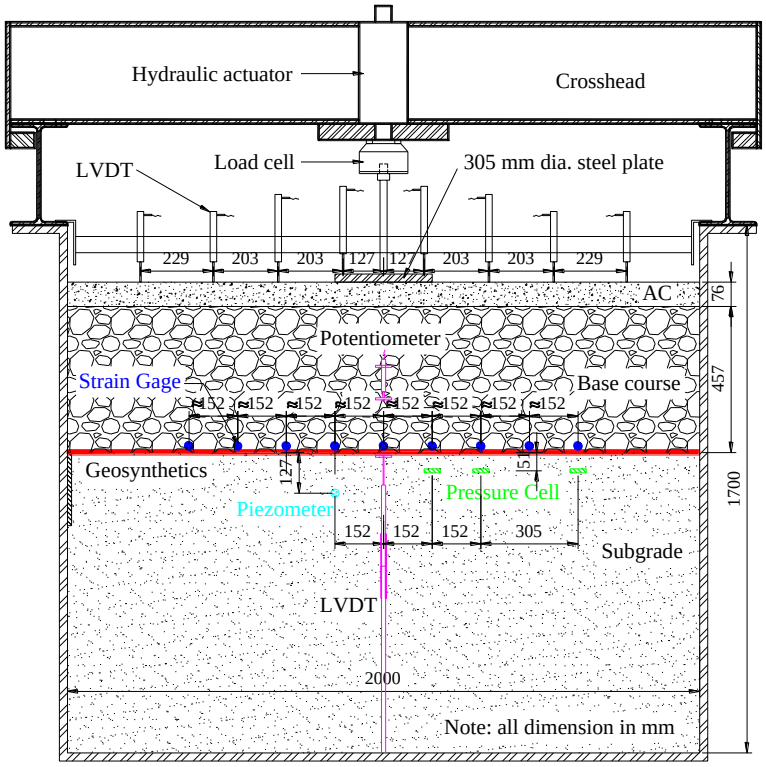

Figure 19
The indoor test box and load actuator for cyclic load testing

Instrumentation. Various types of instruments were installed at different locations within the pavement layers to measure the load associated pavement response and performance. These include pressure cells to measure the total vertical stress at the top of subgrade layer, piezometer to measure the possible excess pore water pressure in the subgrade, customized potentiometer to measure the compressive strain at the mid–height of the base course layer, customized LVDT to measure the total deformation of subgrade layer, strain gauges to measure the strain distribution along the geosynthetics, and LVDTs to measure the surface deformation of pavement test sections. Installation procedures of different instruments can be found in Chen et al. *[2]*.

Pavement Layer Materials

Subgrade. The subgrade soil taken from field pavement test sections were used. To simulate field weak subgrade condition (CBR=0.5), the target moisture content and dry density of subgrade were set as 48% and 69.5 pcf (1,114 kg/m^3), respectively, during construction.

Base Course Material. The same crushed limestone material used in the field test was used in the base course layer for all laboratory test sections. The target moisture content and dry density during construction were set as 7.5% and 123.8 pcf, respectively, to simulate the field test sections.

Hot-mix Asphalt (HMA) Concrete. The HMA used in the construction is a wearing course. It is a 12.5 mm design level 1 Superpave mixture. The asphalt binder was classified as PG 76-22M according to the Performance Grade (PG) specification. The optimum asphalt binder content is 4.1%. The theoretical maximum density of HMA is 154.8 pcf (2,480 kg/m^3).

Geosynthetics. The same geosynthetics used in the field test were used in laboratory tests, i.e., a triaxial geogrid, GG, and a high-strength woven geotextile, GT. The physical and mechanical properties of these geosynthetics as provided by the manufacture are presented in Table 2.

Construction of Test Sections

The subgrade layer was constructed by first mixing the soil with a certain amount of water to achieve the target moisture content with lift thickness of 6 in. (152 mm). Then, the clay was raked level and compacted using an 8-in. (203-mm) × 8-in. (203-mm) plate adapted to a vibratory jack hammer to the predetermined height to achieve the desired density. The nuclear density gauge, Geogauge (Gg), and Vane Shear Testing Apparatus were deployed to measure the in-place properties of subgrade. At least five measurements were performed for

each property. After the completion of subgrade preparation, the instrumentation and the geosynthetics were installed.

After the installation of the geosynthetics, the base course layer was then prepared by placing the crushed limestone in 6-in. (152 mm) thick lifts, mixing with desired water, and then compacting to the predetermined height to achieve the desired density. Once the second lift of the base layer met the requirement, the second geogrid layer of test section 2 with strain gauges was installed. The nuclear density gauge, GG, light falling weight deflectometer (LFWD), and dynamic cone penetrometer (DCP) were deployed to measure the in-place properties of base course. At least five measurements were performed for each property. After the completion of base course preparation, the instrumentations were installed.

The surface asphalt concrete (AC) layer was consequently prepared by placing prime coat on the top of the base layer, followed by placing cold-mix asphalt concrete along the sides of the box with a width of 12 in. (305 mm). The remaining center area of the test box [54 in. (1372 mm) wide square] was left for the HMA. The cold mix asphalt at the boundary area of two mixes was covered with tack coat. The HMA was obtained from a local asphalt plant. It was placed in the oven to age for about 4 hours at a temperature of 300ºF (150ºC). Once the mixture reached the proper compaction temperature [i.e., 300ºF (150ºC)], it was spread over the reserved central area in the test box, raked level, and immediately compacted to the predetermined height using the Bosch Brute breaker hammer. The GG, LFWD, and Portable Seismic Pavement Analyzer (PSPA) were deployed to measure the in-place properties of HMA. At least five measurements were performed for each test.

Test Facility

A steel box was constructed having inside dimensions of 6.5 ft. (2.0 m) (length) × 6.5 ft. (2.0 m) (width) × 5.5 ft. (1.7 m) (height). Two I-beams were fixed on the top of sidewalls of the steel box to serve as the support base for the crosshead. Cyclic plate loads were applied using the hydraulic actuator, which is attached to two I-beams of the crosshead as described earlier. The crosshead was bolted to the support base I beams when the test was running. Figure 20 presents the schematic of the indoor test box. The loading plate was a 1 in. (25 mm) thick steel plate with 12 in. (305 mm) in diameter. The maximum applied load in laboratory tests was 9,000 lb. (40 kN). The same load pulse, as shown in Figure 18, was used here.

Figure 20
Image of the indoor cyclic plate load test facility

DISCUSSION OF RESULTS

In this study, field and large-scale laboratory accelerated loading tests were conducted to evaluate the performance of geosynthetic reinforced/stabilized unpaved/paved road test sections under cyclic moving traffic wheel and cyclic plate loads.

Field Pavement Test Sections

As Constructed Pavement Layer Properties

The importance of characterizing the in situ conditions that affect the road performance was recognized; the in-place material properties of pavement layers were measured at different stages of the study with several different devices, including a nuclear density gauge, a lightweight deflectometer (LWD), a GeoGauge, a dynamic cone penetrometer (DCP), and a vane shear device. Each in situ test was conducted at a minimum of five locations along the longitudinal direction for each test section. The mean values of these properties are summarized in Table 3 to Table 5 for all test pavement sections. The corresponding coefficient of variation (CV), which was calculated by dividing the standard deviation by the mean, is also presented in the tables. As can be seen from Tables 3 and 5, the modulus values obtained from the Geogauge and the LWD are different. These values represent specific stiffness modulus for the testing devices. None of these can be directly used in the mechanistic-empirical analysis of the pavement sections without use of proper correlations with resilient modulus.

Table 3 presents the average value of the native subgrade properties measured before the construction of the aggregate layer. The modulus values from the GeoGauge and the LWD represent the modulus obtained under the testing devices' specific loading conditions, and thus they differ from each other. The range of DCP index (DCPI) in millimeters per blow for the subgrade soil ranges from 160 mm. (6.3 in) to 224 mm (8.8 in.) per blow, which corresponds to a California bearing ratio value of 0.6% to 0.8%.

Table 3 shows that the in situ moisture content of the soil was significantly higher than the optimum, 35%. Sections 2 and 6 had a slightly higher dry density values than the other sections. The different types of modulus values in Table 3 suggest that the subgrade condition is nearly uniform among all the test sections. The minor difference in the stiffness modulus was likely a result of the inherent variability in the heterogeneous nature of soils and the operational variability in testing. However, Section 6 consistently exhibited a slightly higher modulus value through all the different properties, in agreement with Section 6 having a higher subgrade grade level (Figure 6b), less accumulation of moisture from rainfall, and thus a drier and stiffer subgrade condition. Table 4 presents the results of vane shear tests at

various depths of the subgrade. All the test sections again showed similar undrained shear strength, with the exception of Section 6 having a little higher strength.

Table 5 presents the results of in situ tests conducted on the aggregate base layer. The aggregate layer was compacted to meet the requirement of 95% of the maximum dry density determined by the modified Proctor test (ASTM D1557). LWD tests showed similar modulus values for Sections 2, 3, 4, and 5, while Sections 1 and 6 exhibited lower moduli. The reason for this difference is that the LWD measures a composite modulus of the thin aggregate layer and the underlying layer in Sections 1 and 6. The DCP tests in Table 4 show a similar stiffness of the aggregate layer for all the sections except that Section 6 had a little stiffer and drier subgrade.

Table 3

Subgrade conditions tested by nuclear gauge, LWD, GeoGauge, and DCP

Test Section	Moisture Content (%)		Dry Density (lb/ft^3)		LWD (tsf)		GeoGauge (tsf)		DCPI (0-12 in) (inch/blow)		DCPI (12-24 in) (inch/blow)	
	Avg.	Cov.	Avg.	Cov.	Avg.	Cov.	Avg.	Cov.	Avg.	Cov.	Avg.	Cov.
1	49.3	0.05	69.4	0.04	37.6	0.32	145.1	0.14	8.8	0.19	5.1	0.39
2	46.0	0.07	71.3	0.02	47.0	0.16	214.0	0.07	8.0	0.10	6.5	0.16
3	49.5	0.11	68.4	0.07	42.8	0.30	215.1	0.10	7.9	0.03	3.7	0.35
4	49.5	0.12	69.3	0.04	41.8	0.26	190.0	0.15	8.2	0.12	3.6	0.15
5	51.2	0.05	68.1	0.03	41.8	0.18	219.2	0.13	7.9	0.09	6.2	0.06
6	46.5	0.04	70.8	0.02	51.2	0.17	239.1	0.06	6.3	0.17	6.8	0.19

Table 4

Subgrade in-situ undrained shear strength from vane shear tests, units in psi

Test Section	30.5 cm (12 in) below surface		61.0 cm (24 in) below surface		91.4 cm (36 in) below surface	
	Avg.	Cov.	Avg.	Cov.	Avg.	Cov.
1	7.82	0.23	10.76	0.23	10.76	0.27
2	8.41	0.15	11.34	0.13	12.36	0.12
3	8.27	0.17	10.09	0.37	12.61	0.22
4	8.50	0.18	10.73	0.21	13.34	0.10
5	8.34	0.34	9.95	0.38	11.98	0.30
6	8.87	0.13	11.22	0.09	13.34	0.04

Table 5

Base conditions tested by nuclear gauge, LWD, GeoGauge, and DCP (before pre-rut)

Test Section	Moisture Content (%)		Dry Density (lb/ft^3)		LWD (tsf)		GeoGauge (tsf)		DCPI (Base) (inch/blow)		DCPI (Subgrade) (inch/blow)	
	Avg.	Cov.	Avg.	Cov.	Avg.	Cov.	Avg.	Cov.	Avg.	Cov.	Avg.	Cov.
1	8.8	0.03	122.9	0.01	1200.6	0.17	1261.2	0.12	0.5	0.08	5.0	0.03
2	7.6	0.07	122.6	0.01	1306.0	0.14	1325.9	0.16	0.4	0.10	5.6	0.11
3	6.9	0.04	125.5	0.02	1273.7	0.14	1331.1	0.13	0.4	0.10	5.5	0.33
4	8.2	0.06	122.7	0.02	1279.9	0.12	1712.2	0.18	0.2	0.15	3.6	0.37
5	5.0	0.09	123.0	0.01	1299.8	0.20	1784.2	0.13	0.2	0.08	3.2	0.38
6	9.7	0.05	125.6	0.01	786.1	0.14	1320.7	0.22	0.3	0.04	3.8	0.17

Moving Wheel Load Tests on Unpaved Test Sections (Phase 1 Pre-Rut)

Because the primary purpose of the accelerated traffic testing on the unpaved test sections is to pre-rut the aggregate layer and mobilize the geosynthetics, care was exercised to minimize the damage to the structural integrity of the aggregate layer for the subsequent Phase 2 study. At the end of testing, 2,000 wheel passes had been applied to the sections with geosynthetic reinforcement, while only 400 wheel passes had been applied to the two control sections. By using a wireless laser profilometer, the transverse surface profile of the test sections was measured at selected intervals of load repetitions at eight locations along the wheel path. The pavement responses to the moving loads of ALF were recorded. Static measurements were also taken, without the ALF surcharge load, to monitor the accumulation of the permanent deformation of the aggregate layer and the subgrade layer.

Resilient Responses under Moving Traffic Load. The pavement resilient responses to moving traffic load are of great importance because they can be used to calibrate and verify the mechanistic models for ME analysis and design. Figure 21a shows the vertical stresses at the top of subgrade layer in Sections 5 and 6 measured by the pressure cells. Because the aggregate layer of Section 5 is 8 in. (203 mm) thicker than that of Section 6 [18 in. (457 mm) versus 10 in. (254 mm)] (Figure 6b), the peak value of the vertical stresses in Section 5 is considerably less than the peak value in Section 6. In addition, the duration of the stress pulse in Section 5 is greater than that of Section 6, mainly due to a wider stress distribution caused by increased depth.

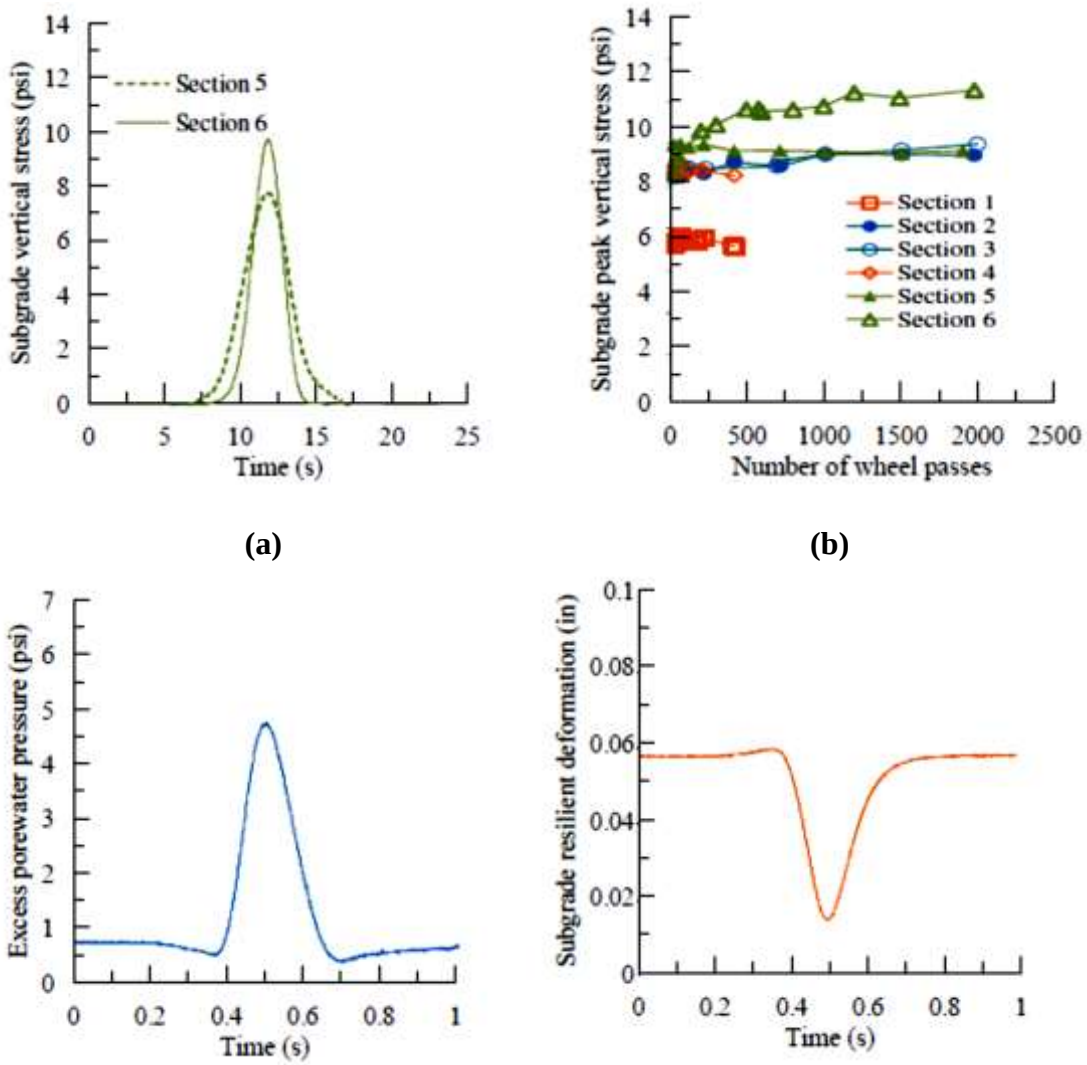

Figure 21
Resilient responses: (a) transient vertical subgrade stress in Section 5 and Section 6 at wheel pass of 1500; (b) peak subgrade vertical stress along with number of wheel passes; (c) subgrade excess pore pressure of section 6; (d) resilient subgrade deformation of Section 6

Figure 21b shows the peak vertical stress at the top of subgrade at different stages of traffic loading for all the test sections. In general, the vertical stresses on top of the subgrade slightly decreased (Sections 1, 4, and 5) or remained a relatively stable state (Sections 2 and 3) throughout the testing with an exception of Section 6. The decrease in vertical stress at the top of subgrade indicates the increase in stiffness of the aggregate layer overlying the subgrade, which is probably due to further compaction of granular aggregates under the repetitive traffic load and/or due to the increase in the modulus of the gravel layer provided by the geosynthetic reinforcement. In contrast, the vertical stress at the top of subgrade in

Section 6 increases; this finding suggests the possibility of degradation in the thinner aggregate layer from moving wheel loading.

As Figure 21b shows, for Sections 2, 3, 4, and 5 with the same aggregate layer thickness, the magnitudes of the peak subgrade stress vary between 55 and 60 kPa. No consistent influence on subgrade vertical stress due to the presence of geosynthetics was noted for any of the test sections, indicating that geosynthetics may have limited contribution to the resilient properties of pavement (during Phase 1 Pre-Rut testing). Section 1 with a sand embankment exhibited a considerably lower subgrade vertical stress, which is likely attributed to the thicker sand layer (Figure 6b).

During repeated traffic loading, possible buildup of excess pore water pressure in the subgrade is of concern as it has a weakening effect on the stiffness and strength of the subgrade caused by the decrease in effective stresses. Figure 21c presents the measurements from the piezometer installed in the subgrade for Section 6. As the figure shows, the excess pore water pressure dissipates completely after the wheel pass, indicating no (or limited) accumulation of excess pore water pressure with moving wheel loading. Figure 21d shows the elastic vertical displacement measured at the top of the subgrade layer in Section 6, which illustrates the resilient deformation behavior of the subgrade soil under the repeated traffic wheel loading.

Permanent Deformation/Surface Rutting for Phase 1. Figure 22a presents the accumulation of the total permanent deformation along with the number of wheel passes for the six test lane sections. The total permanent deformation for each test lane section shown in Figure 22a is the average of the measurements taken at the eight different locations along the wheel path in each section. The control sections, Section 1 and Section 4, exhibited significantly greater total permanent deformation than the reinforced sections under the same number of wheel load passes, indicating the benefits of geosynthetics in reducing permanent deformation in unpaved roads built over soft soil subgrade (i.e., geosynthetics were mobilized).

Compared with the test sections reinforced with the triaxial geogrids (Sections 2 and 3), the test sections with the high-strength geotextile (Sections 5 and 6) showed less permanent deformations. Between Sections 2 and 3, Section 2 reinforced with two layers of geogrids showed less permanent deformation at the end of the testing. Less deformation occurred at the early stage of the traffic in Section 2, a situation that may be the result of early mobilization of the geogrid layer installed at the upper one-third of the aggregate layer in

Section 2. The two control sections, Sections 1 and 4 showed almost similar performance in total permanent deformation.

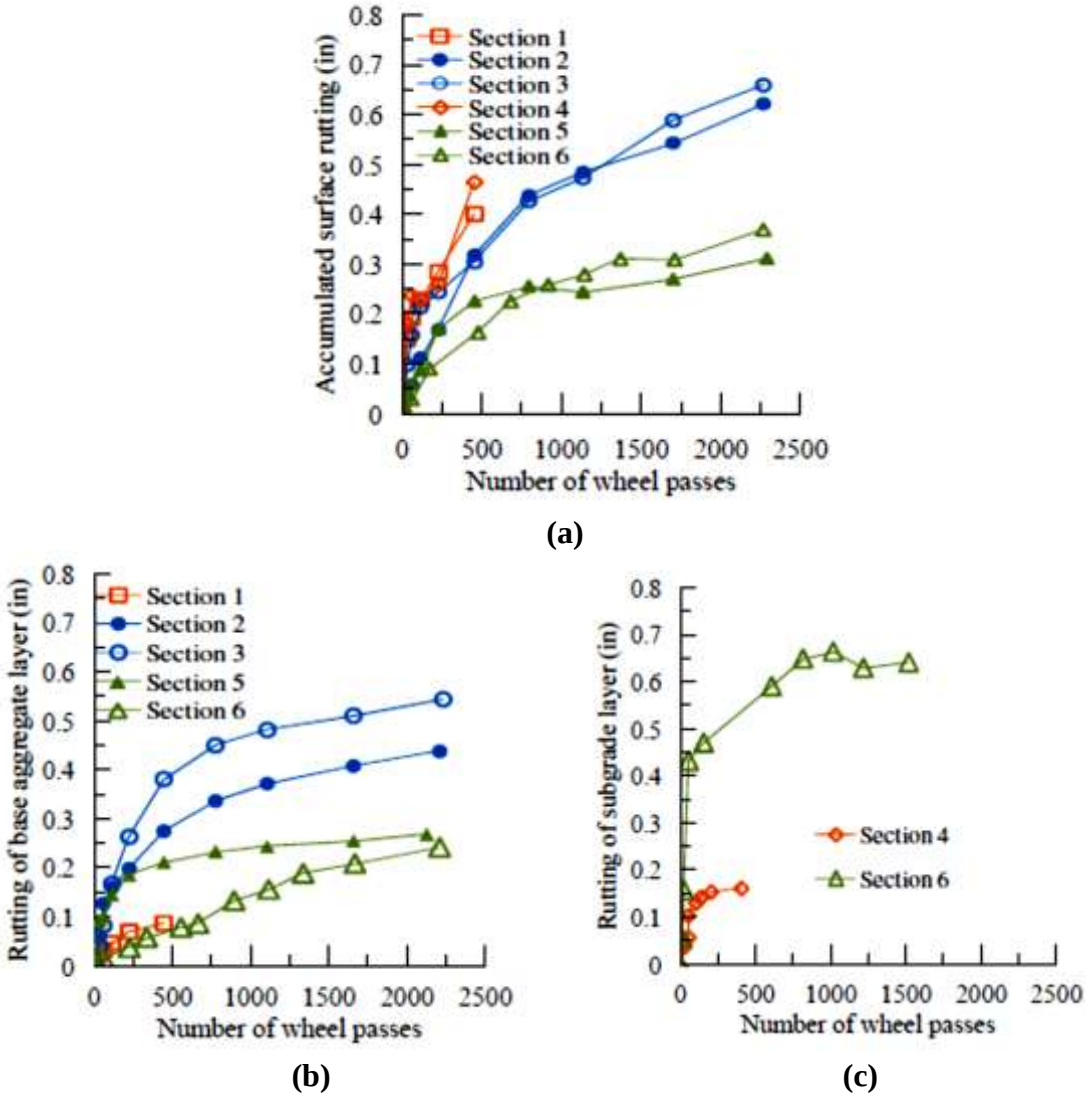

Figure 22
Accumulated permanent deformation: (a) total permanent deformation/surface rutting; (b) in aggregate layer; (c) in subgrade

In addition to the presence of geosynthetics or geosynthetic types, other factors can affect the performance of the test sections in resisting the surface rutting. Although efforts were made to ensure consistent or similar in-situ conditions for all test sections, as noted earlier, the change of the subgrade soil and aggregate layer conditions throughout the testing process may affect the sections' performance. A relatively higher subgrade stiffness of Section 6 may contribute to its superior performance. Variations in construction, such as material placing and degree of compaction, may also affect the section performance. In addition, given the limited number of wheel passes in phase 1 pre-rut testing, the performance of the different

geosynthetics may not be conclusive (i.e., the geosynthetics could be further mobilized and perform differently at a larger number of wheel passes in the subsequent phase 2 accelerated pavement testing).

Permanent Deformation in Aggregate Layer and Subgrade. Two 6-in. long customized potentiometers were installed at mid-height of the aggregate layer for each test section. Measurements from the potentiometer were relative distances between its two end plates. The change of the distance is converted into the compressive strain that was subsequently used to estimate the deformation of the aggregate layer by multiplying by the overall thickness of the aggregate layer. The use of the potentiometer measurements for estimating the aggregate layer deformation is based on the assumption that the compressive strain of the aggregate layer is represented by the mid-height compressive strain. Figure 22 (b) presents the derived permanent deformation of the aggregate layer for each test section except for Section 4 because of potentiometer malfunction.

Compared with Section 3, Section 2, with two layers of geogrids, showed noticeably less aggregate layer deformation. Unlike other test sections, Section 6 showed a nearly linear increase in the permanent deformation of the aggregate layer. Although Section 1 showed a higher total permanent deformation at the same number of wheel passes [Figure 22, (a) and (b)], the deformation in the aggregate layer in Section 1 is relatively smaller, a result indicating that the underlying sand embankment may significantly contribute to the overall permanent deformation in Section 1.

The subgrade was instrumented to measure both the permanent and elastic deformations of the subgrade at select intervals of the ALF traffic passes. As noted earlier, the LVDTs were mounted in a steel rod, which had one end relatively fixed to a great depth of the soil foundation. Therefore, the permanent deformation measured by LVDTs represented the overall deformation of the entire subgrade layer. Some of the LVDTs were damaged due to the construction or moisture intrusion. Figure 22 (c) depicts the accumulation of permanent deformation of the subgrade along with the number of wheel passes for Sections 4 and 6. LVDTs in other test sections were inoperable during the accelerated pavement testing.

As Figure 22c indicates, control Section 4 has a significantly less deformation in the subgrade surface than Section 6, which is reinforced by the high-strength geotextile. The reason for this difference may be that the aggregate layer of Section 4 is 8 in. (203 mm) thicker than that of Section 6, suggesting that the additional 8 in. (203 mm) aggregate layer provides more protection to the subgrade layer than the high-strength geotextile layer does.

The total permanent deformation of the surface (rutting) for each test section, measured by using the laser profilometer at various intervals of traffic load applications, consists of permanent deformations in the aggregate layer and in the subgrade layer. Figure 22 shows that the majority of the total permanent deformation is generally attributed to the permanent deformation in the aggregate layer. The load-induced permanent deformation is usually a result of material densification, shear-related deformation, or a combination of both, which can occur in any layer of the pavement system. The measurements of aggregate layer deformation demonstrate that the aggregate layer makes the greatest relative layer contributions to the total permanent deformation of the test sections.

Strain Developed in Geosynthetics. Foil strain gauges were installed on opposite surfaces at each location to measure tensile strains developed in geosynthetics with repetitions of the traffic load. The measurements from the strain gauges on opposite surfaces were averaged to account for the flexural bending effects. Figure 23 shows the geosynthetic tensile strains measured at the centerline of the test sections. No reliable results from strain measurements were obtained in Section 5 due to the loss of strain gauges.

As Figure 23 indicates, the geosynthetics installed at the subgrade - aggregate layer interface generated a strain around 0.2% at the end of the traffic loading. Between the two layers of geogrids in Section 2, the geogrid installed at the upper one-third of the aggregate layer developed the tensile strains that are more than twice those of the geogrid installed at the subgrade-aggregate layer interface. Overall, Figure 23 demonstrates that the geosynthetics were all mobilized to some extent at the end of the Phase 1 pre-rut accelerated loading.

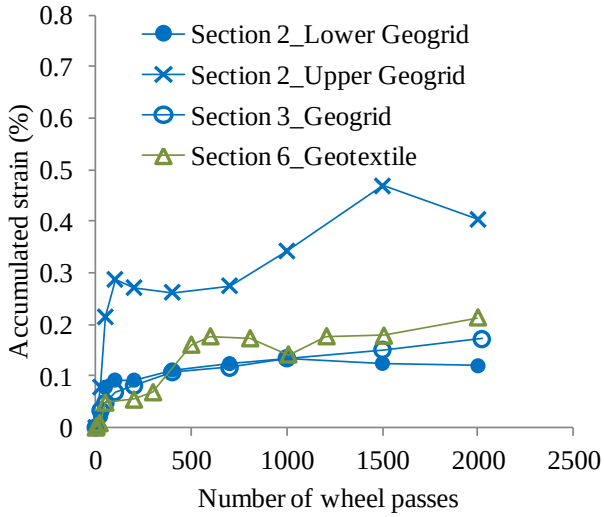

Figure 23
Geosynthetic strains measured at center of test sections

Moving Wheel Load Tests on Paved Test Sections (Phase 2)

As previously mentioned, the test was conducted in two phases for all sections: (1) pre-rut loading phase, prior to construction of HMA layer, and (2) main loading phase, after HMA construction. During the main loading phase, the sections was loaded to 19 mm (¾ in.) rut depth. The starting load was 9,750 lb (43.4 kN). The load was increased to 12,050 lb (53.6 kN) after 110,000 cycles (which is equivalent to 151,510 ESALs according to the fourth power relationship), and then to 14,350 lb (63.8 kN) after 210,000 cycles (which is equivalent to 472,860 ESALs according to the fourth power relationship) or until reaching 0.75 in rut depth. The tire pressure was set to 105 psi (724 kPa).

In-Situ Pavement Layer Properties. The in-situ material properties of base and subgrade were measured prior to the placement of HMA layer with devices such as dynamic cone penetrometer (DCP), and ground penetrating radar (GPR). Each in situ test was conducted at a minimum of five locations along the longitudinal direction for each test section. After the construction of HMA layer, at least five core samples were taken from each section to determine the thickness, air voids, density, and dynamic modulus of HMA. The mean values of the properties, which are related to the AASHTOWare Pavement ME design inputs, are summarized in Table 6 for all pavement test sections. The corresponding coefficient of variation (CV) is also presented in the tables. The resilient moduli of base and subgrade, evaluated using the California bearing ratio CBR-DCPI relationship suggested by Webster et al. and M_r-CBR relationship suggested by Powell et al., are also presented in the table. Here, DCPI is the dynamic cone penetration index defined as penetration/drop *[41, 42]*.

$$\left.\begin{aligned} CBR &= 292/(DCPI)^{1.12} \\ M_r(MPa) &= 17.58 \times CBR^{0.64} \end{aligned}\right\} \overset{yields}{-} M_r(MPa) = 665.06/(DCPI)^{0.7168} \qquad (4)$$

As can be seen from the table, the estimated subgrade resilient moduli range from 183.7 tsf (17.6 MPa) to 211.9 tsf (20.3 MPa); while estimated resilient moduli of base varies from 1169.3 tsf (112.0 MPa) to 1451.2 tsf (139.0 MPa), which are consistent with the results of laboratory resilient modulus tests. The laboratory resilient modulus tests on subgrade soil, compacted at the average in-situ moisture content of 49% and density of 69.5 lb/ft^3, give a resilient modulus of 187.9 tsf (at a confining pressure of 2 psi and a deviator stress of 6 psi); while laboratory resilient modulus tests on base materials, compacted at optimum moisture content and maximum dry density, gives a resilient modulus of 1440.7 tsf (at a confining pressure of 3 psi and a deviator stress of 12 psi).

Table 6
In-situ properties of subgrade, base, and asphalt layer (moving wheel load test)

Test Section		Subgrade		Base			Asphalt			
		DCPI[1] inch/blow	M_r[2] (tsf)	D[3] (inch)	DCPI[1] inch/blow	M_r[2] (tsf)	D[3] (inch)	Density[4] ton/ft^3	Air Voids[4] (%)	E*[5] (tsf)
Section 1	Mean	6.29	183.7	13.8	0.48	1169.3	3.26	0.07	4.8	41,342
	CV(%)	22.2		8.5	9.2		11.1	1.20	19.1	16.5
Section 2	Mean	5.79	194.2	18.8	0.35	1451.2	3.23	0.07	5.75	38,534
	CV(%)	15.8		6.3	10.5		2.2	1.20	20.3	15.8
Section 3	Mean	6.04	189.0	20.7	0.38	1367.6	3.14	0.07	6.53	38,409
	CV(%)	21.3		10.1	9.9		12.0	1.00	16	15
Section 4	Mean	6.09	187.9	18.8	0.38	1367.6	3.10	0.07	6.33	39,296
	CV(%)	16.1		7.9	8.6		6.4	1.60	24.4	16.1
Section 5	Mean	5.43	203.6	21.5	0.36	1440.7	3.30	0.07	4.34	37,939
	CV(%)	14.9		5.8	8.1		3.1	0.70	15.1	14.6
Section 6	Mean	5.13	211.9	10.9	0.40	1325.9	3.35	0.07	6.23	33,617
	CV(%)	21.7		7.2	12.3		8.5	1.90	27.9	9

[1]Dynamic cone penetrometer index; [2]Resilient modulus estimated from DCPI; [3]*D* is the thickness; [4]Determined from the core samples taken from each test lane; [5]Dynamic complex modulus at a temperature of 30^{o}C and a loading frequency of 10 Hz.

Mechanical Response of Pavement Sections. As mentioned earlier, a variety of sensors were installed to measure the load associated pavement responses and performance. Figure 24 (a) shows the dynamic response of the pressure cells installed near the top of subgrade for one wheel pass at the 10,000-pass level.

Figure 24 (b) shows the dynamic vertical stresses versus number of wheel passes for all the test sections. In general, the vertical stresses on top of the subgrade remained a relatively stable state throughout the testing. As expected, Section 6 registered the highest pressure due to shallow depth of subgrade layer while Section 1 registered lowest pressure due to deeper subgrade layer, compared to the other sections. The difference in magnitudes of the peak subgrade stress between unreinforced (Section 4) and reinforced (Sections 2, 3, and 5) sections is not significant when the applied load is 9,750 lb (43.4 kN), With the increase of

load, however, the benefit of geosynthetics on the reduction of maximum stress on top of subgrade becomes more distinguishable.

Figure 24 (c) presents the dynamic response of customized LVDTs, which illustrates the resilient deformation behavior of the subgrade soil under the moving wheel load. As can be seen from the figure, the difference in magnitudes of the resilient subgrade deformation between unreinforced (Section 4) and reinforced (Sections 2 and 3) sections is not significant, indicating that geosynthetics may have limited contribution to the resilient properties of subgrade.

Figure 24 (d) shows the dynamic response of customized potentiometers, which illustrates the resilient deformation behavior of the base layer under the moving wheel load. The benefit of geosynthetics on the resilient properties of base layer is clearly demonstrated in the figure, with the least base resilient deformation recorded in the section with double layer geosynthetic reinforcement (Section 2). The pavement dynamic responses observed in this study provided very valuable information, which can be used to calibrate and verify the mechanistic models in Pavement ME design low and medium volume roads.

Measured Permanent Deformation Behavior of Pavement Sections. Figure 25 presents the accumulation of the total permanent surface deformation along with the number of EASLs for the six test lane sections. The total permanent deformation for each test lane section shown in Figure 25 is the average of the measurements taken at the six different locations along the wheel path in each section. The results show that sections constructed with geosynthetics experienced less rut depth than the control section. As compared to the single layer geogrid reinforcement section, more reduction in the pavement surface deformation was observed for the double layer geogrid reinforcement (Section 2) and the woven geotextile reinforcement (Section 5).

Noticeably, there was a drastic increase in surface rutting after 1,119,165 ESALs for section 2 and 796,012 ESALs for section 3. This sudden increase in surface rutting is believed to be related to the heavy intense of rainfall rate that occurred during the period and the designed drainage system could not handle that amount of rain. The DCP data showed that the bottom one-third of base material was significantly weakened, with DCPI increased from around 10 mm/blow to around 70 mm/blow. This clearly demonstrates the significant importance of

drainage in the performance of pavement structure, both reinforced and unreinforced sections. The AASHTOWare Pavement ME was utilized by the authors to simulate the weakening effect of the bottom of base layer by dividing the base layer of sections 2 and 3 into two layers (upper strong base and bottom weak base). The permanent deformations were then adjusted by assuming the bottom weak base having the same property as the upper strong base. The adjusted permanent deformation curves were also presented in Figure 25. The traffic benefit ratio (TBR) was used to evaluate the benefit of geosynthetic reinforcement on the performance of pavement test sections. The results obtained for the different control and reinforced pavement test sections are summarized in Table 7.

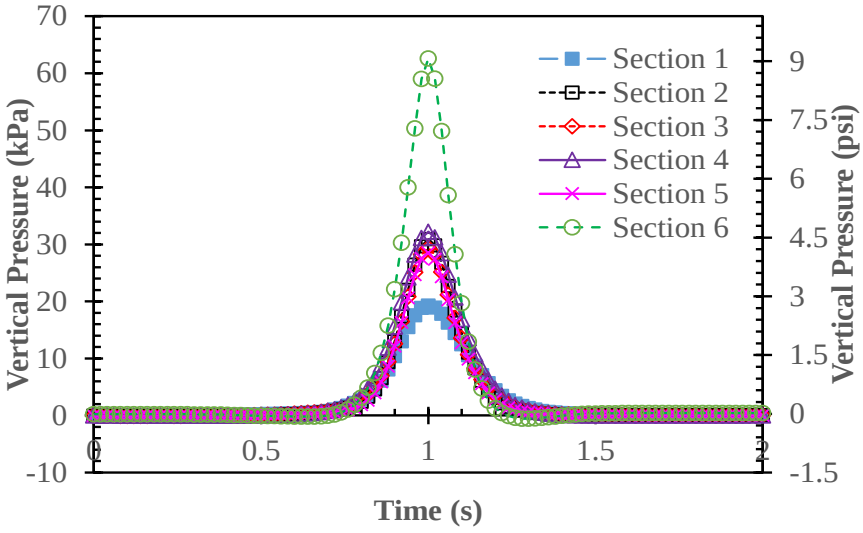

(a)

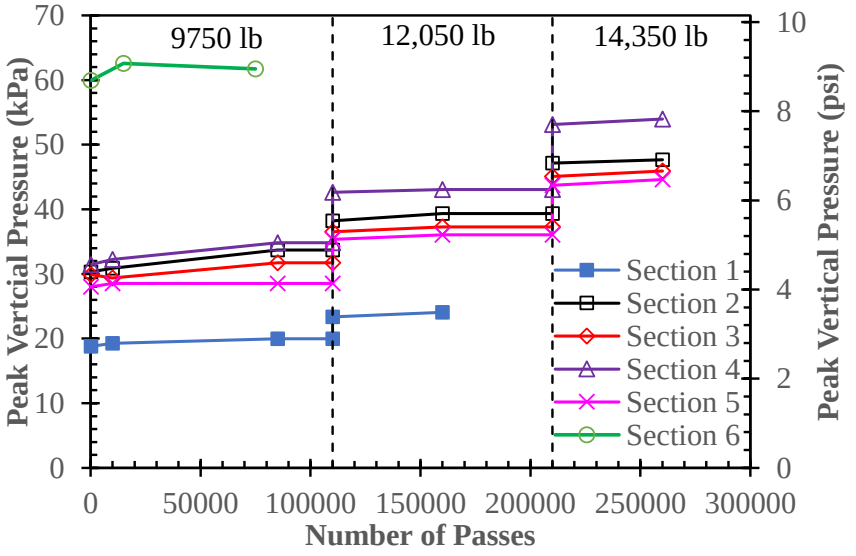

(b)

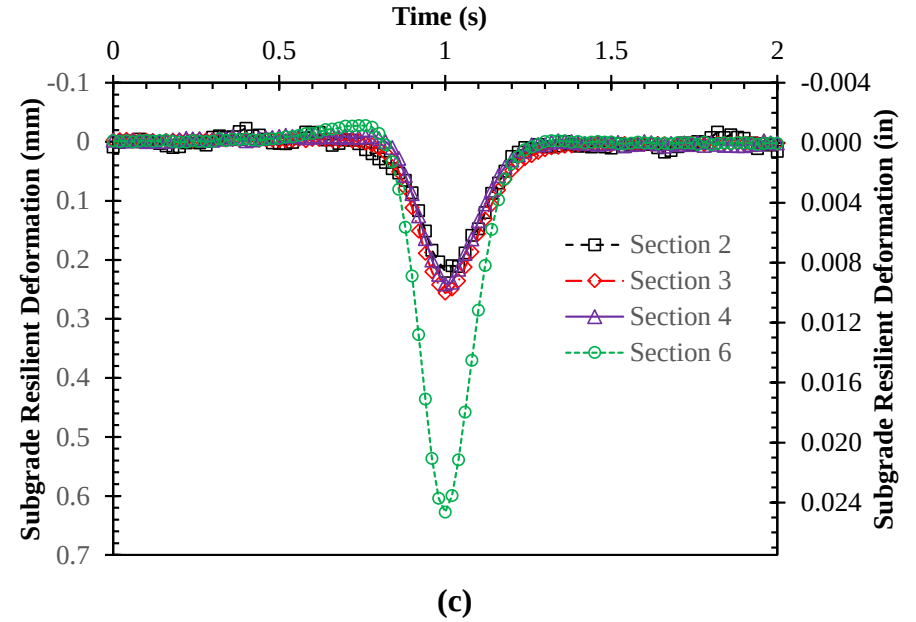

(c)

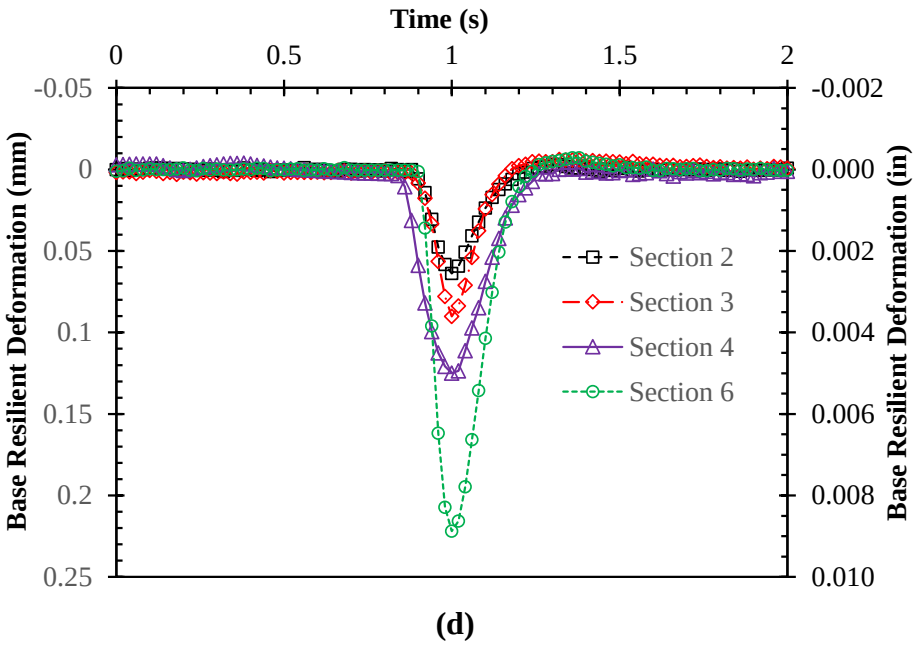

(d)

Figure 24
Mechanical responses: (a) transient vertical subgrade stress at wheel pass of 10,000; (b) peak subgrade vertical stress along with number of wheel passes; (c) resilient subgrade deformation at wheel pass of 10,000; (d) resilient strain in base at wheel pass of 10,000

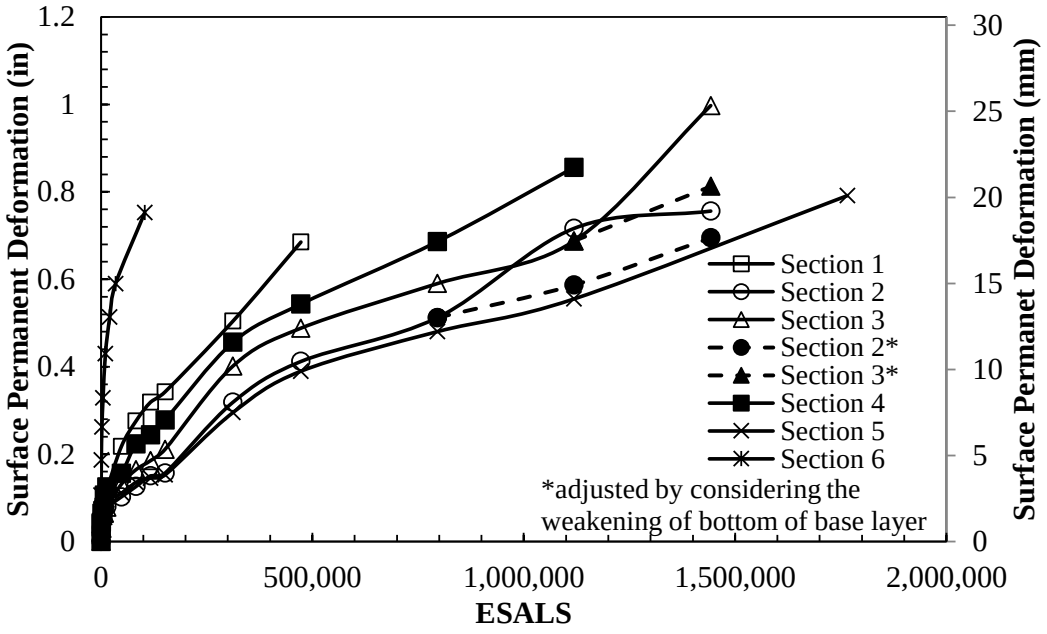

Figure 25
Accumulated total permanent surface deformation

Table 7
Summary of moving wheel load tests at ALF

Test Section	Rut depth = 0.5 in		Rut depth = 0.75 in	
	ESALs	TBR*	ESALs	TBR*
Section 1	307,808	-	-	-
Section 2	756,315	1.92	1,393,729	1.52
Section 3	510,260	1.30	1,184,287	1.29
Section 4	393,246	1	917,500	1
Section 5	881,051	2.24	1,652,365	1.80
Section 6	19,009	-	102,356	-

*TBR values before adjustment for variations in test sections

It should be noted here that the TRB values calculated in Table 7 for the reinforced sections are based on comparison with the results of control section 4 with a nonwoven geotextile separator assuming it has a TRB of 1. It is expected that the TBR values would be higher if the results of reinforced sections were compared with a control section without a geotextile separator.

Effect of Variations in Pavement Layer Properties on Surface Permanent Deformation. As with any other construction, there are always some variations in the constructed layer thicknesses and properties of the pavement test lane sections (Table 6). The change of the pavement conditions throughout the testing process also affects the sections' performance since each pavement section was loaded at different time periods. To evaluate the effect all these factors on the performance of pavement test sections, the measured TBR is simply broken down into two components: one associated with property variation of payer layer materials and the other associated with geosynthetic reinforcement, i.e.,

$$TBR = VF \times TBR_{adj} \quad (5)$$

where, *TBR* is the measured traffic benefit ratio; *VF* is the factor associated with property variation of pavement layer materials/thicknesses due to construction and seasonal change; TBR_{adj} is the traffic benefit ratio associated with geosynthetic reinforcement. A relatively simple analysis, using AASHTOWare Pavement ME Design software, was then performed to quantify the impact of variation in pavement layer properties, introduced by construction and seasonal change, on the performance of pavement test sections (i.e., *VF*) *[43]*.

The traffic load was applied using dual wheels through special axle configuration available in Pavement-ME software. The center-to-center distance of two wheels is 15 in. (380 mm). The load is 9,000 lbf (40 kN) with a tire pressure of 105 psi (724 kPa). Since each test section was loaded alternately and also due to a couple of breakdowns of ALF testing facility during testing, no test section was continuously loaded. As such, the individual climate file was generated for each test section by the authors to simulate the environmental conditions of that test section during testing.

The TDR measurement indicates that the subgrade stayed nearly saturated over the testing period. This is expected when considering the high ground water table at the testing site. As such, the subgrade resilient modulus of each test section was kept constant through the testing period and the corresponding value is presented in Table 6.

Meanwhile, the TDR measurement shows that the moisture content of base layer kept changing during the test period. To consider this seasonal variation effect, the resilient moduli of the base layer were evaluated using the prediction model adopted in AASHTOWare Pavement ME and are plotted in Figure 26.

$$log\left(\frac{M_R}{M_{Ropt}}\right) = a + \frac{b-a}{1+EXP\left(\beta+k_s\left(S-S_{opt}\right)\right)} \quad (6)$$

Where, M_R is the resilient modulus at degree of saturation of S, M_{Ropt} is the resilient modulus at maximum dry density and optimum moisture content; S is the degree of saturation, (%); S_{opt} is the degree saturation at maximum dry density and optimum moisture content, (%); a, b, β, and k_s are model coefficients, (a=-0.3123, b=0.3, β = -0.0401, and k_s = 6.8157 for coarse grained soil).

It should be pointed out here that in the Pavement ME analysis of this study, the number of ESALs experienced by each pavement test section is evenly distributed into twelve months as an input to the designed monthly traffic repetitions. As such the month shown in Figure 26 does not represent the real month, e.g., 10th month does not mean October. But instead means the number of months that the pavement test section has been loaded in the Pavement ME analysis. In other words, the same month in Figure 26 may represent different time periods for each pavement test section.

By considering the measured/estimated in-situ pavement layer's thickness and properties (Table 6 and Figure 26), the number of ESALs needed to reach 0.5 in. and 0.75 in. rut depth was calculated for each test section to quantify the effect of construction and seasonal variations on the test results. For the reinforced test sections, the comparison was made with respect to its corresponding unreinforced condition, i.e., the same pavement structure and layer properties but without geosynthetic reinforcement. The results of the analyses are presented in

Table 8. The *VF* is evaluated here as the number of ESALs at a specific rut depth (i.e., 0.5 in. and 0.75 in.) carried by the corresponding unreinforced condition of the reinforced test section divided by that of the control test section. By dividing the measured *TBR* values by the *VF* factors, the *TBR* associated with geosynthetic reinforcement (TBR_{adj}) was obtained for each reinforced test section and is also presented in

Table 8. It should be pointed out here that the TBR_{adj} values can be affected by the accuracy of modulus test results for HMA, the variation in DCP test profiles for subgrade layer, accuracy in measuring thicknesses of HMA and base layer, and reliability of the correlation equations used.

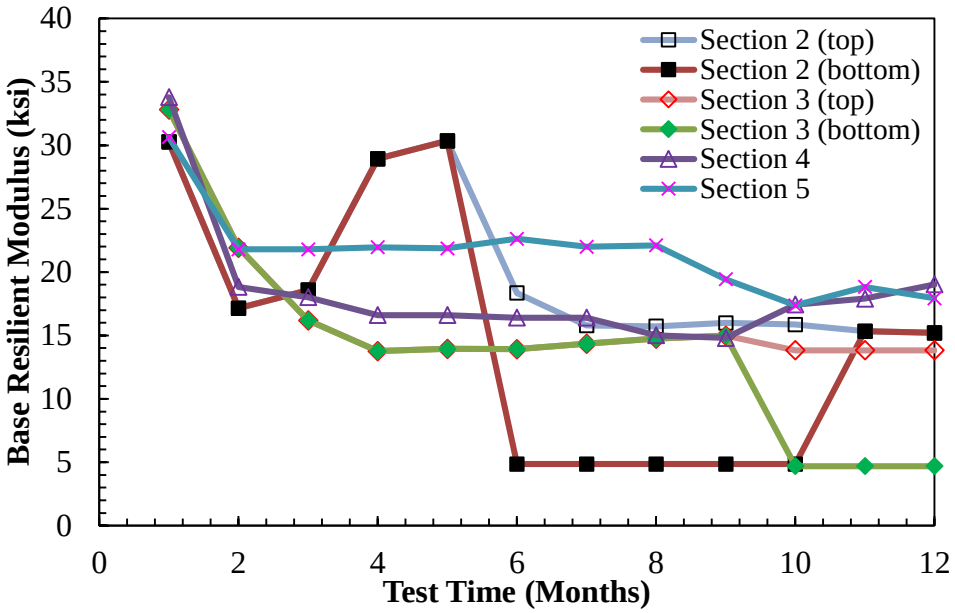

Figure 26

Variation of base resilient modulus

Table 8
Effect of differences in constructed pavement layer properties (moving ALF test)

Test Sections	Rut depth = 0.5 in			Rut depth = 0.75 in		
	ESALs	VF	TBR_{adj}[#]	ESALs	VF	TBR_{adj}[#]
Section 2	349,311	0.88	2.18	720,349	0.77	1.96
Section 3	308,611	0.78	1.67	922,497	0.99	1.30
Section 4	396,239	-	1	931,146	-	1
Section 5	573,445	1.45	1.55	1,269,623	1.36	1.32

[#]TBR_{adj} = TBR/VF

Permanent Deformation in Subgrade and Base. As previously mentioned, a customized potentiometer was installed at the mid-height of base layer to estimate the deformation of the base layer, and a customized LVDT was used to estimate the deformation of the subgrade layer. Figure 27 (a) and 27 (b) illustrate the development of subgrade and base permanent deformation with number of EASLs for Sections 2, 3, 4 and 6 (data is missing for Section 5). It is interesting to note that the permanent deformation of base layer, estimated from the potentiometer measurement, didn't show the heavy rainfall induced weakening effect of the bottom of base layer in Sections 2 and 3. This may be because the potentiometers were installed above the weakened bottom base layer. As can be seen from the figures, for the control section (Section 4), the base layer makes more significant contribution to the total permanent deformation, when compared to the subgrade layer. The use of geogrids in Sections 2 and 3 resulted in reducing the permanent deformations in both the base and subgrade layers. Similar behavior is also expected for Section 5 with high strength geotextile reinforcement. Compared with Section 3, Section 2 with two layers of geogrids, showed similar reduction of permanent deformation in subgrade layer but noticeably less aggregate layer deformation. This suggests that while the performance of base and subgrade was improved by the geogrid at the base-subgrade interface, the performance of base layer was further enhanced by the geogrid placed at the upper one-third of the base layer. While geosynthetics showed appreciable benefits in reducing the permanent deformation of subgrade here, the geosynthetics, as previously indicated, have little effect on the resilient properties of subgrade. As such, the benefits of geosynthetics on subgrade performance should be considered in permanent deformation properties part within the framework of Mechanistic Empirical Pavement Design Guide (MEPDG); i.e., the model for predicting permanent deformation in the subgrade.

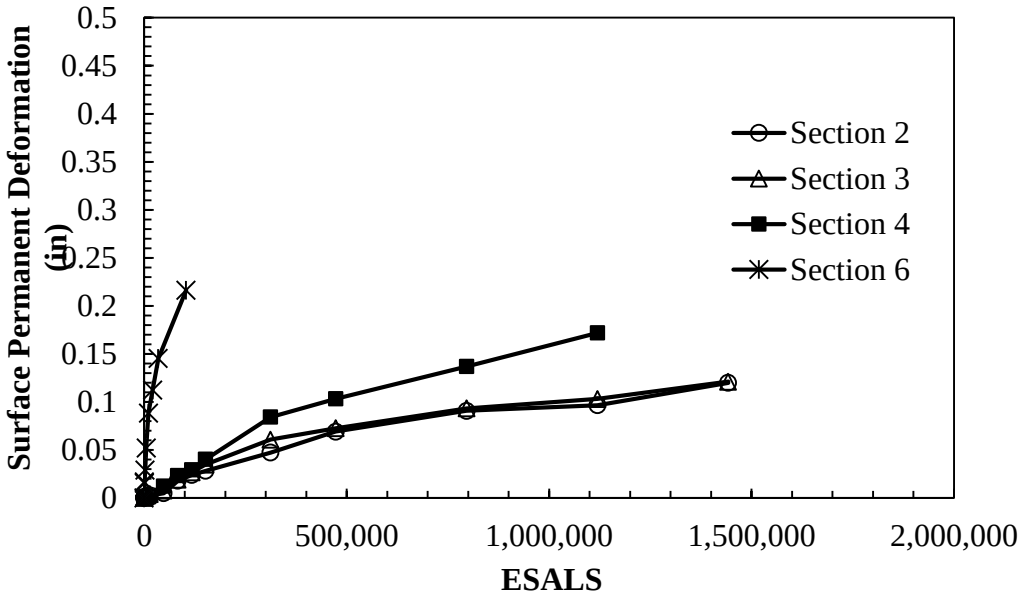

(a) Subgrade

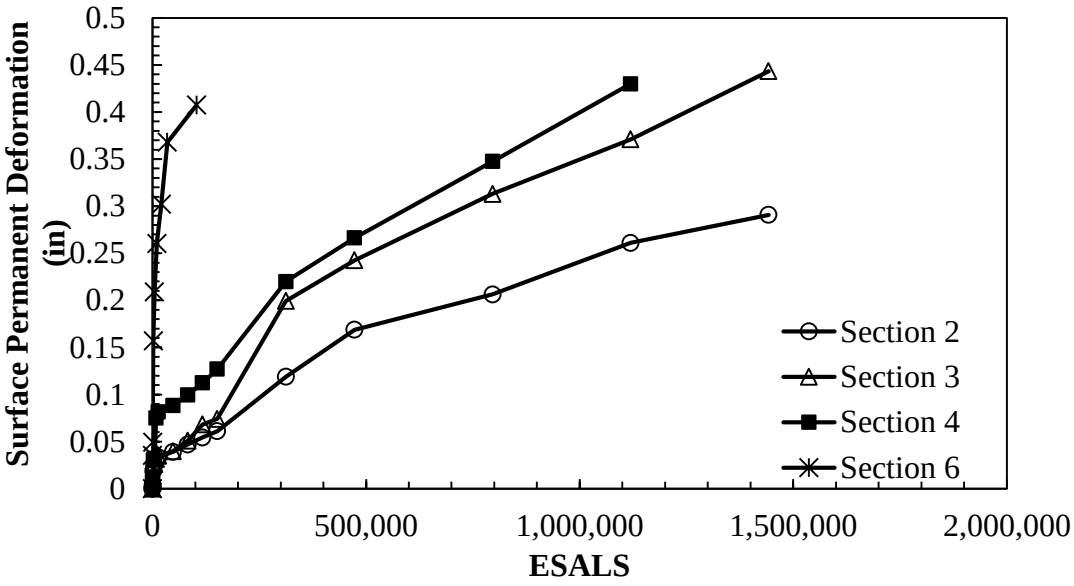

(b) Base

Figure 27

Accumulated permanent deformation in subgrade and base layer

Cyclic Plate Load Tests on Paved Test Sections (Phase 3)

In addition to the six field pavement sections shown in Figure 6 (b), another small-scale test section (Section 7) with dimensions 12 ft. x 12 ft. was constructed as a control section of Section 6 for cyclic plate load tests on the field pavement test sections.

In-Situ Pavement Layer Properties

The in-situ material properties of base and subgrade were measured prior to the cyclic plate testing of each section with dynamic cone penetrometer (DCP). Three DCP test were conducted around the cyclic plate test location for each test section. A core sample was taken from each section to determine the thickness, air voids, density, and dynamic modulus of HMA. The values of the properties, which are related to the AASHTOWare Pavement ME design inputs, are summarized in Table 9 for all pavement test sections. The resilient moduli of base and subgrade, evaluated using equation (4), are also presented in the table.

Table 9

In-situ properties of subgrade, base, and asphalt layer (cyclic plate load tests at ALF)

Test Section		Subgrade		Base			Asphalt			
		DCPI[1] in/blow	M_r[2] (tsf)	D[3] (in)	DCPI[1] in/blow	M_r[2] (tsf)	D[3] (in)	Density[4] (pcf)	Air Voids[4] (%)	E*[5] (ksi)
Section 1	Mean	7.3	164.3	10.3	0.37	1393.5	3.45	149.9	3.7	555.7
	CV(%)	28		6.5	11		-	-	-	-
Section 2	Mean	7.2	166.0	18.95	0.31	1581.9	3.21	146.67	5.75	461.2
	CV(%)	15		7.2	10		-	-	-	-
Section 3	Mean	6.61	176.5	19.4	0.24	1900.4	2.82	145.47	6.53	452.8
	CV(%)	17		5.9	17		-	-	-	-
Section 4	Mean	6.5	178.6	19.3	0.24	1900.4	3.01	145.77	6.33	461.7
	CV(%)	10		7.7	13		-	-	-	-
Section 5	Mean	7.03	168.8	20.7	0.27	1746.5	3.25	148.90	4.34	445.8
	CV(%)	7		6.8	21		-	-	-	-
Section 6	Mean	5.74	195.3	10.5	0.28	1701.6	3.23	145.90	6.23	475.2
	CV(%)	35		7.1	24		-	-	-	-
Section 7	Mean	5.51	201.1	11.0	0.31	1581.9	3.30	145.90	6.23	475.2
	CV(%)	25	-	7.2	24	-	-	-	-	-

[1]Dynamic cone penetrometer index; [2]Resilient modulus estimated from DCPI; [3]*D* is the thickness; [4]Determined from the core samples taken from each test lane; [5]Dynamic complex modulus at a temperature of 30^{o}C and a loading frequency of 10 Hz.

Measured Permanent Deformation Behavior of Pavement Sections. Figure 28 illustrates the development of rut depth (permanent deformation) with number of ESALs for the seven pavement test sections. The results obtained for the different control and reinforced pavement test sections are also summarized in Table 10. The surface permanent deformation

was calculated by averaging the readings of two LVDTs rest on top of the loading plate. The results show that the surface permanent deformation accumulated with the number of EASLs; sections constructed with geosynthetics experienced less rut depth as compared to the control section; and more reduction in the pavement surface deformation was observed for the double layer reinforcement section (Section 2). Sections 2, 3 and 5 can sustain 2,212,143, 1,577,043, and 1,784,762 ESALs at a rut depth of 0.75 in. (19.1 mm), which result on traffic benefit ratios (TBR) of 1.81, 1.29, and 1.46 (Table 10), respectively. Meanwhile, Section 6 can sustain 92,971 ESALs at a rut depth of 0.75 in., which result on TBR of 2.42.

The increased TBR for Section 6 compared to the other reinforced sections mainly attributed to the decreased base course thickness. The corresponding TBR values for Sections 2, 3, 5 and 6 at 0.5 in. rut depth are 2.08, 1.40, 1.70, and 2.41, respectively.

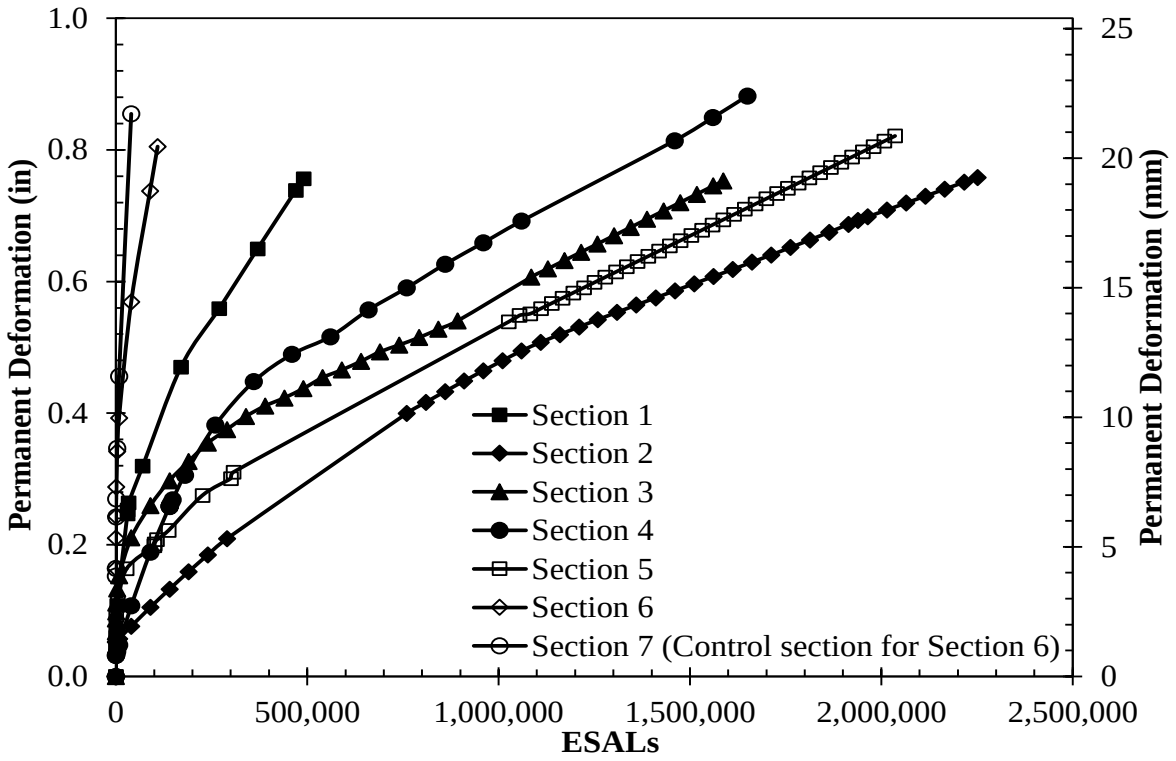

Figure 28
Accumulated total permanent deformation

Table 10
Summary of cyclic plate load tests on field pavement test sections

Reinforcement configuration	HMA Thickness (in)	Base Thickness (in)	Base Modulus (tsf)	Subgrade Modulus (tsf)	Rut depth = 0.5 in		Rut depth = 0.75 in	
					ESALs	TBR	ESALs	TBR
Section 1	3.45[&]	10.3	1379.7	164.6	-	-	-	-
Section 2	3.21[&]	18.95[&]	1562.0[#]	166.4[#]	1,077,865	2.08	2,212,143	1.81
Section 3	2.82[&]	19.4[&]	1890.6[#]	176.6[#]	723,723	1.40	1,577,043	1.29
Section 4	3.01[&]	19.3[&]	1875.3[#]	178.6[#]	518,653	1	1,225,115	1
Section 5	3.25[&]	20.69[&]	1742.9[#]	168.8[#]	881,797	1.70	1,784,762	1.46
Section 6	3.13[&]	10.5[&]	1596.3[#]	201.1[#]	25,110	2.41	92,971	2.42
Section 7	3.30[&]	11[&]	1690.5[#]	195.6[#]	10,416	-	38,357	-

[&] Measured actual thickness; [#]From DCP

Effect of Variations in Pavement Layer Properties on Surface Permanent Deformation

A relatively simple analysis, using AASHTOWare Pavement ME Design software (43), was again performed to quantify the impact of variation in pavement layer properties on the performance of pavement test sections (i.e., *VF*).

The traffic load was applied using single wheel through special axle configuration available in Pavement-ME software. The load is 9,000 lbf (40 kN) with a tire pressure of 105 psi (724 kPa). Since each test section was loaded in very short time, the base and subgrade resilient modulus of each test section was assumed to be constant through the testing period and the corresponding value is presented in Table 10.

By considering the measured/estimated in-situ pavement layer's thickness and properties (Table 9), the number of ESALs needed to reach 0.5 in. and 0.75 in. rut depth was calculated for each test section to quantify the effect of construction and seasonal variations on the test results. The results of the analyses are presented in Table 11. The *TBR* associated with geosynthetic reinforcement (TBR_{adj}) was obtained for each reinforced test section and is also presented in Table 11.

Table 11
Effect of differences in constructed layer properties and thickness (cyclic plate load tests at ALF)

Test Sections	Rut depth = 0.5 in			Rut depth = 0.75 in		
	ESALs	VF	TBR_{adj}[#]	ESALs	VF	TBR_{adj}[#]
Section 2	820,744	0.83	2.52	3,589,584	0.85	2.12
Section 3	546,692	0.86	1.62	2,586,811	0.86	1.51
Section 4	392,400	-	-	1,992,000	-	1
Section 5	666,884	1.03	1.65	2,905,531	1.02	1.43
Section 6	71,817	1.15	2.09	495,178	1.19	2.09
Section 7	29,880	-	-	150,840	-	-

[#]TBR_{adj} = TBR/VF

Large-Scale In-box Laboratory Pavement Test Sections

As-Constructed Pavement Layer Properties

As with any other construction, there are always some variances in the constructed layer thicknesses and properties of the test sections in the box.

Table 12 presents the average value of the measured subgrade and base properties. Table 13 shows the results of in-situ tests conducted on the AC layer.

In-box Cyclic Plate Load Tests

A total of six tests were conducted on different pavement sections, as shown in Figure 6b. The traffic benefit ratio (TBR) was used to evaluate the benefit of geosynthetic reinforcement. TBR is defined as the number of ESALs carried by a reinforced section at a specific rut depth divided by that of an equivalent control section. The results obtained for the different control and reinforced pavement test sections are summarized in Table 14.

Table 12

In-place properties of subgrade and Base (In-box Test)

Test Section		Subgrade						Base				
		MC[1] (%)	DD[2] (lb/ft^3)	Shear Strength[3] (tsf)		E_{GG}[4] (tsf)	DCPI inch/blow	MC[1] (%)	DD[2] (ton/ft^3)	E_{LFWD}[5] (tsf)	E_{GG}[4] (tsf)	DCPI inch/blow
				12 inch	24 inch							
Section 1	Mean	48.42	68.5	0.57	0.76	224.878	5.91	7.30	124.1	1269.8	1200.50	0.22
	CV(%)	1.44	2.12	7.32	4.23	3.410	6.01	2.61	2.34	19.2	13.36	8.52
Section 2	Mean	48.14	68.2	0.58	0.76	224.147	5.75	7.83	121.0	1173.8	1387.68	0.20
	CV(%)	1.52	3.12	6.24	3.27	31.710	5.48	11.14	2.36	38.9	11.19	11.56
Section 3	Mean	48.22	69.4	0.56	0.75	244.400	6.22	6.90	120.9	1260.1	1357.20	0.21
	CV(%)	1.96	1.02	6.97	2.97	3.120	5.48	3.26	2.98	1.0	4.94	9.02
Section 4	Mean	48.66	68.3	0.56	0.75	237.614	5.98	7.10	122.8	1107.2	1413.47	0.21
	CV(%)	2.12	1.98	5.12	2.96	6.170	6.99	14.26	3.50	12.3	1.93	8.24
Section 5	Mean	48.9	69.0	0.57	0.77	232.290	6.14	7.94	122.1	1189.4	1356.47	0.20
	CV(%)	3.90	1.29	6.99	3.99	0.95	6.97	2.98	3.02	7.10	8.71	11.10
Section 6	Mean	48.52	69.5	0.52	0.72	231.83	6.10	7.52	122.1	1041.81	1254.29	0.22
	CV(%)	1.42	2.98	2.69	2.01	0.97	5.95	6.10	2.01	1.00	8.15	5.94

[1]Moisture content; [2]Dry density; [3]In-situ vane shear test, conducted at two different depths (304.8 mm and 609.6 mm); [4]$E_{GG}=P(1-\nu^2)/1.77R.\delta$, P= the applied force, ν=Poisson's ratio, R=outside radius of the Geogauge ring foot, δ=the displacement; [5]$E_{LFWD}=P(1-\nu^2)\sigma.R/\delta_c$, σ=the applied stress, R=the loading plate radius of LFWD, δ_c=center deflection of the loading plate.

Table 13

In-place properties of HMA (In-box Test)

Test Section		HMA						
		Before test				After test		
		E_{LFWD}[1] tsf	Air Voids[2] (%)	Density[2] lb/ft^3	Shear Modulus[3] tsf	Air Voids[4] (%)	Density[4] lb/ft^3	E*[5] tsf
Section 1	Mean	2363.6	7.3	135.3	172845.1	6.7	145.1	23696.2
	CV(%)	8.3	30.2	3.24	19.6	19.3	1.02	10.3
Section 2	Mean	2467.6	8.3	134.9	211867.9	7.1	144.7	26445.8
	CV(%)	9.0	1.9	1.89	17.6	9.9	0.99	17.9
Section 3	Mean	2499.8	6.9	135.5	195519.2	6.6	145.4	24731.4
	CV(%)	13.5	15.2	3.64	17.1	15.9	1.50	13.2
Section 4	Mean	3013.2	7.2	138.6	245096.2	6.2	146.0	26550.4
	CV(%)	13.0	19.9	4.83	10.2	6.8	1.50	16.2
Section 5	Mean	2914.4	6.6	142.3	231185.9	6.6	146.0	24829.0
	CV(%)	20.8	11.7	3.01	11.2	15.2	1.02	17.6
Section 6	Mean	2302.0	7.2	136.9	191758.2	6.9	144.8	27867.3
	CV(%)	16.3	15.2	2.98	16.0	7.0	1.50	12.0

[1] $E_{LFWD}=P(1-\nu^2)\sigma.R/\delta_c$, σ=the applied stress, R=the loading plate radius of LFWD, δ_c=center deflection of the loading plate; [2] Determined from the core samples taken after test; [3] Measured by Pavement Quality Indicator; [4] Measured from core samples; [5] Dynamic complex modulus.

Table 14

Summary of in-box cyclic plate load tests

Test Sections	Base Thickness (mm)	HMA Thickness (mm)	Rut depth = 0.5 in		Rut depth = 0.75 in		Rut depth = 1 in	
			ESALs	TBR	ESALs	TBR	ESALs	TBR
Section 1	451.8	74.1	147290	-	526704	-	1183043	-
Section 2	454.6	76.0	3167943	4.73	-	-	-	-
Section 3	452.1	75.2	822955	1.23	1921712	1.51	3367399	2.19
Section 4	459.7	73.6	669960	-	1270908	-	1537749	-
Section 5	447	74.9	800341	1.19	2073279	1.63	3439960	2.24
Section 6	256.5	69.9	20822	-	90483	-	240542	-

Effect of Variances in Constructed Layer Thickness and Properties

In order to quantify the uncertainty introduced by the differences in the constructed test sections, a relatively simple analysis, using AASHTOWare Pavement ME Design software, was performed to assess the impact of variation in layer properties and thicknesses, and thereby provide insight into the significance of the observed TBR values *[43]*. The traffic load was applied using a single tire through special axle configuration available in Pavement-ME software. The load is 9000 lbf (40 kN) with a tire pressure of 80 psi (550 kPa), which results in a circular loading area of radius 6 in. (152 mm). This load magnitude is consistent with that in cyclic plate load tests. The self-defined climate file, which includes temperature, precipitation, wind speed, percent sunshine, and hourly ground water depth, was used to simulate the environmental condition of the laboratory cyclic plate load tests. The resilient moduli (M_r) for the base and subgrade layer were evaluated using the California bearing ratio CBR-DCPI relationship suggested by Webster et al. and M_r-CBR relationship suggested by Powell et al., i.e., equation (4) *[41, 42]*.

The number of ESALs needed to reach 0.5 in. (12.5 mm), 0.75 in. (19.1 mm), and 1 in. (25.4 mm) rut depth was calculated for each test section taking into consideration the measured layer's thickness and properties (Tables 13 and 14) to quantify the effect of construction variations on the analysis of test results. For the reinforced test sections, the comparison was made with respect to its corresponding unreinforced condition, i.e., without geosynthetic reinforcement. The results of the analyses are presented in Table 15. In the table, the variation factor (VF) was introduced to evaluate the effect of differences in constructed layer thickness and properties on the calculated TBR values. The VF is defined here as the number of ESALs at a specific rut depth (i.e., 0.5 in., 0.75 in., and 1 in.) carried by the corresponding unreinforced condition of the reinforced test section divided by that of the control test section. By dividing the TBR values by the VF factors, the adjusted TBR (TBR_{adj}) was obtained for each reinforced test section and are presented in Table 15. It should be pointed out here that the estimated TBR_{adj} values can be affected by the accuracy of modulus test results for HMA, the variation in DCP test profiles for base layer, accuracy in measuring thicknesses of HMA and base layer, and reliability of the correlation equations used.

Table 15
Effect of differences in constructed layer properties and thickness

Test Sections	Rut depth = 0.5 in.			Rut depth = 0.75 in.			Rut depth = 1 in.		
	ESALs	VF	TBR_{adj}[#]	ESALs	VF	TBR_{adj}[#]	ESALs	VF	TBR_{adj}[#]
Section 2	39480	1.15	4.11	232800	1.12	-	734400	1.09	-
Section 3	35520	1.03	1.19	211752	1.02	1.48	681600	1.02	2.16
Section 4	34320	-	-	207600	-	-	670800	-	-
Section 5	37200	1.08	1.10	222144	1.07	1.52	710400	1.06	2.11

[#]TBR_{adj} = TBR/VF

Pavement Surface Deformation of In-box Tests

Figure 29 illustrates the development of rut depth (permanent deformation) with number of ESALs for the six pavement test sections. The surface permanent deformation was calculated by averaging the readings of two LVDTs rest on top of the loading plate. The results show that the surface permanent deformation accumulated with the number of EASLs; sections constructed with geosynthetics experienced less rut depth as compared to the control section; and more reduction in the pavement surface deformation was observed for the double layer reinforcement section (Section 2). Sections 3 and 5 can sustain 3,367,399 and 3,439,960 ESALs at a rut depth of 1 in., which result on adjusted traffic benefit ratios (TBR) [the adjusted traffic benefit ratio (TBR_{adj})] of 2.19 (2.16) and 2.24 (2.11) (Tables 14 and 15), respectively. Section 2, with double reinforced layers, never reached the 1 in. rut depth during the test and the rut depth of 0.5 in. was obtained at 3,167,943 ESALs. The performance of Section 1 was much lower than Section 4, which indicates that the 8 in. thick Mexican limestone is more effective than the 12-in. thick nonwoven geotextile-wrapped sand embankment in reducing the pavement rutting. Section 6 showed the lowest performance among the six test sections mainly due to its much thinner base layer (10 in. vs. 18 in.).

The profiles of surface deformation were measured using eight LVDTs, as shown in Figure 19. Figure 30 clearly demonstrates that the reinforced sections exhibited a lower level of surface deformation than the control section. The figure also shows that a small amount of tilt occurred in the loading plate. This may be due to variations in the loading apparatus and/or local variations in the properties of the HMA, base course, or subgrade (1).

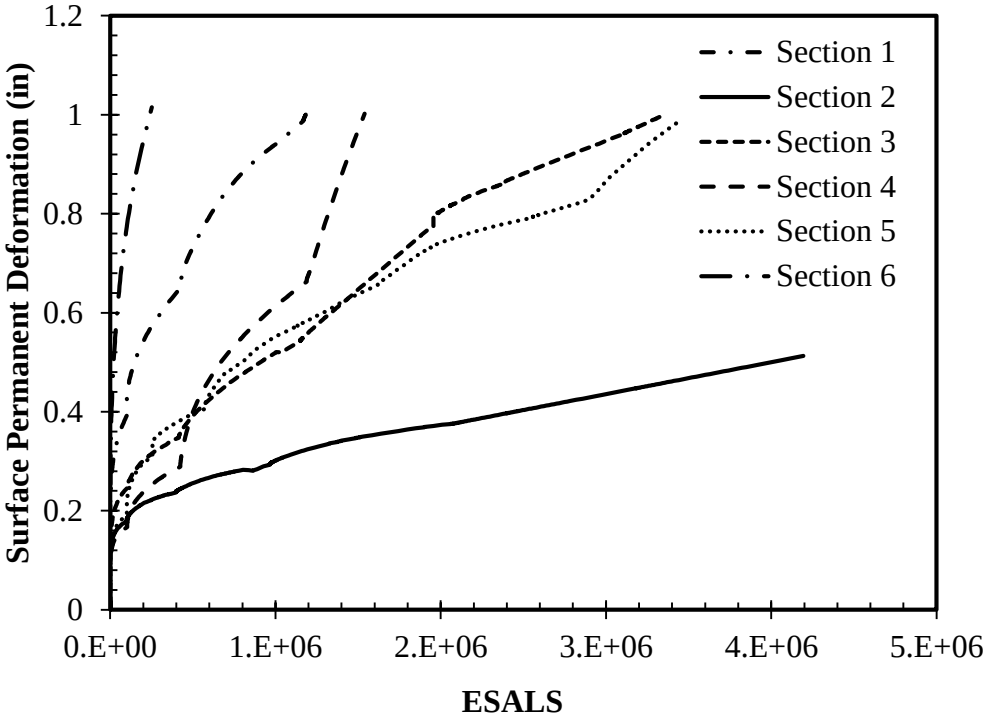

Figure 29

Development of surface permanent deformation

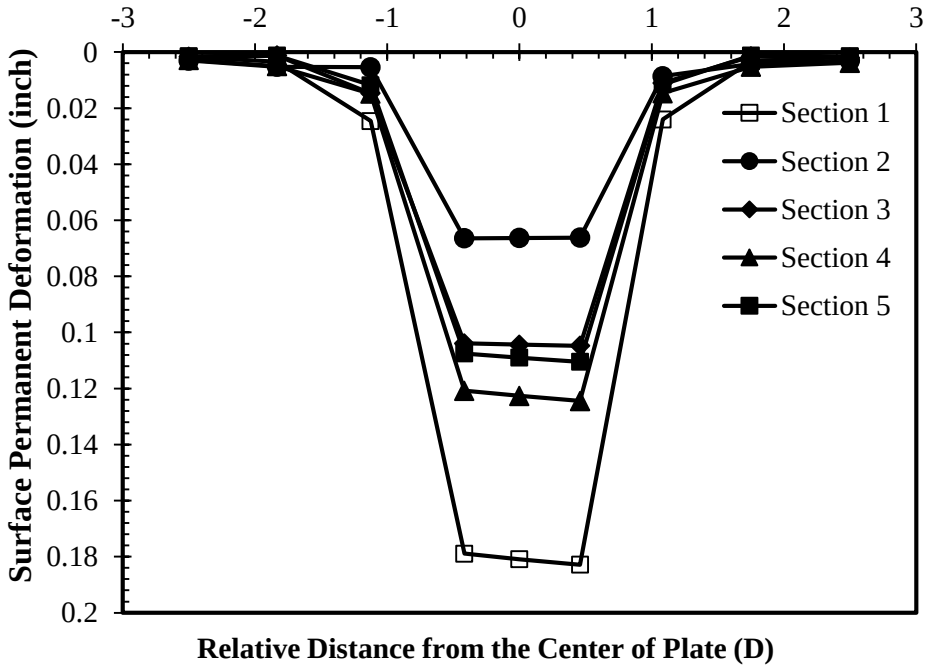

Figure 30

Profile of surface deformation at 1,000,000 ESALs

Permanent Deformation in Base and Subgrade

As previously mentioned, the customized potentiometer was installed at the mid-height of base layer to measure the compressive strain. It is assumed here that the compressive strain at the mid-height represents the mean compressive strain of the whole layer. As such, the overall deformation of the entire base layer was determined by multiplying the measured compressive strain by the thickness of base layer. In the subgrade layer, a customized LVDT was mounted on a steel rod, which has an end fixed to the bottom of the steel box. Therefore, the deformation measured by the LVDT is the overall deformation of the entire subgrade layer. Figure 31 (a) and 31 (b) illustrate the development of base and subgrade permanent deformation with number of EASLs. As can be seen from the figures, for the control section (Section 4), the subgrade layer makes more significant contribution to the total permanent deformation, when compared to the base layer. The use of geosynthetics resulted in reducing the permanent deformations in both the base and subgrade layers (Sections 2 and 5, and Section 3 up to 1.5E+06 ESALs). However, when the geosynthetic is placed at the base-subgrade interface, significant reduction of permanent deformation occurred in subgrade; while only small reduction of permanent deformation was observed in the base layer (Section 3 and 5). This means that the geosynthetic at the base-subgrade interface mostly enhance the performance of the weak subgrade, i.e., it functions more as stabilizing the weak subgrade layer than reinforcing the base aggregate layer. For the double reinforced layer (Section 2), the permanent deformations were significantly reduced in both the base and the subgrade layers. This suggests that while the performance of subgrade was signicantly improved by the geogrid at the base-subgare interface, the performance of base layer was enhanced by the geogrid placed at the upper one–third of the base layer. Meanwhile, the measured absolute permanent deformation in the base aggregate layer of Section 1 (relatively weak section) is close to Section 2 (relatively strong section) due to the use of a much thinner base layer in Section 1 (10 in. vs. 18 in.). This means that considerable deformation is expected in the geotextile-wrapped sand layer in Section 1, although unfortunatly, no deformation measurement is available for this layer.

Vertical Stress in the Subgrade

The vertical stress distribution at the subgrade/base interface and along the centerline of the loading plate for both the reinforced and control sections are shown in Figure 32. The stresses measured were the total vertical stresses induced by the peak load during each cycle, and the stresses induced by the weight of the soil are not included. Because the customized LVDT used to measure the deformation of subgrade layer was installed directly underneath the center of the loading plate, the stress measurement at this location was not available. However, from the figure, one can see that the magnitude of vertical stress was increased

away from the plate in the reinforced test sections compared to the control section. This may suggest that the load was redistributed to a wider area in the geosynthetic reinforced test sections, resulting in an improved stress distribution on top of the subgrade layer. As expected, Section 6 registered the highest pressure near the center due to shallow depth of subgrade layer while Section 1 registered lower pressure near the center due to deeper subgrade layer, compared to the other sections.

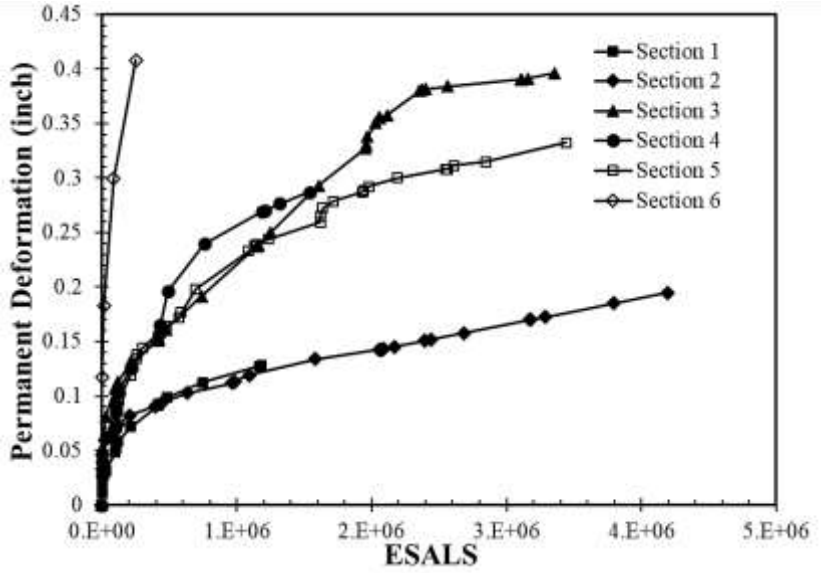

(a) Permanent Deformation in Base

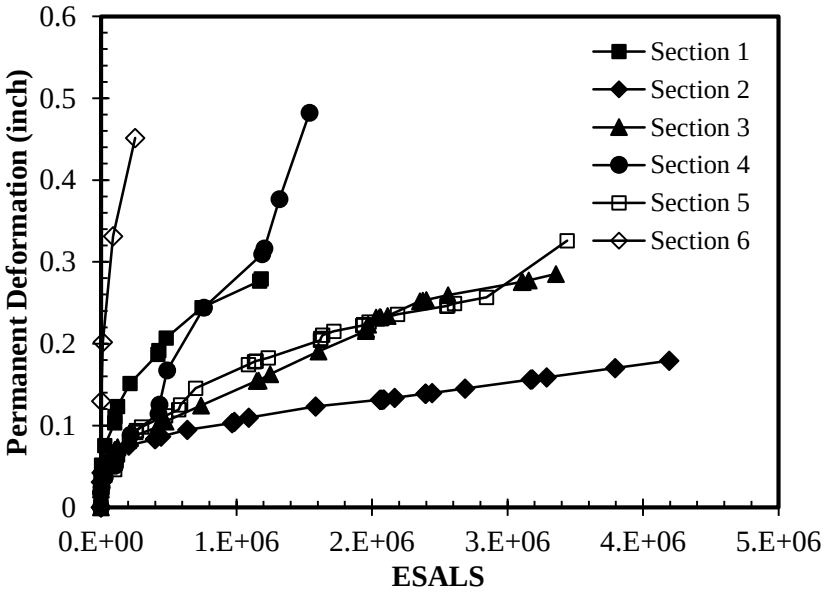

(b) Permanent Deformation in Subgrade

Figure 31
Development of permanent deformation in base and subgrade

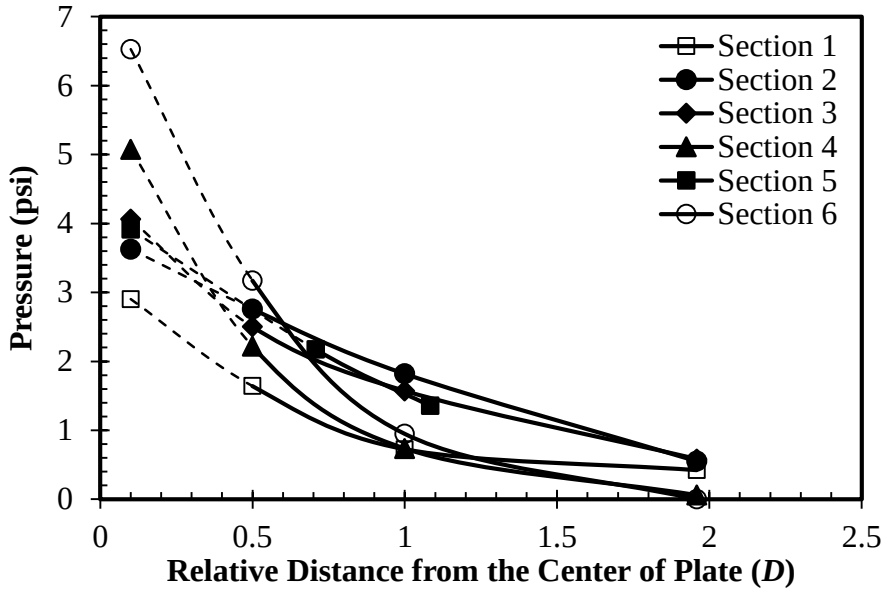

Figure 32
Vertical stress distribution at 100,000 ESALs

Development of Excess Pore Water Pressure in the Subgrade

The development of excess pore water pressures for both unreinforced and control pavement sections as measured at 0.5 in. below the subgrade surface are presented in Figure 33. It should be pointed out that the start of loading was taken as the zero point for the excess pore water pressure values in Figure 33. The starting excess pore water pressure, i.e., the excess pore water pressure at the start of loading (dictated by the compaction energy and the time between the end of construction and the start of the loading), was kept in a small range of 1 ~ 3 kPa in this study as it can strongly influence the magnitude of excess pore water pressure during the test *[31]*. It is interesting to notice that the excess pore water pressure was initially built up at a relatively fast rate until reaching a peak value, after that it remained almost constant. It is also noted that the maximum excess pore water pressure generated in reinforced sections (Sections 2, 3, and 5) was less than that in the control section. This is maybe due to the separation function of geosynthetics, which helped reduce pore water pressure developed from aggregate penetration into subgrade layers *[44]*. In general, the excess pore water pressure generated in subgrade was found to be directly related to the amount of permanent deformation, such that the larger the rutting, the higher the pore water pressure was developed. This is because the excess pore water pressures generated during repeated loading usually reduce the strength of the subgrade soil. The greater the excess pore water pressure generated in subgrade, the greater the strength loss for subgrade soil *[45]*.

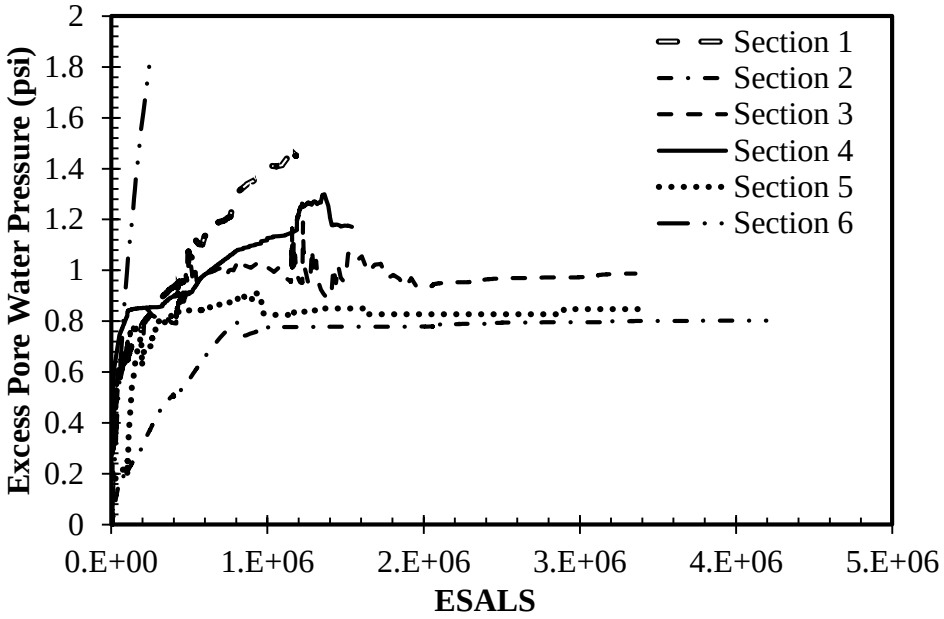

Figure 33

Development of excess pore pressure in top of subgrade

Strain Distribution along the Geosynthetics

The variations of strains measured along the centerline of the geosynthetics for different load cycles are presented in Figure 34. Under cyclic load testing, strain gages experienced both accumulation of residual (plastic) strains and a relatively high dynamic strain level, causing them to stop working after about 5,000 loading cycles *[2]*. Similarly, the strain gages used in Perkins's study and Chen et al.'s study survived 7,500 cycles and 1,000 cycles, respectively *[2, 12]*. As such, the figures only present the strain distribution up to 5,000 cycles. As expected, the measured strain in geosynthetics kept increasing in the tensile direction, as shown in Figure 35, because of plastic strain accumulation. The data demonstrate that appreciable permanent tensile strains were developed in geosynthetics, which are believed to help restrain the lateral movement of the base course aggregates, an important reinforcing mechanism. The highest tensile strains (around 0.4 ~ 0.8%, depending on the type and location of geosynthetic reinforcement) were measured directly beneath the center of the loading plate, where the maximum lateral movement of the base courses were expected to occur, and became almost negligible at a certain distance. This distance is about 1.5 *D* (*D*: loading plate diameter) from the center of the loading plate for the geosynthetics placed at subgrade/base interface and about 1.0 *D* from the center of the loading plate for the geosynthetics placed at the upper one third of the base layer. The maximum measured strains in geosynthetics were well below the failure strain for geosynthetics. Similar pattern of strain development was also reported by Perkins and Chen et al. *[2, 12]*. It also should be

mentioned here that the residual tensile strains (around 0.2~0.3%) were observed in geosynthetics after compaction. These residual tensile strains in geosynthetics can increase the locked-in initial stresses in the base course, thus improving the performance of pavement structure.

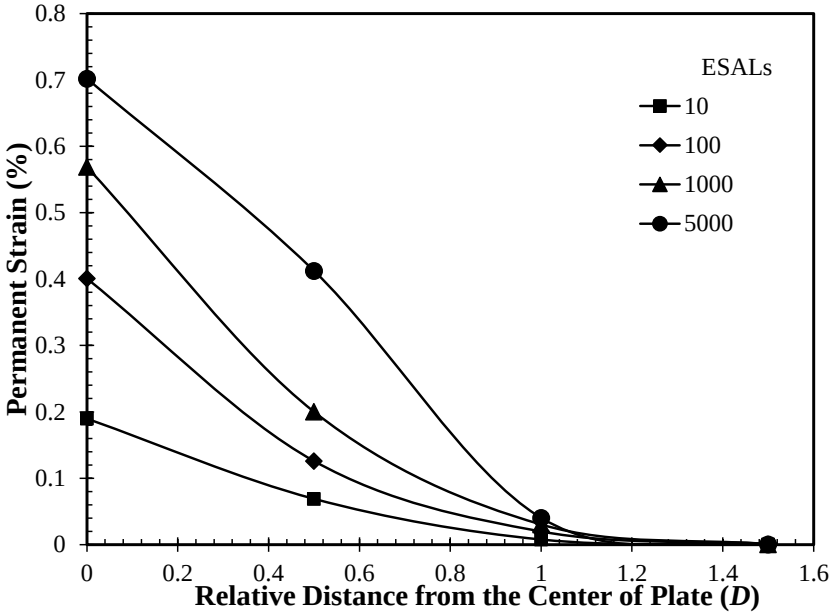

(a) Section 2 (upper one third)

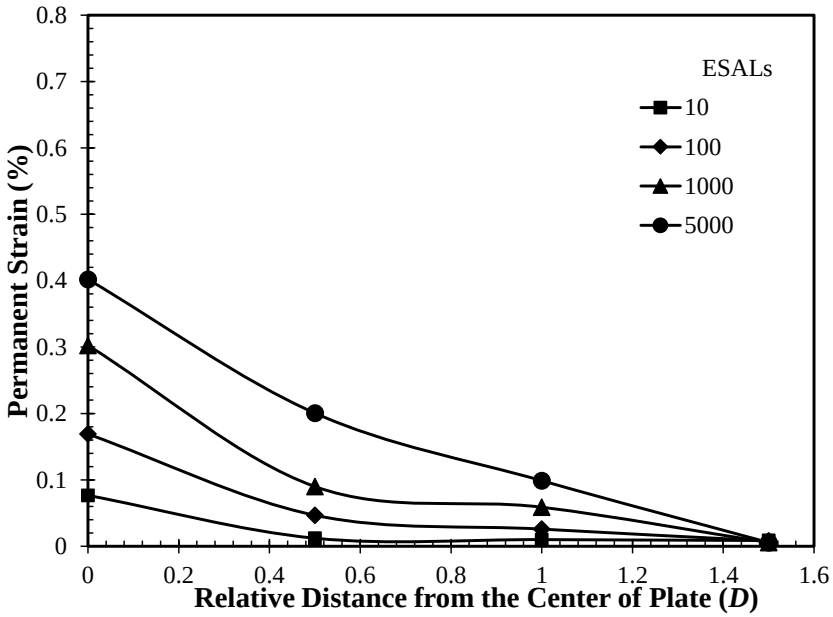

(b) Section 2 (at base-subgrade interface)

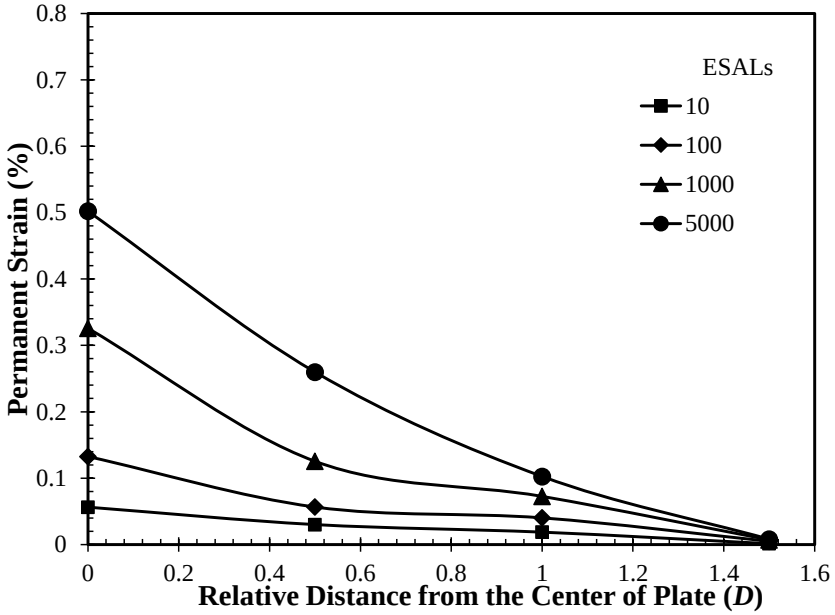

(c) Section 3 (at base-subgrade interface)

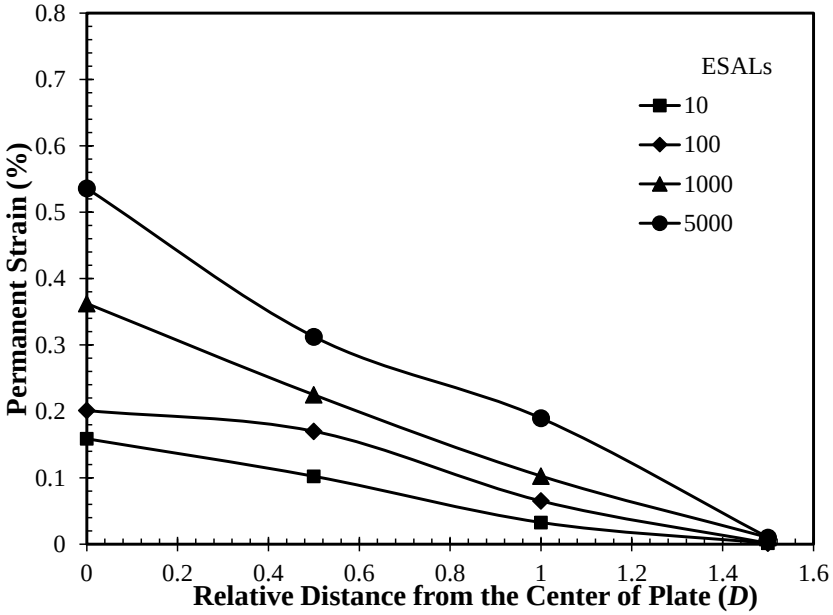

(d) Section 5 (at base-subgrade interface)

Figure 34
Permanent strain distribution along the centerline of geosynthetics (D: loading plate diameter)

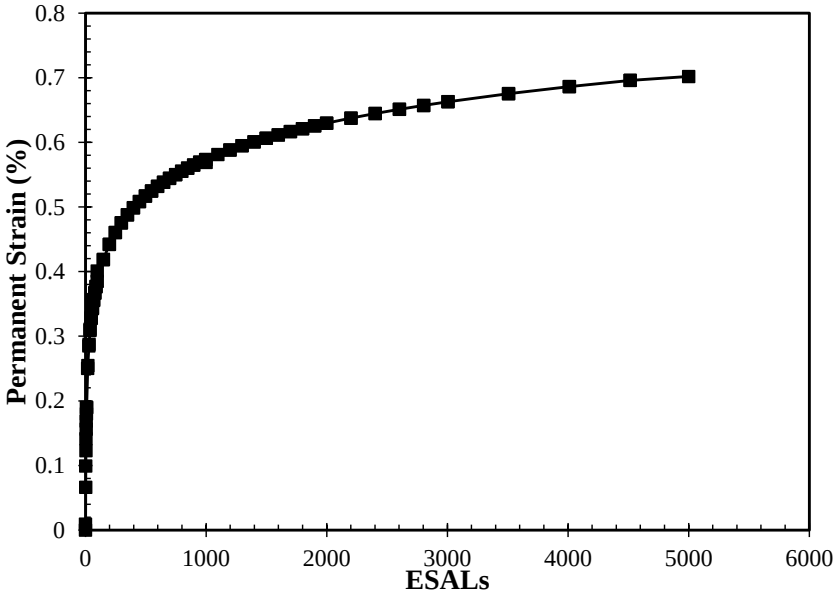

Figure 35
Typical development of permanent strain in geosynthetics (at the point directly beneath the center of the loading plate in Section 2)

Structural Contribution of Geosynthetic Reinforcement

Both AASHTOWare PavementME Design software and 1993 AASHTO Pavement Design Guide were used in this study to analyze the pavement testing sections constructed in the field and laboratory. The failure criterion of a 0.75 in. (19.1 mm) rut depth was used in this study for all test sections [except for Section 2 inside the large-scale in-box laboratory test, the failure criterion of 0.5 in. (12.7 mm) was used since it never reached 0.75 in. (19.1 mm) rut depth]. The benefits of geosynthetic reinforcement were demonstrated through the input parameter of the mechanistic part (i.e., resilient modulus) and/or empirical part (i.e., local calibration factor) of the design method. Geosynthetics have three primary applications in pavement: base reinforcement, mechanical subgrade stabilization and seperation, especially when placed at the base-subgrade interface. However, when geogrids are placed within the base layer (i.e., at upper one-third of base) they function as base reinforcement/stabilization only. For design purpose, the geosynthetics at base-subgrade interface were evaluated as base reinforcement only in this report.

Geosynthetics as Base Reinforcement

For design purpose, the geosynthetic reinforcement benefit can be incoprated into the Pavement ME Design by adjusting the base resilient modulus (M_r) to account for the improved strength of the base by the geosynthetics, i.e. base reinforcement effect of geosynthetics, as shown in Figure 36. In this approach, it is assumed that geosynthetic has no

stabilization effect on the subgrade layer, i.e. the subgrade resilient modulus of reinforced sections is kept the same as the corresponding unreinforced condition.

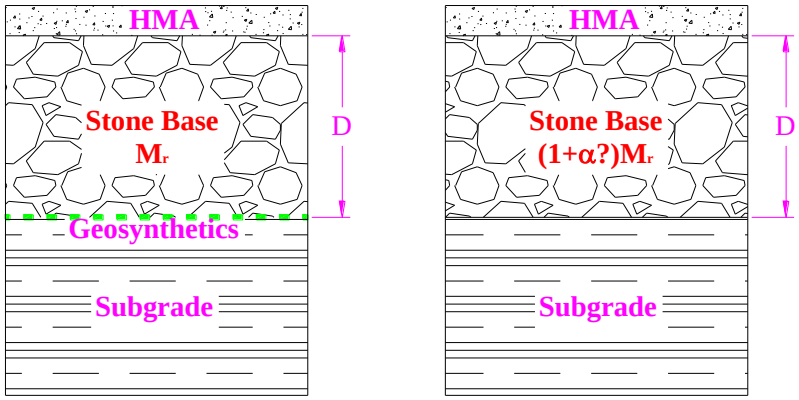

Figure 36
Structural Contribution of Geosynthetic Reinforcement

There are differences between the number of load cycles obtained from the experimental program and those estimated from the Pavement ME Design at different rut depths due to the differences in loading conditions between the plate loading test and vehicular loading and other variables related to the experimental tests. To account for these differences in evaluating the of geosynthetic benefits in terms of improving the base resilient modulus (M_r), two approaches of analyses were used, Approach 1: evaluate the effective base resilient modulus at 0.75 in. rut depth, and Approach 2: evaluate the effective base resilient modulus that best match the entire rut depth-load cycle curve.

Approach 1: Evaluate the Effective Base Resilient Modulus at 0.75-in. Rut Depth

A correction factor was first evaluated on the control section to account for the differences between the experimental results and the Pavement ME Design, which is equal to 6.1. The number of load cycles for the different reinforced sections used in Pavement ME Design are then estimated by multiplying the number of load cycles obtained from the experimental study by the correction factor. The obtained number of load cycles was then used to back-calculate the effective base resilient modulus for the reinforced sections using the Pavement ME Design software with a failure criterion of a 0.75 in. (19.1 mm) rut depth [0.5 in. (12.7 mm) for Section 2 inside the large-scale in-box laboratory test]. The results of back-calculation are summarized in Table 16 through Table 18. For each reinforced section, the base layer's resilient modulus of its corresponding unreinforced section was obtained using the CBR-DCPI relationship suggested by Webster et al. and M_r-CBR relationship suggested by Powell et al., as presented earlier in equation (4) *[41, 42]*. As can be seen from Table 16,

the resilient modulus of the base layer under moving wheel loading condition was increased by 55-65 percent by adding one layer of geosynthetics at the base-subgrade interface and 200 percent by using two layers of geosynthetics (Section 2). Meanwhile, from Table 17 and Table 18, one can see that the resilient modulus of the base course layer under cyclic plate loading was increased by 24-35 percent by adding one layer of geosynthetics at the base-subgrade interface, and 57-136 percent by using two layers of geogrids. This increase in the base resilient modulus will result in extending the service life of a pavement (measured in terms of Traffic Benefit Ratio, TBR).

Table 16
Effective base resilient modulus for moving wheel load test at ALF (M_r, psi)

	Section 2				Section 3				Section 5	
	M_r		Effective M_r		M_r		Effective M_r		M_r	Effective M_r
	Top	Bottom	Top	Bottom	Top	Bottom	Top	Bottom		
1st Month	30259	30259	90778	90778	32817	32817	50867	50867	30641	50558
2nd Month	17146	17146	51439	51439	21915	21915	33968	33968	21793	35959
3rd Month	18575	18575	55724	55724	16182	16182	25082	25082	21793	35959
4th Month	28930	28930	86791	86791	13769	13769	21341	21341	21952	36221
5th Month	30341	30341	91024	91024	13945	13945	21615	21615	21873	36090
6th Month	18343	4850	55030	14550	13923	13922	21580	21580	22623	37327
7th Month	15790	4850	47370	14550	14342	14342	22230	22230	21992	36286
8th Month	15724	4850	47171	14550	14743	14743	22852	22852	22110	36482
9th Month	15990	4850	47971	14550	14982	14981	23221	23221	19437	32071
10th Month	15856	4850	47569	14550	13834	4692	21443	7273	17371	28662
11th Month	15335	15335	46005	46005	13834	4692	21443	7273	18830	31070
12th Month	15208	15208	45625	45625	13834	4692	21443	7273	17928	29581
Percent Improvement (%)			200				55			65

Table 17
Effective base resilient modulus for cyclic plate load test at ALF (M_r, psi)

Test Sections	Base Resilient Modulus[1] (psi)	Effective base Resilient Modulus[2] (psi)	Percentage Improvement (%)
Section 2	21694	34050	57
Section 3	26258	32700	25
Section 5	24207	29910	24
Section 6	23480	40870	74

[1]From DCP [2]Backcalculated from Pavement ME Design software

Table 18
Effective base resilient modulus for cyclic plate load test in the laboratory (M_r, psi)

Test Sections	Base Resilient Modulus[1] (psi)	Effective base Resilient Modulus[2] (psi)	Percentage Improvement (%)
Section 2	30277	71400	136
Section 3	29326	38200	30
Section 5	29050	39300	35

[1]From DCP [2]Backcalculated from Pavement ME Design software

If the service life of the reinforced section is assumed to be the same as that of the unreinforced section, then the base layer thickness can be reduced with the increase of base resilient modulus. This benefit of geosynthetic reinforcement is usually evaluated in terms of the Base Course Reduction (BCR) factor, which is defined as the base thickness of the reinforced section divided by the base thickness of the unreinforced section for a given traffic level (up to 5 million ESALs service life). As can be seen from Tables 19 through 21, the values of BCR range from 0.46 to 0.63 for pavement sections with a single layer of geosynthetics placed at the base-subgrade interface. This means that the thickness of base layer can be reduced by about half or more with the inclusion of one layer of geosynthetics placed at the base-subgrade interface. Thus an 18 in. (457 mm) thick base layer of unreinforced base layer can be reduced to about 9 in. (229 mm) of one-layer geosynthetic reinforced base of same performance. For the pavement section with double layer of geogrid reinforcement/ stabilization, the values of BCR range from 0.64 to 0.78 in this study, which means that an 18 in. (457 mm) thick unreinforced base layer can be reduced to about 6 in. (152 mm) or more of double-layer of geogrid reinforced base of same performance. These reduction values seem to be not realistic in engineering practice. The PavementME may be not suitable for evaluation of base course reudction and should be further investigated.

Table 19
Reduction in base layer thickness for moving wheel load test at ALF

Test Sections	Base Thickness in	Reduced Thickness in	BCR (%)
Section 2	18.8	4.1	78
Section 3	20.7	8.3	60
Section 5	21.5	8	63

Table 20
Reduction in base layer thickness for cyclic plate load test at ALF

Test Sections	Base Thickness In	Reduced Thickness in	BCR (%)
Section 2	18.95	6.8	64
Section 3	19.4	9.27	52
Section 5	20.69	10.83	48
Section 6	11	4	64

Table 21
Reduction in base layer thickness for cyclic plate load test in the laboratory

Test Sections	Base Thickness in	Reduced Thickness in	BCR (%)
Section 2	17.9	4.5	75
Section 3	17.8	9.4	47
Section 5	17.6	9.5	46

Approach 2: Evaluate the Effective Base Resilient Modulus for Entire Rut Depth-load Cycle Curve

In this approach, the material input parameters for the AASHTOWare Pavement ME Design software were first calibrated for the four unreinforced test sections to achieve the best match fit with the entire measured rut depth-load cycle curves, as evaluated in terms of least square of errors between the measured and predicted values. The surface, base and subgrade rut curves were used in this calibration and comparison. Figures 37 to 40 present the comparison between the measured rut-load cycle curves and the best match AASHTOware curves for the unreinforced test sections for the moving wheel at ALF (Section 4), in-box CPLT (Section 4), and the CPLTs at ALF (Sections 4 and 7), respectively. The corresponding calibrated input parameters, Br1 and Br3 for asphalt layer, Bs1 for subgrade layer and Bs1 for base layer, for the four unreinforced test sections, are summarized in Table 22. The calibrated material input materials were then used to develop the rut depth - cyclic load curves for the corresponding reinforced/stabilized geosynthetic sections. The effective resilient modulus for the base layer of each reinforced/stabilized section was increased gradually until the entire predicted AASHTOware rut depth - cyclic load curve achieve best match fit with the entire measured curve, as evaluated in terms of least square of errors. The comparison between the measured and AASHTOWare best match rut-cycle load curves for the reinforced/stabilized geosynthetic test sections are presented in Figures 41 to 43 for the ALF moving wheel sections, in Figures 44 to 46 for the in-box CPLT sections, and in Figures 47 to 50 for the ALF CPLT sections. The percent improvement in resilient modulus for each section due to geosynthetics was then calculated as the ratio of effective resilient modulus for the reinforced/stabilized section to the resilient modulus of corresponding unreinforced section. The percent improvement for all reinforced/stabilized test sections are presented in Table 23.

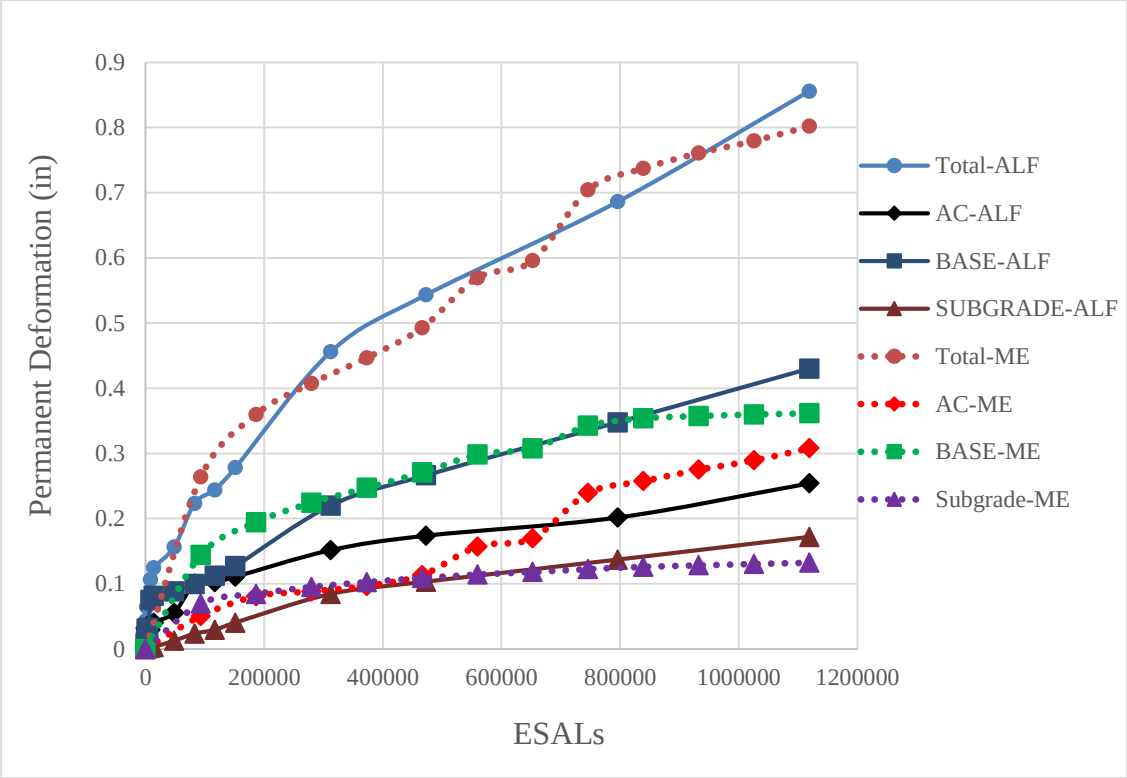

Figure 37
Predicted versus measured rut curves for the moving wheel of unreinforced Section 4

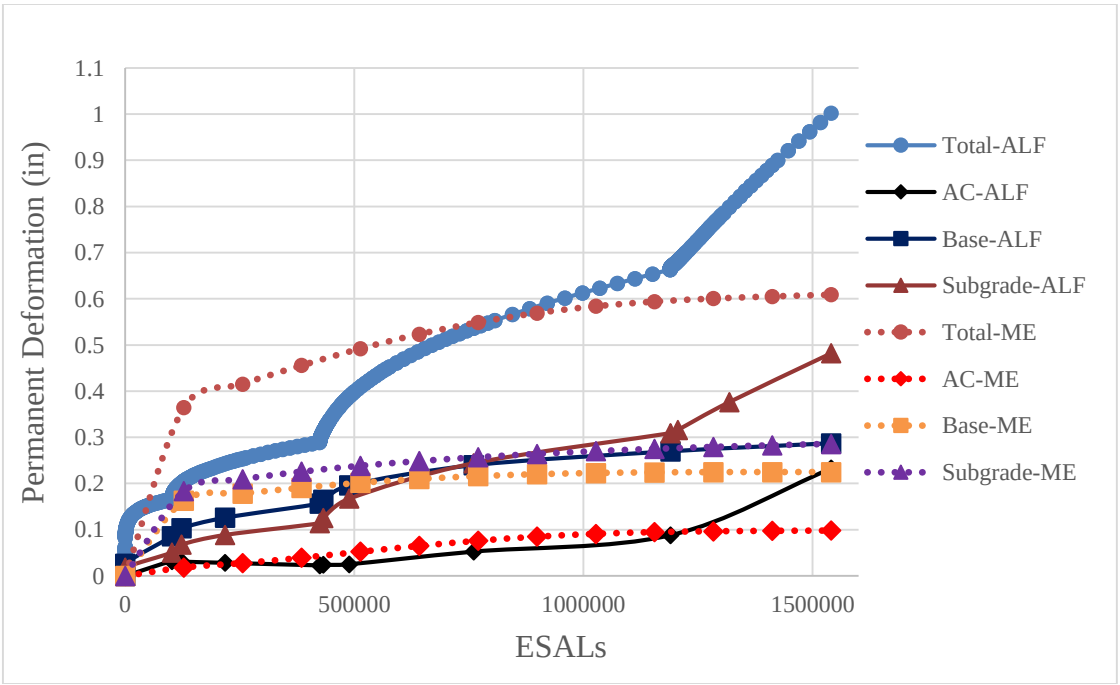

Figure 38
Predicted versus measured rut curves for the in-box CPLT of unreinforced Section 4

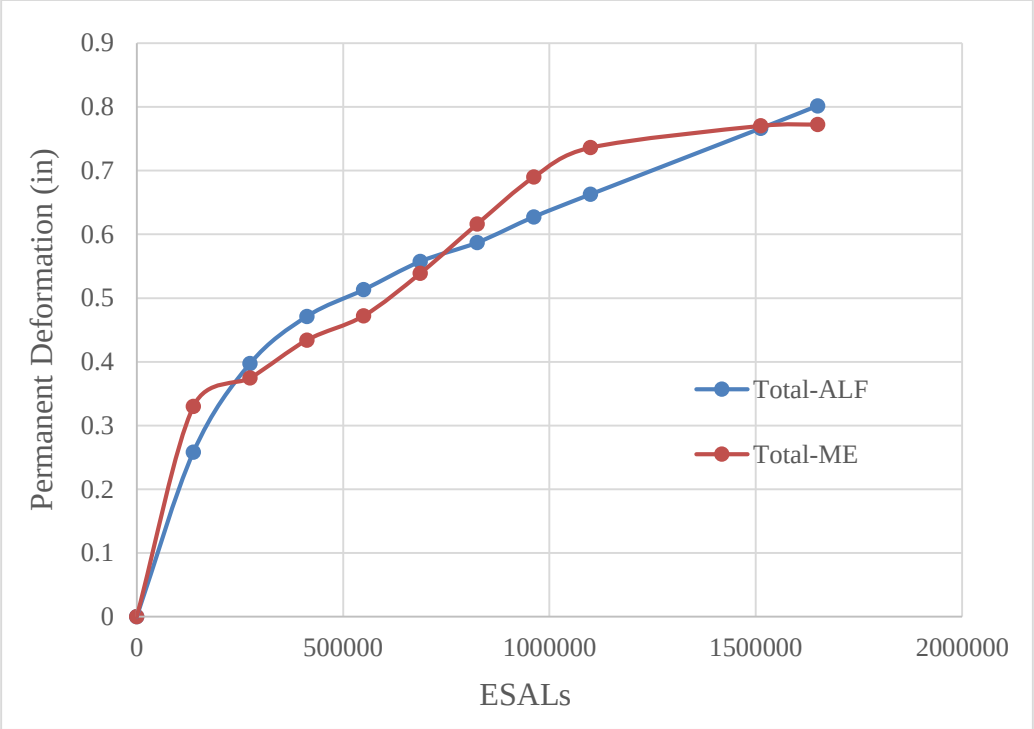

Figure 39
Predicted versus measured rut curves for ALF CPLT of unreinforced Section 4

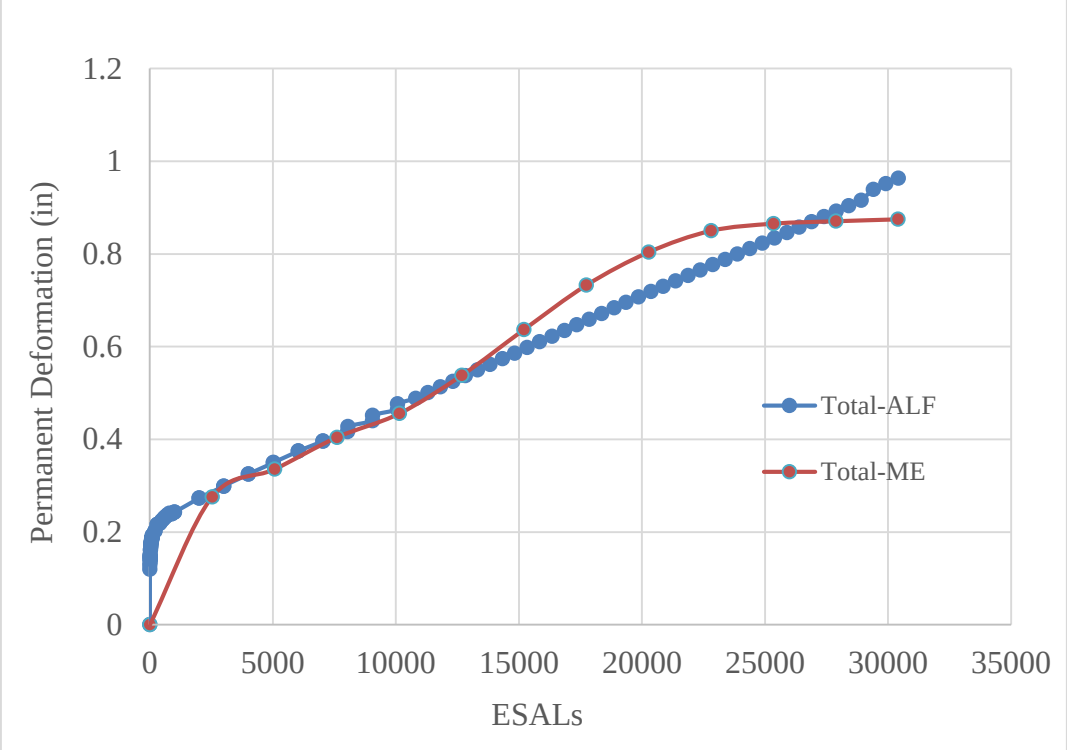

Figure 40
Predicted versus measured rut curves for ALF CPLT of unreinforced Section 7

Table 22
Calibrated AASHTOWare material input parameters for unreinforced test sections

Material Input Parameter	Moving wheel at ALF (Lane 4)	In-box Cyclic Plate Load Test	Cyclic Plate Load Test at ALF (Lane 4)	Cyclic Plate Load Test at ALF (Lane 7)
Br1	2.8	0.45	1.00	1.25
Br3	0.95	0.85	0.85	1.25
Bs1 (base)	0.45	0.90	0.80	1.30
Bs1 (subgrade)	1.55	0.6	0.70	1.20

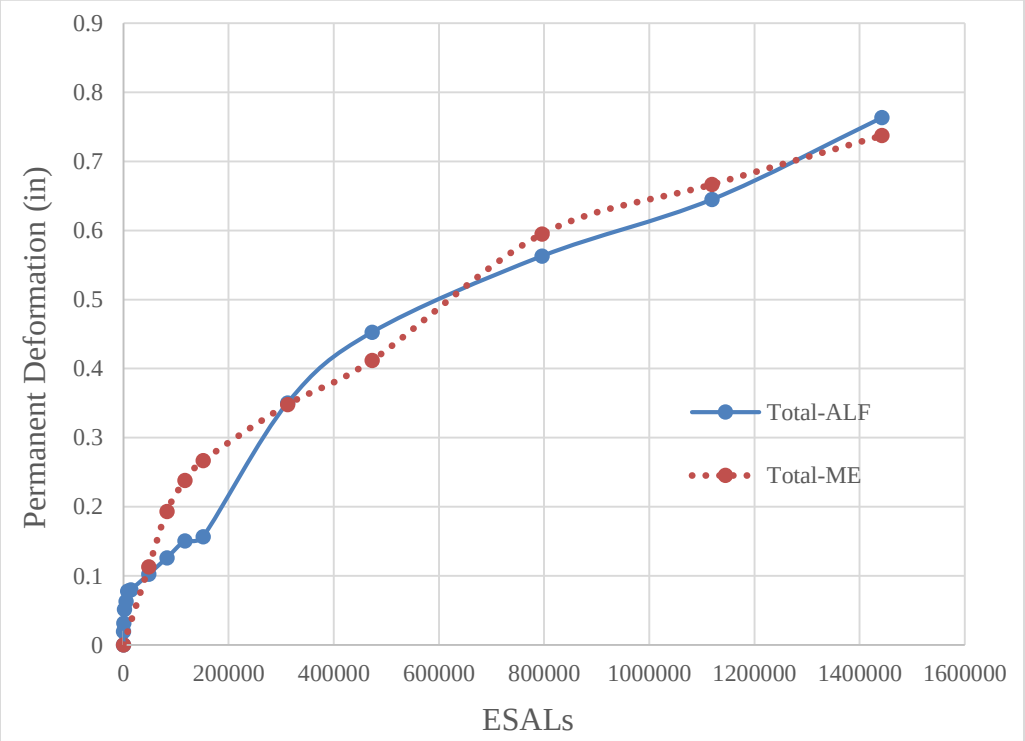

Figure 41
Predicted versus measured rut curves for ALF moving wheel Section 2

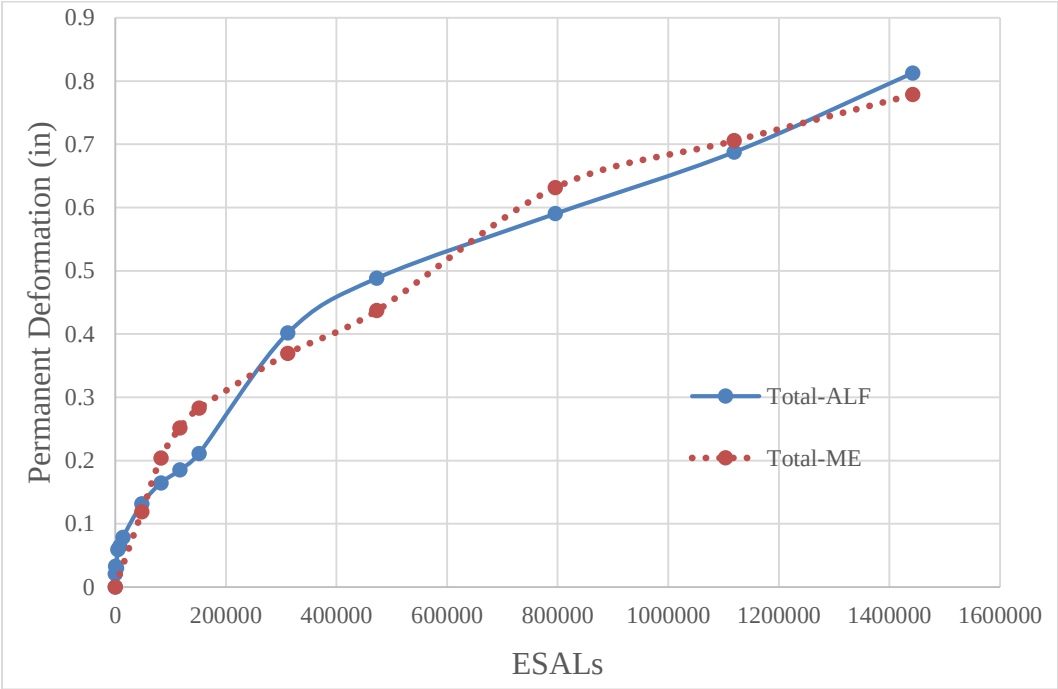

Figure 42
Predicted versus measured rut curves for ALF moving wheel Section 3

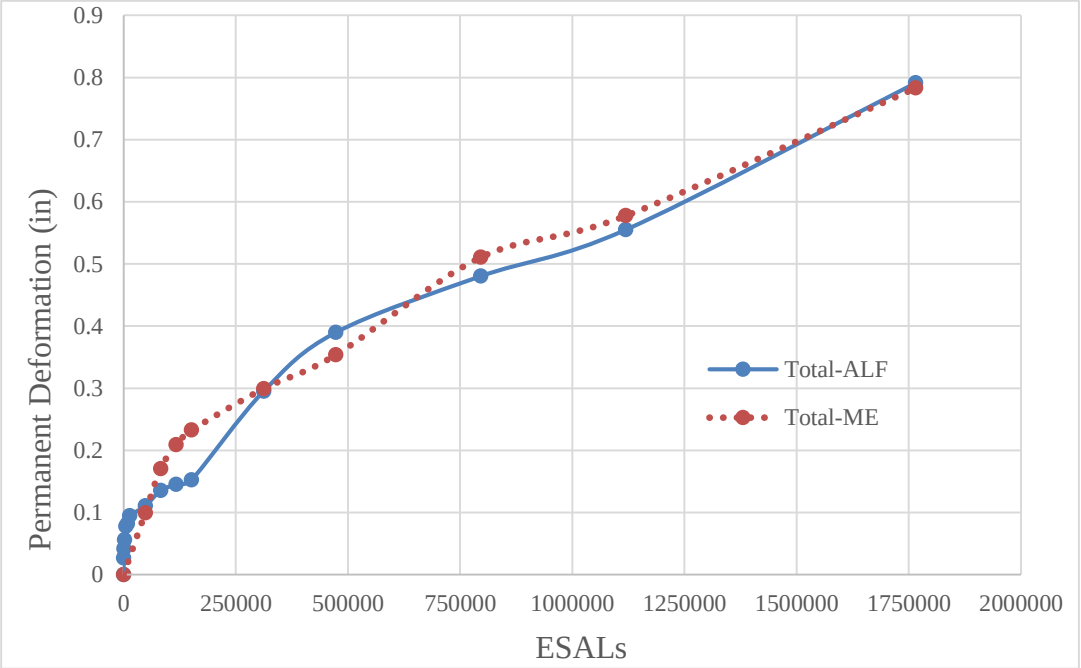

Figure 43
Predicted versus measured rut curves for ALF moving wheel Section 5

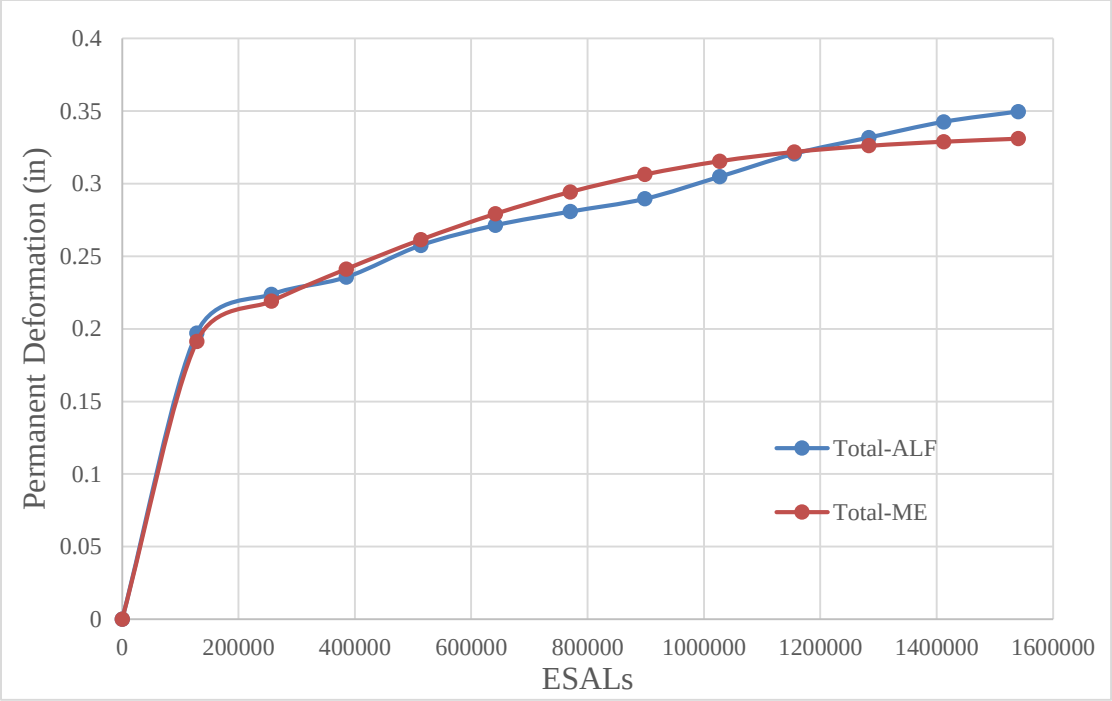

Figure 44
Predicted versus measured rut curves for in-box CPLT Section 2

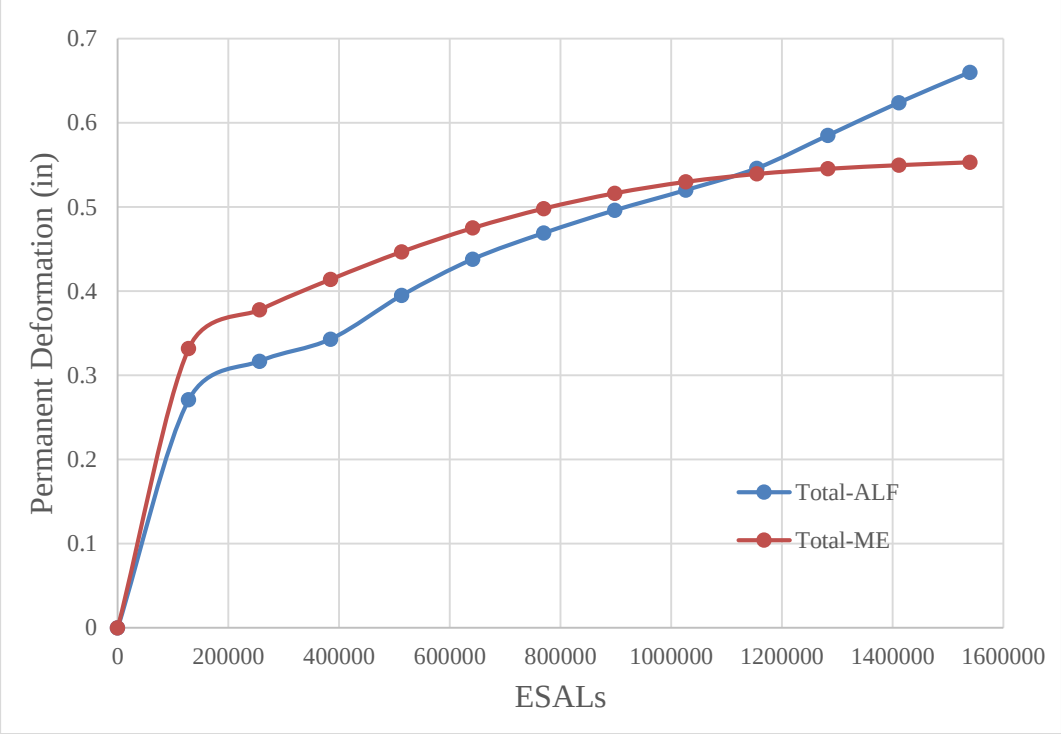

Figure 45
Predicted versus measured rut curves for in-box CPLT Section 3

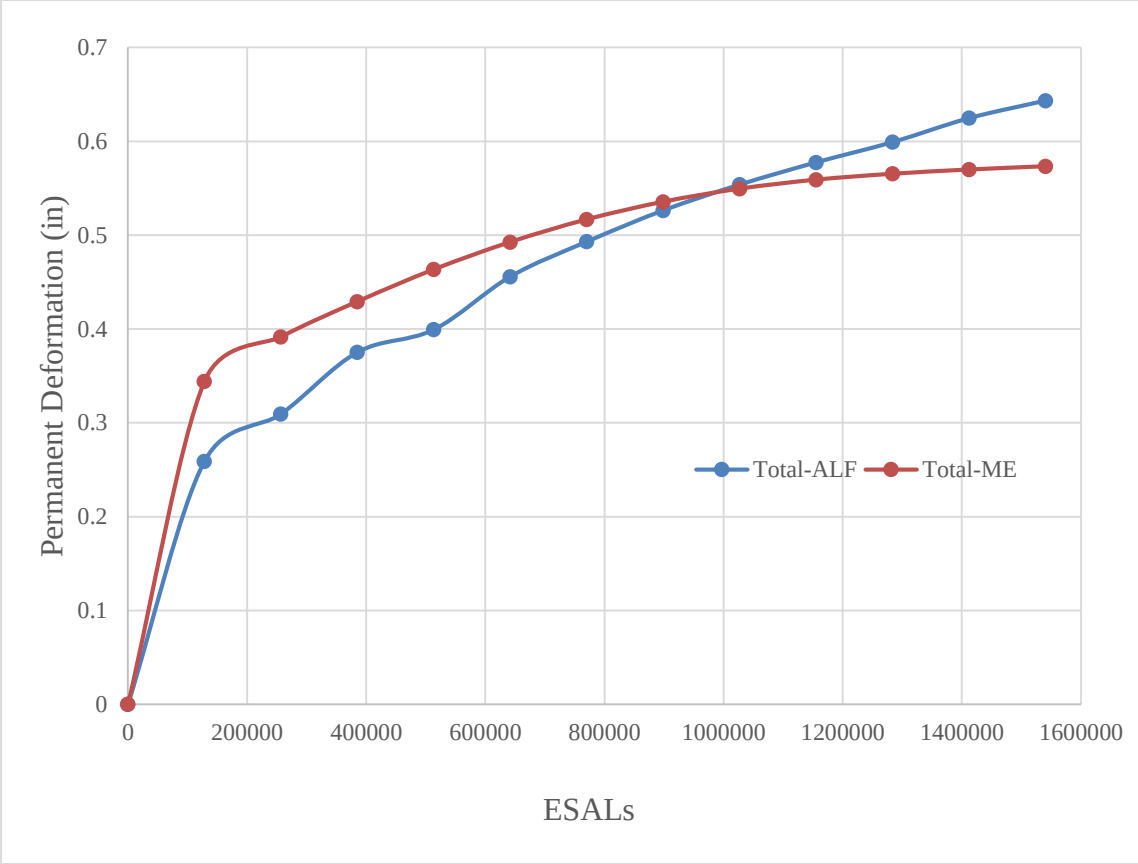

Figure 46
Predicted versus measured rut curves for in-box CPLT Section 5

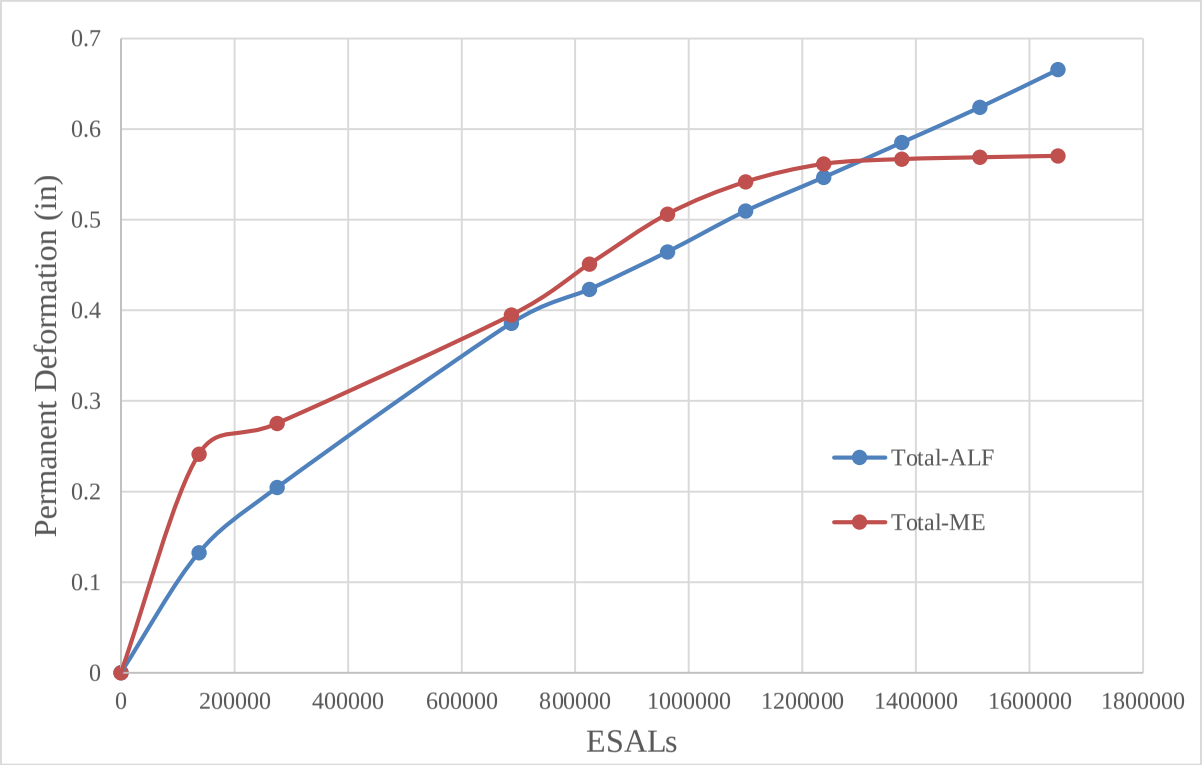

Figure 47
Predicted versus measured rut curves for ALF CPLT Section 2

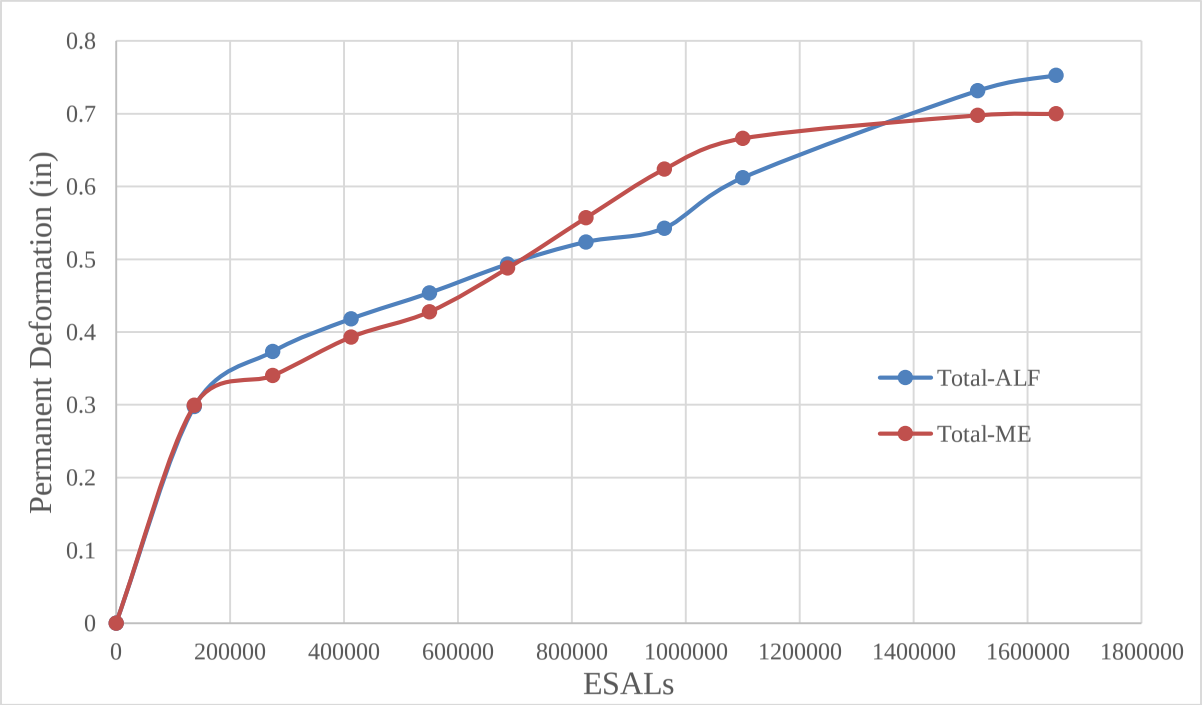

Figure 48
Predicted versus measured rut curves for ALF CPLT Section 3

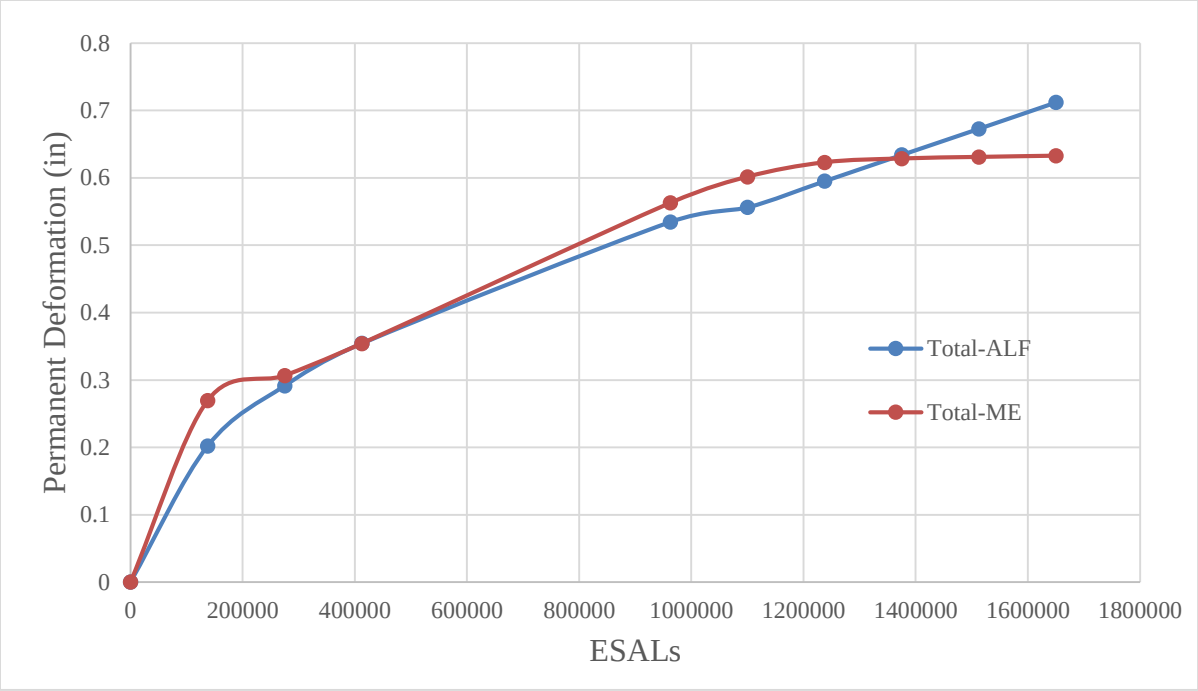

Figure 49
Predicted versus measured rut curves for ALF CPLT Section 5

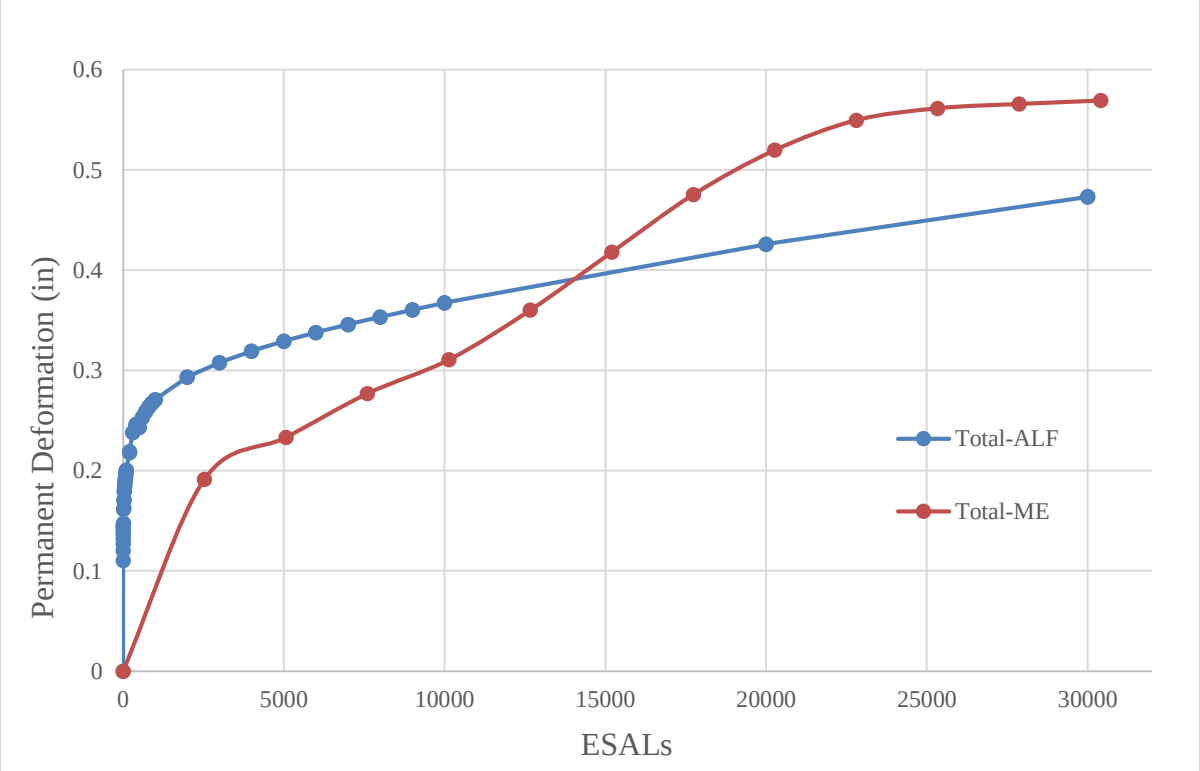

Figure 50
Predicted versus measured rut curves for ALF CPLT Section 6

Table 23
Percent improvement in base resilient modulus for all test sections – Approach 2

Test Sections	Moving wheel at ALF		In-box Cyclic Plate Load Test		Cyclic Plate Load Test at ALF	
	% Improvement	SSE*	% Improvement	SSE*	% Improvement	SSE*
Section 2	82	0.02827	162	0.04514	114	0.03321
Section 3	36	0.01810	27	0.03660	28	0.01100
Section 5	65	0.01465	25	0.02451	50	0.01644
Section 6	-	-	-	-	210	0.05469

SSE*: Sum of square of errors

The benefits of geosynthetic reinforcement/stabilization can be evaluated for approach 2 in terms of reducing the thickness of base course layer (defined by BCR factor) through assuming the service life of the reinforced section to be the same as that of the unreinforced section. The BCR values for the different geosynthetic reinforced/stabilized sections using Approach 2 are calculated and summarized in Table 24. As can seen from the table, the values of BCR range from 0.40 to 0.62 for pavement sections with a single layer of geosynthetics placed at the base-subgrade interface, which means that the thickness of base layer can be reduced by about half or more with the inclusion of one layer of geosynthetics placed at the base-subgrade interface. i.e., an 18 in. (457 mm) thick base layer of unreinforced base layer can be reduced to about 9 in. (229 mm) of one-layer geosynthetic reinforced base of same performance. However, for the pavement Section 2 with double layer of geogrids, the values of BCR range from 0.62 to 0.78, which means that an 18 in. (457 mm) thick unreinforced base layer can be reduced to about 6 in. (152 mm) or more of double-layer of geogrid reinforced base of same performance. Again these reduction values seem to be not realistic in engineering practice. The PavementME may be not suitable for evaluat of base course reudction and should be further investigated.

Table 24
Reduction in base layer thickness for all tests

Test Sections	Moving wheel	In-box CPLT	Field CPLT
Section 2	62	78	65
Section 3	51	44	47
Section 5	62	40	55
Section 6	-	-	80

Geosynthetics as Both Base Reinforcement and Mechanical Subgrade Stabilization

The more reasonable approach to incorporate the benefits of placing geosynthetics at the base-subgrade interface within the context of the Pavement ME Design is to consider both their reinforcement/stabilization effect on base layer and their stabilization effect on subgrade, as shown in Figure 51. In this approach, the effect of geosynthetics increases resilient modulus of the base in the vicinity of the geosynthetics (i.e., within the influence zone of geosynthetics) and reduces critical subgrade vertical strains/stresses, thus, the permanent deformation of subgrade, which can be considered in permanent deformation properties part within the framework of Mechanistic Empirical Pavement Design Guide (MEPDG), i.e., in the model for predicting permanent deformation in the subgrade as follows:

$$\delta_{SG}(N) = k_{GS}\left[\beta_{SG}\left(\frac{\varepsilon_0}{\varepsilon_r}\right)e^{-\left(\frac{\rho}{N}\right)^{\beta}}\varepsilon_v h\right] \quad (7)$$

where, δ_{SG} is the permanent deformation for the subgrade layer at N repetitions of load; N is he number of load repetitions; ε_o; β and ρ are material parameters; ε_r is the resilient strain imposed in laboratory tests to obtain material properties; ε_v is the vertical strain of the asphalt material; h is the thickness of the subgrade layer; β_{SG} is the national model calibration factor for subgrade material and k_{GS} is the reduction factor due to geosynthetics reinforcement.

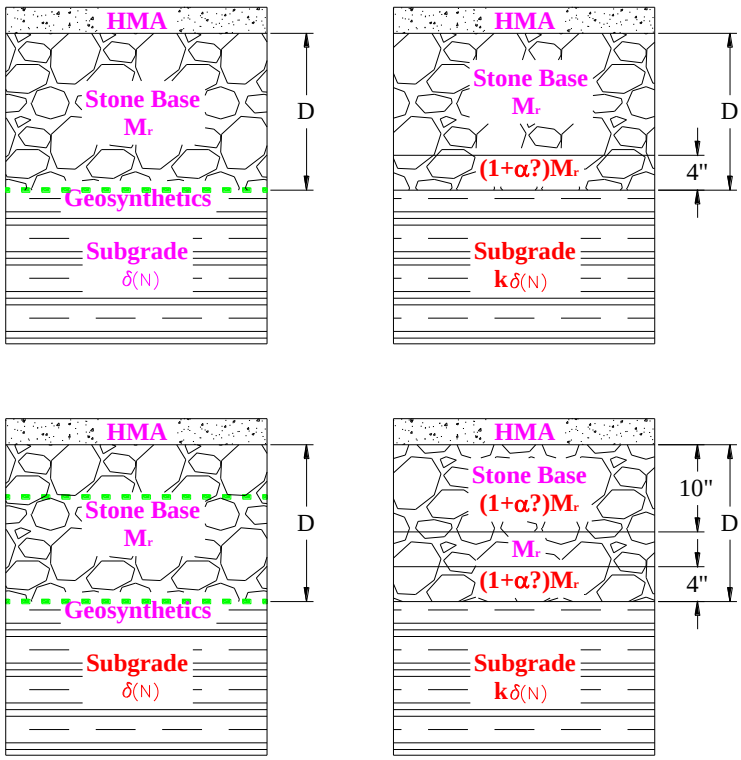

Figure 51
Geosynthetics as both base reinforcement/stabilization and mechanical subgrade stabilization

Since there are two unknowns, it is assumed here that the improved resilient modulus of the base layer in the vicinity of the geosynthetics is due to the increased confining pressure provided by the confinement effect of geosynthetics. This increased confining pressure can be evaluated as:

$$\Delta\sigma_3 = \frac{T}{S} \tag{8}$$

where, *T* is the tensile force in geosynthetics, which is taken at 2% strain in this study; *s* is the influence zone of geosynthetics, which is assumed to be 4 in. in this study. The estimated increased confining pressure is about 7 psi, which results in a confining pressure about 10 psi for limestone within influence zone of geosynthetics. This increase in confining pressure results in about a two-thirds increase of resilient modulus, as shown in Figure 52.

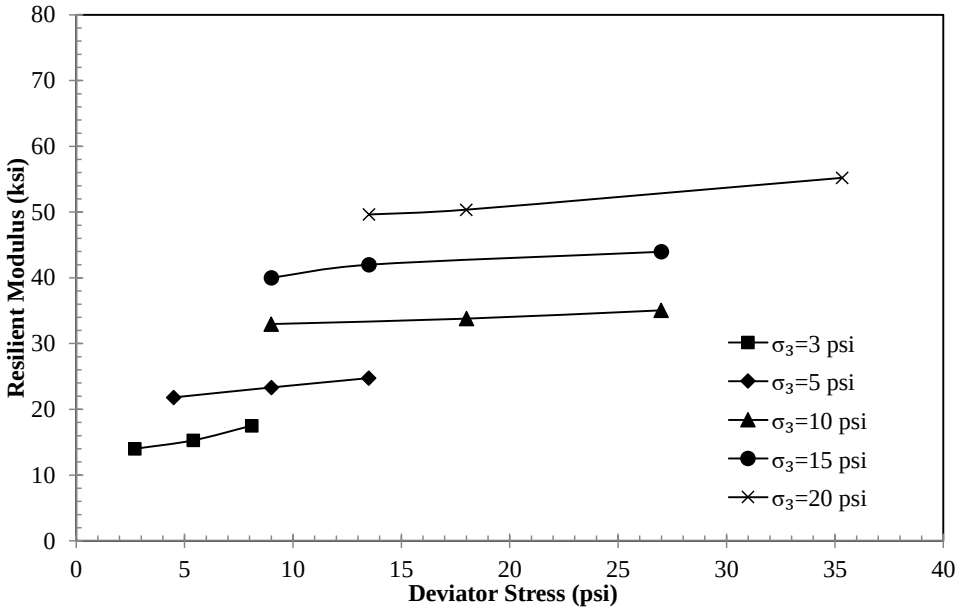

Figure 52
Resilient modulus of crushed limestone

Again, the Pavement ME Design software was used here to back calculate the subgrade permanent deformation reduction factor for the reinforced sections. The results of back calculated permanent deformation reduction factors for the reinforced/stabilized sections are summarized in Table 25 for the two approaches: at 0.75 in. rut depth, and best match to entire rut curve. As can be seen from the table, the subgrade permanent deformation reduction factor under moving wheel loading condition ranged from 0.46 to 0.53 by adding one layer of geosynthetics at the base-subgrade interface and ranged from 0.37 to 0.49 by using two layers of geosynthetics (Section 2). Meanwhile, the subgrade permanent deformation reduction factor under cyclic plate loading ranged from 0.70 to 0.90 by adding one layer of

geosynthetics at the base-subgrade interface and 0.56 to 0.68 by using two layers of geosynthetics.

Table 25
Subgrade permanent deformation reduction factor

Test Sections	RWLT at ALF		CPLT at ALF		CPLT in the Lab	
	At 0.75 in. rut	Match the entire rut curve	At 0.75 in. rut	Match the entire rut curve	At 0.75 in. rut	Match the entire rut curve
Section 2	0.37	0.49	0.68	0.63	0.61	0.56
Section 3	0.53	0.62	0.72	0.65	0.86	0.88
Section 5	0.46	0.46	0.70	0.57	0.87	0.90
Section 6	-	-	0.52	0.35	-	-

Comparisons of Different Tests

The performance comparisons of pavement sections under the cyclic plate load and under the moving wheel load are presented in Figure 53. Under the unidirectional moving wheel load, a pavement element within the plane of the wheel track generally experienced various combinations of vertical, horizontal, and shear stresses with an extension-compression-extension multiple stress path and continuous rotation of the principal stress. On the other hand, under the cyclic plate load, various magnitudes of vertical and horizontal stresses are experienced by a pavement element beneath the center of loading plate with a single compression stress path. There is no rotation of principal stress under the cyclic plate load. This lack of rotation is a fundamental difference between the cyclic plate load and the moving wheel load. The more detailed descriptions of stress experienced by a pavement element under these two types of loading conditions can be found in Abu-Farsakh and Chen *[46]*.

As can be seen from Figure 53, the rut depths of Sections 2, 3, 4, and 6 under moving wheel load test are higher than those under cyclic plate load. This indicates that in general, the moving wheel load is a more damaging loading condition than the cyclic plate load, which confirms the observation from authors' previous study *[46]*. However, Section 1 showed inconsistent results with lower rut depth under moving wheel load as compared to those under cyclic plate load. Interestingly, there are good agreement between the results of moving wheel load tests and cyclic plate load tests for Section 5 and 6. This indicates that except for the types of loading conditions, there are many other factors affecting the performance of pavement sections, for example, variations in constructed pavement layer properties and environmental conditions experienced by different pavement test sections. These variables make it very complex to develop an accurate "correction factor" to account for the principal stress rotation as proposed by the authors in their previous study *[46]*.

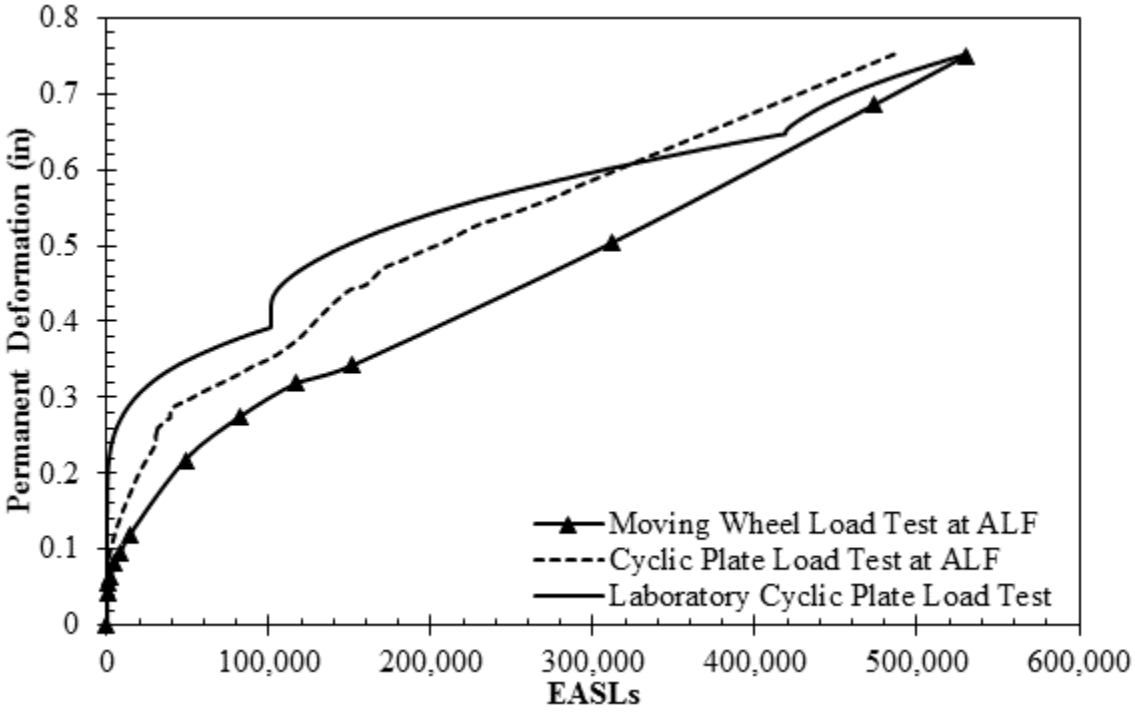

(a) Section 1

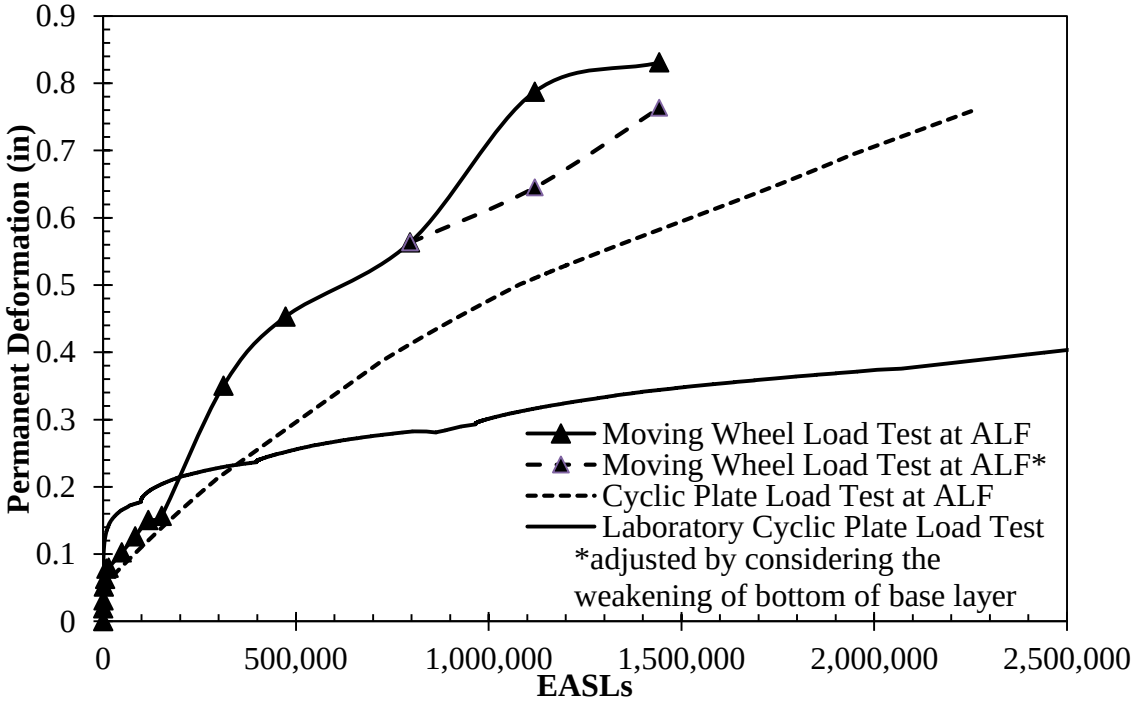

(b) Section 2

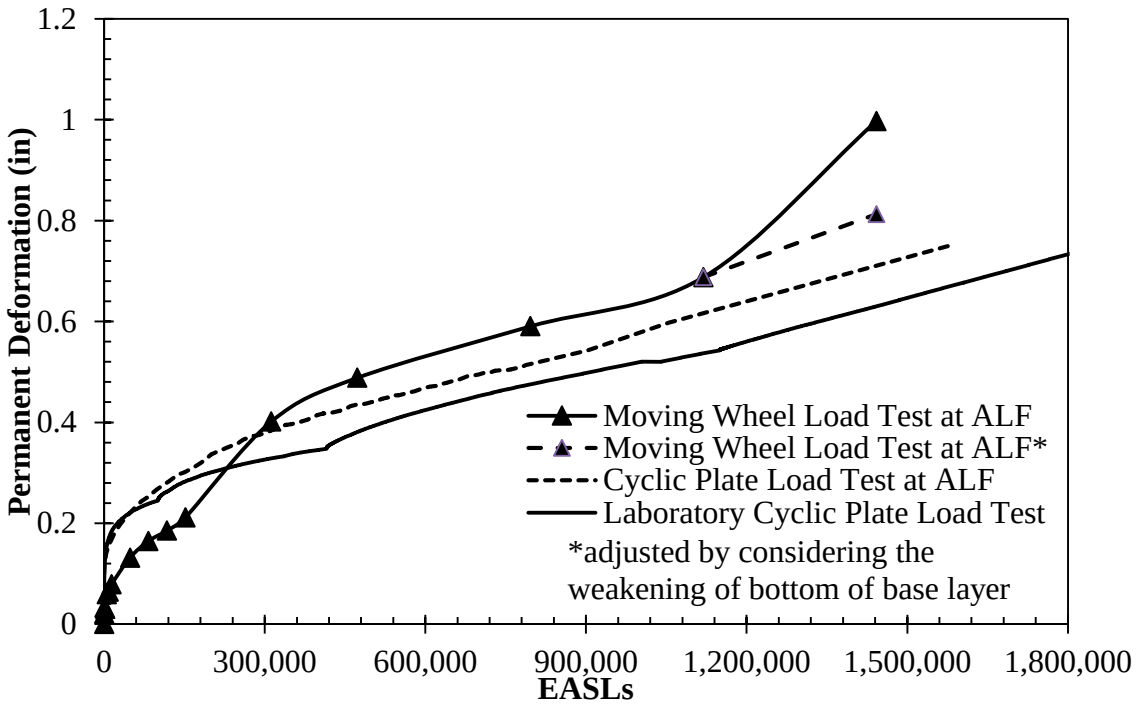

(c) Section 3

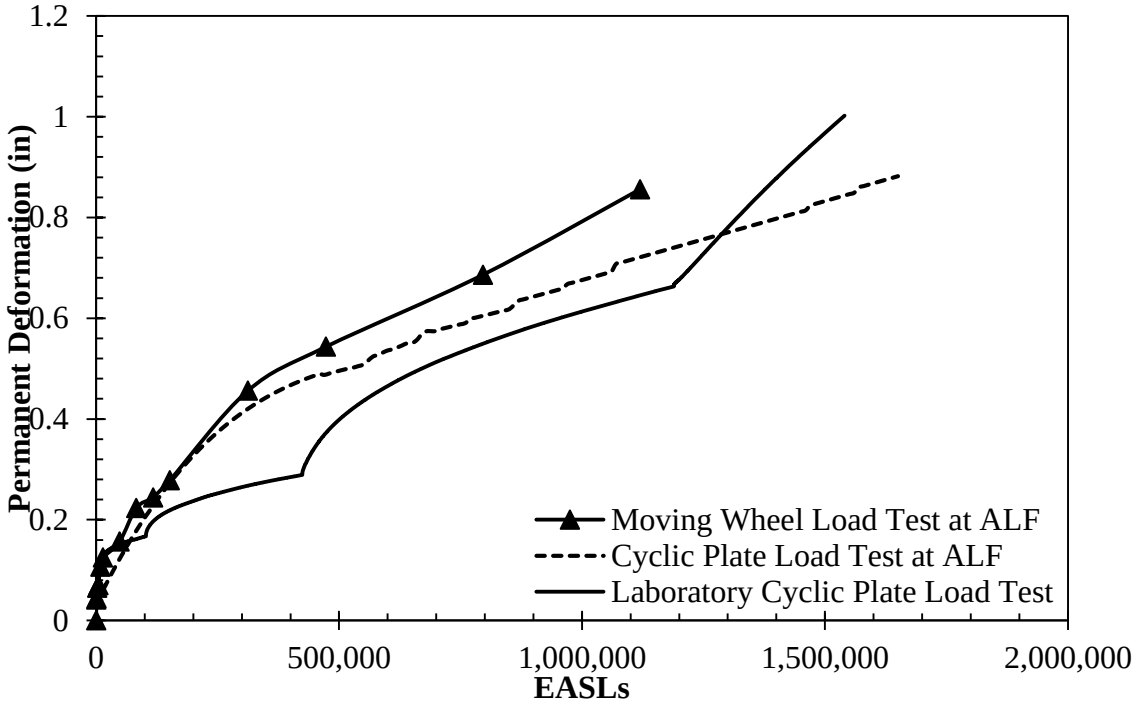

(d) Section 4

(continued)

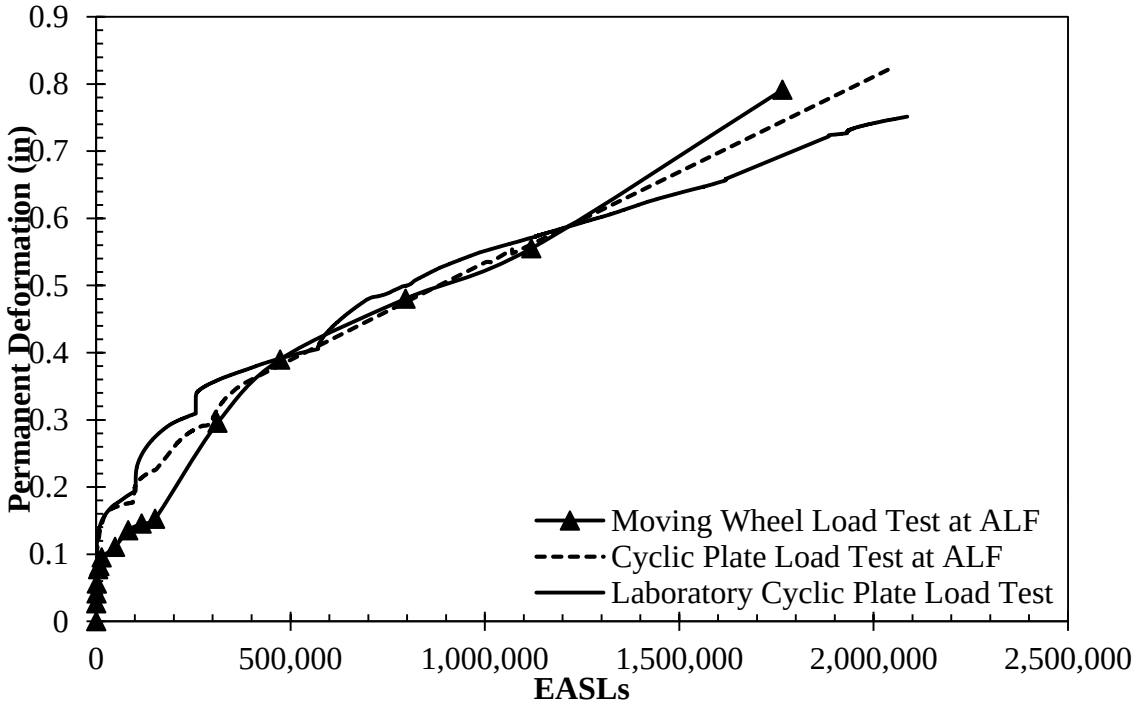

(e) Section 5

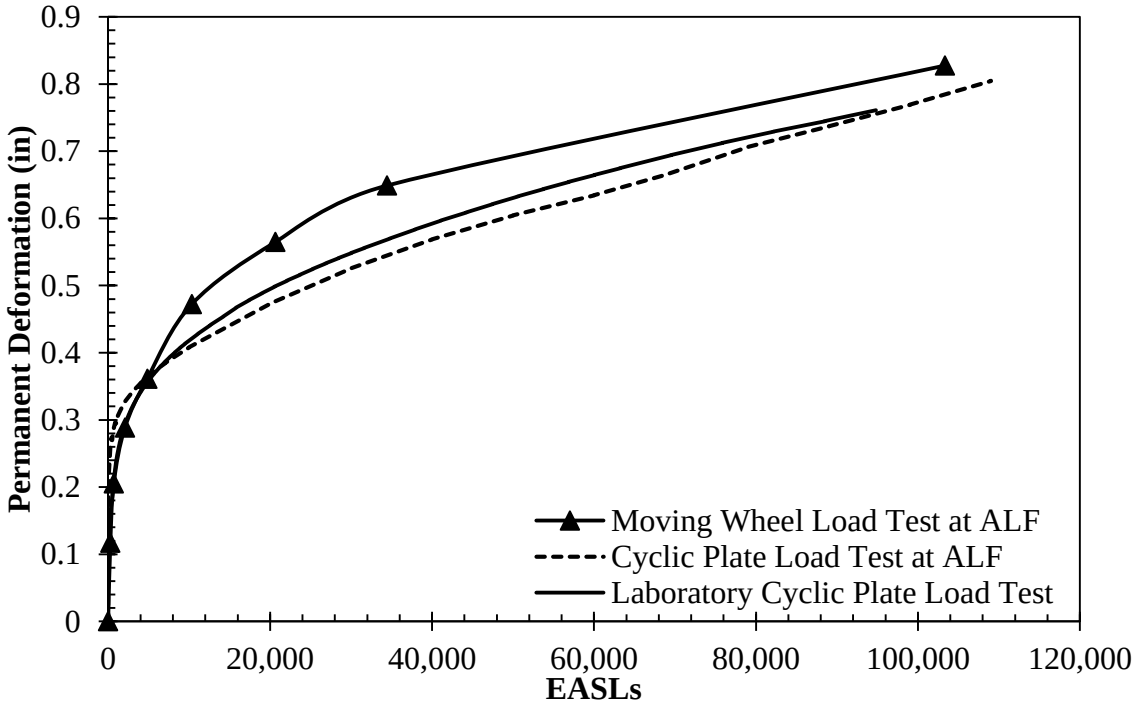

(f) Section 6

(continued)

Figure 53
Comparisons of moving wheel load test and cyclic plate load test

DESIGN GUIDELINE AND COST BENEFIT ANALYSIS

Design Guideline

In the design, for simiplicity, the benefit of geosynthetic reinforcment is assumed to be completely taken by the base layer as base reinforcement, i.e., the effective base resilient modulus (M_{r_eff}) alone is used to account for the benefit of geosynthetic reinforcement, as shown in Figure 54. The effective base resilient modulus (M_{r_eff}) can be expressed as:

$$M_{r\_eff} = (1+\alpha)M_r \tag{9}$$

where, α is the percentage increase in base layer modulus; M_r is the resilient modulus of base course without reinforcement. Based on the results of analysis presented in subsection "Geosynthetics as Reinforcement," for Approach 2 (best match of the entire rut depth-load cycle curve), a conservative value of α = 30% was selected for a single layer of geosynthetic reinforcement placed at the base-subgrade interface, and a value of α = 90% was selected for double layers of geogrid reinforcement. Note here that the benefits of using a single layer of triaxial geogrid underlain by nonwoven geotextile separator and the high strength woven geotextile used in this study are very close, and thereforethey were assigned same α value.

Theoretically, the effect of geosynthetics only increases resilient modulus of the base in the vicinity of the geosynthetics (i.e., within the influence zone of geosynthetics). The influence zone is assumed to be 4 inch above/below the geosynthetics in this study, as shown in Figure 54. The α_1 and α_2 are related to the α by the following equations:

$$(1+\alpha)M_r = \frac{(1+\alpha_1)M_r \times 4 + M_r \times (D-4)}{D} \tag{10}$$

$$(1+\alpha)M_r = \frac{(1+\alpha_1)M_r \times 4 + (1+\alpha_2)M_r \times 8 + M_r \times (D-12)}{D} \tag{11}$$

By substituting α value of 30% for single layer of geosynthetic reinforcement into Equation (10), the α_1 is back-calculated as about 135%. By substituting α value of 90% for double layer of geogrid reinforcement into Equation (11), the α_2 is back-calculated as about 135% too. The α_1 and α_2 values are almost identical. These values (i.e., $\alpha_1 = \alpha_2 = 135\%$) are then used to calculate the α values for pavement sections with different base thickness, which are presented in Table 26.

Once the effective base resilient modulus (M_{r_eff}) is determined, it can then be input into PavementME Design Guide to estimate the service life of the reinforced pavement section. The corresponding TBR is then evaluated and presented in Table 27.

As indicated earlier in Tables 19 to 21 and Table 24, the current version of PavementME gives unreasonable reduction in base layer thickness, so it is not recommended to use PavementME to determine the thickness of base layer of reinforced pavement section. Instead, AASHTO 1993 Pavement Design Guide is used here to determined the BCRs, which are presented in Table 28.

Based on analyses, the α values presented in Table 26, the TBR values presented in Table 27 and the BCR factors presented in Table 28 are recommended for the design of geosynthetics reinforced flexbile pavement built over the weak subgrade (CBR = 0.5-3).

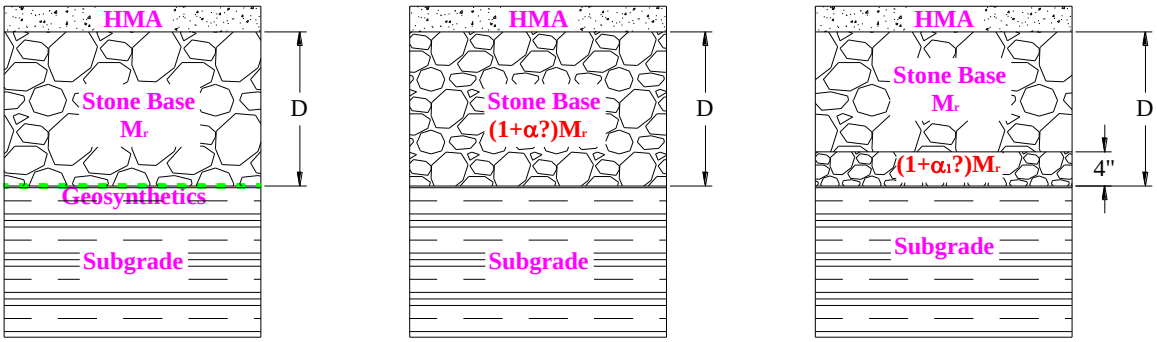

(a) Single layer of geosynthetic reinforcement

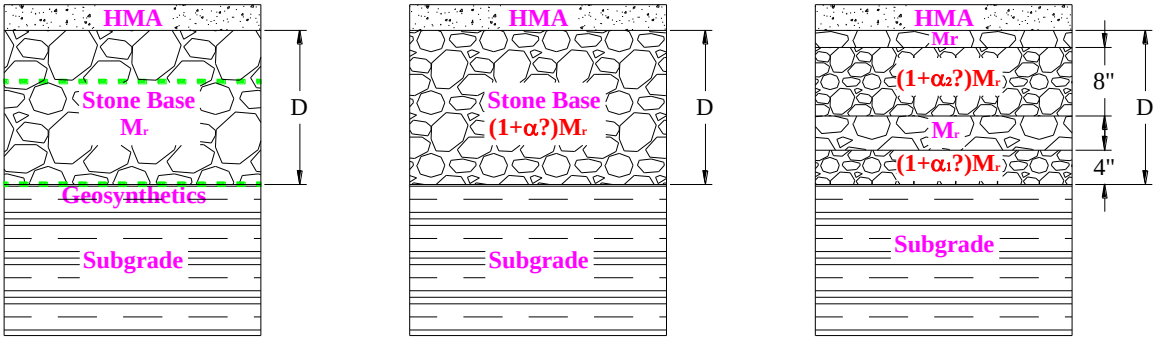

(b) Double layers of geogrid reinforcement

Figure 54
Effect of geosynsthetics on resilient modulus of base material

Table 26

Percentage improvement of base resilient modulus

Base Thickness (in)	α	
	Single Layer of geosynthetics	Double Geogrid Layers
12	45%	135%
14	40%	115%
16	35%	100%
18	30%	90%

Table 27

Traffic benefit ratio (Based on AASHTOWare PavementME)

Base Thickness (in)	TBR	
	Single Layer of geosynthetics	Double Geogrid Layers
12	1.55	2.25
14	1.50	2.15
16	1.47	2.10
18	1.45	2.00

Table 28

Base course reduction factors (Based on 1993 AASHTO Design Method)

Base Thickness (in)	BCR	
	Single Layer of geosynthetics	Double Geogrid Layers
12	23%	50%*
14	21%	45%*
16	20%	45%
18	19%	40%

*Not realistic

Cost Benefit Analysis

Cost savings when using a geosynthetic reinforcement in a pavement system will vary for each project. Here, the analysis will be based on the above design recommendations of geosynthetic reinforced pavements (i.e., triaxial geogrid and high strength woven geotextile) as compared to the 12-in. cement/lime treated subgrade with class II cement stabilized base and the unreinforced/untreated sections with aggregate base. The cost benefit analysis of using geosynthetic reinforcement can be performed in terms of two different prospects ways: (a) reduced base thickness as defined by the base course reduction (BCR), and (b) extended

serviced life of pavement as defined by the traffic benefit ratio (TBR). It should be noted here that instead of including all pay items, only the pay items that make the cost differences between the three different pavement sections will be included for analysis: cost of geosynthetic reinforcement, cost of aggregate base, cost of class II cement stabilized base, and cost of 12-in. cement/lime treated subgrade (i.e., assume that the thickness of asphalt layer is the same for all sections).

Cost Benefit Analysis – BCR

The economic benefit of using geosynthetics, in terms of reduced base thickness, lies in the saving of initial construction cost, i.e., short-term benefit. This can be easily evaluated by the cost of following pay items in Table 29.

Table 29

Pay Items for base course reduction (BCR)

Item Name	Unit Cost
Base Aggregate Cost	$\$90/yd^3$
12” Cement/lime treated subgrade	$\$12.8/yd^2$
8” Class II cement stabilized base	$\$14.55/yd^2$
12” Class II cement stabilized base	$\$18.85/yd^2$
Geosynthetics Cost	$\$3.5/yd^2$

The results of cost benefit analysis for different geosynthetic reinforced base thicknesses are presented in Table 30. The results show that the cost saving due to reduced base thickness can reach up to $\$4.5/yd^2$ and $\$11.0/yd^2$ for a single layer and double layers of geosynthetic reinforcements, respectively, as compared to unreinforced/untreated pavement section. Compared to the 12-in. cement/lime treated subgrade with the cement stabilized base section, the use of a single geosynthetic layer is cost effective for base thickness < 12 in.; whereas, the use of 12-in. treated subgrade with cement stabilized base is somehow cost effective for base thickness ≥ 12 in. This is mainly due to relative high cost of aggregate stone compared to cement stabilized materials. However, the cost benefit of using double geogrid layers exceeds the cost savings of 12-in. treated subgrade with cement stabilized base, up to $\$11.0/yd^2$ compared to up to $\$6.3/yd^2$.

Table 30
Cost Saving in Terms of BCR

Base Thickness (in) (Single reinf. layer/treated, unreinf.)	Construction Cost (Geosynthetics, Treated subgrade, Stabilized base, Aggregate base)				Cost Saving		
	Unreinf. section	12" Treated subgrade & cement stabilized base	Single reinf. layer	Double reinf. Layers*	12" Treated subgrade& cement stabilized base	Single reinf. layer	Double reinf. layers
(8, 10.8)	$27.0/yd^2	$27.4/yd^2	$23.5/yd^2	-	-$0.4/yd^2	$3.5/yd^2	-
(10, 13.0)	$32.5/yd^2	$29.5/yd^2	$28.5/yd^2	$22.5/yd^2	$3.0/yd^2	$4.0/yd^2	$10.0/yd^2
(12, 15.2)	$38.0/yd^2	$31.7/yd^2	$33.5/yd^2	$27.0/yd^2	$6.3/yd^2	$4.5/yd^2	$11.0/yd^2
(14, 16.4)	$41.0/yd^2	$34.8/yd^2	$38.5/yd^2	$30.0/yd^2	$6.2/yd^2	$2.5/yd^2	$11.0/yd^2

* The layer base thickness for the double reinforcement layers are less than those for a single reinforcement layer (According to BCR in Table 28).

Cost Benefit Analysis – TBR

The evaluation of economic benefits of using geosynthetics, in terms of extended service life, is a little bit more complex because except for the initial construction cost, the long-term rehabilitation cost also makes impact on the total cost of pavement now. The pay items involved here are presented in Table 31. The rehabilitation is assumed to have 2-in. asphalt mill and 3.5-in. asphalt overlay (1.5 in. AC wearing course and 2 in. AC binder course).

Table 31
Pay Items (TBR)

Item Name	Unit Cost
Geosynthetics Cost	$3.5/yd^2
HMA Milling Cost	$2.0/yd^2
HMA Overlay Cost	$87/ton

An analysis period of 40 years is used here. Based on DOTD's policy, the rehabilitation schedule of unreinforced flexible pavements include mill and overlay at years 18 and 30. The rehabilitation schedule of reinforced flexible pavements is calculated by multiplying the rehabilitation schedule of unreinforced flexible pavement by TBR. The activity timing for

future rehabilitation of reinforced pavements are indicated in Table 32. The net present value (NPV) is used here for comparisons and it is calculated as follows:

$$NPV = Initial\ Construction\ Cost + \sum_{n=1}^{N} Rehabilitaion\ Cost_n \times PVF \qquad (12)$$

where, the present value factor (PVF) is evaluated as:

$$PVF = \left[\frac{1}{(1+r)^n}\right] \qquad (13)$$

where, *n* is the number of years; and *r* is the discount rate, taken as 4% in this study.

Table 32
Scenarios for future pavement rehabilitation

Base Thickness (in) (Single reinf./treated, unreinf.)	Years			
	1st Rehabilitation		2nd Rehabilitation	
	Single Layer	Double Layers	Single Layer	Double Layers
(8, 10.8)	28.0	40.5	46.5	-*
(10, 13.0)	27.0	38.5	45.0	-*
(12, 15.2)	26.5	37.5	44.0	63.0
(14, 16.4)	26.0	36.0	43.5	60.0

* Usually, researchers do not use double geogrid layers for thin base thickness (< 12").

The results of life-cycle cost analysis (LCCA) for unreinforced/untreated pavement are presented in Table 33, and the results of LCCA for the 12-in. cement/lime treated subgrade pavement with the cement stabilized base are presented in Table 34. Here the rehabilitation cost of treated subgrade pavement is assumed to be the same as the unreinforced/untreated pavement with the difference in the initial cost. Only the pay items that make the differences in the initial cost between the three different pavement sections will be included in analyses. Please note that the benefits of geosynthetics were described here in terms of extending the pavement service life (evaluated by TBR), and therefore the thicknesses of reinforced sections are kept the same as that for the unreinforced section, which results in increasing the initial cost as compared with Table 30. In contrary, the benefits of geosynthetics in Table 30 were described in terms of reducing the base thickness (evaluated by BCR), and therefore, the thicknesses of reinforced sections are lower than those for the unreinforced sections. The results of LCCA for the single and double layers of geosynthetic reinforcement are presented in Tables 35 and 36, respectively. The cost saving due to extended service can reach up to \$6.2/yd^2 for a single geosynthetic layer and up to \$8.0/yd^2 for double geogrid layers, as

compared to unreinforced/untreated pavements. However, the cost savings from using 12-in. cement/lime treated subgrade pavement with the cement stabilized base, as compared to unreinforced/untreated pavements, can reach up to 6.3/yd^2 for base thickness of 12 in. The LCCA results demonstrate more cost effective to use one geosynthetic layer or double geogrid layers for base aggregate thickness < 15 in. (or < 12 in. of cement stabilized base). However, the cost benefit becomes close for base thickness > 12 in. (or > 15 in. of aggregate base).

Table 33
Cost of unreinforced/untreated pavement

Base Thickness (in)	Cost (per yd^2)							
	Initial Cost	1st Rehabilitation #1			2nd Rehabilitation			NPV
		Milling	Overlay	Total	Milling	Overlay	Total	
10.8	$27	$2	$16.7	$18.7	$2	$16.7	$18.7	$42.0
13.0	$32.5	$2	$16.7	$18.7	$2	$16.7	$18.7	$47.5
15.2	$38	$2	$16.7	$18.7	$2	$16.7	$18.7	$53.0
16.4	$41	$2	$16.7	$18.7	$2	$16.7	$18.7	$56.0

Table 34
Cost of 12-in. treated subgrade with cement stabilized base

Base Thickness (in)	Cost (per yd^2)								
	Initial Cost	1st Rehabilitation #1			2nd Rehabilitation			NPV	Cost Saving
		Milling	Overlay	Total	Milling	Overlay	Total		
8	$27.4	$2	$16.7	$18.7	$2	$16.7	$18.7	$42.4	-
10	$29.5	$2	$16.7	$18.7	$2	$16.7	$18.7	$44.5	$3.0/yd^2
12	$31.7	$2	$16.7	$18.7	$2	$16.7	$18.7	$46.7	$6.3/yd^2
14	$34.8	$2	$16.7	$18.7	$2	$16.7	$18.7	$49.8	$6.2/yd^2

Table 35
Cost of reinforced pavement with single layer of geosynthetics

Base Thickness (in)	Cost (per yd^2)						Cost Saving
	Initial Cost	1st Rehabilitation			Residual Value	NPV	
		Milling	Overlay	Total			
10.8	$30.5	$2	$16.7	$18.7	$0.9	$35.8	$6.2/$yd^2$
13.0	$36	$2	$16.7	$18.7	$0.7	$41.8	$5.7/$yd^2$
15.2	$41.5	$2	$16.7	$18.7	$0.7	$47.4	$5.6/$yd^2$
16.4	$44.5	$2	$16.7	$18.7	$0.7	$50.5	$5.5/$yd^2$

Table 36
Cost of Reinforced pavement with double layer of geosynthetics

Base Thickness (in)	Cost (per yd^2)						Cost Saving
	Initial Cost	1st Rehabilitation			Residual Value	NPV	
		Milling	Overlay	Total			
10.8	$34	-	-	-	$0.0	$34.0	$8.0/$yd^2$
13.0	$39.5	-	-	-	$0.0	$39.5	$8.0/$yd^2$
15.2	$45	$2	$16.7	$18.7	$0.7	$48.6	$4.4/$yd^2$
16.4	$48	$2	$16.7	$18.7	$0.7	$51.9	$4.1/$yd^2$

CONCLUSIONS

Accelerated load testing was conducted to evaluate the benefits of using geosynthetics to reinforce/stabilize base aggregate layer/subgrade in pavement. Six test lane sections and an additional small-scale control Section 7 (for test lane 6) were constructed over native weak subgrade soil. Two geosynthetic reinforcements were used, one triaxial geogrid and one high strength woven geotextile. The sections were extensively instrumented to measure the load- and environment-associated pavement responses and performance. Three series of tests, moving wheel load tests and field and laboratory cyclic plate load tests, were conducted to investigate the performance of geosynthetic reinforced/stabilized unpaved/paved roads and to identify the differences in pavement response to moving wheel and cyclic plate loads.

Please note that the findings of this study are based on using one triaxial geogrid and one high strength woven geotextile (properties in Table 2) for reinforcing/stabilizing pavement test sections built over weak subgrade soil; and therefore the conclusions of this study cannot be generalized for all geogrids and/or all geotextiles.

Based on the results of field and laboratory accelerated loading tests on pavement test sections with and without geosynthetic reinforcement inclusion, the following conclusions can be drawn:

- The test results demonstrate that both the triaxial geogrid and the high strength woven geotextile significantly improved the performance of the pavement section in terms of reducing the surface permanent deformation and extending the service life of pavement sections. The adjusted traffic benefit ratio (TBR_{adj}) associated with geosynthetic reinforcement can be increased up to 2.12 at a rut depth of 0.75 in. for pavement constructed using 18 in. (457 mm) thick base layer on top of weak subgrade soil and two layers of geogrid reinforcement.
- The inclusion of geosynthetic reinforcement (triaxial geogrid or high strength woven geotextile) results in redistributing the applied load to a wider area, thus reducing the stress concentration and achieving an improved vertical stress distribution on top of subgrade layer. This behavior results in less accumulated permanent deformation in the subgrade; i.e., lower maximum vertical stress on subgrade, and hence the lower permanent vertical strain in subgrade. The benefits of geosynthetics on the reduction of maximum vertical stress on top of subgrade are more appreciable at higher load levels.
- Among the six pavement sections tested in this study, the best performance was observed for the pavement section reinforced with double geogrid layers. However, the cost of

having two geogrid layers is higher than a single layer of geosynthetic reinforcement, and therefore life cycle cost analyses (LCCA) are needed to evaluate the cost savings associated with using two geogrid layers versus a single geosynthetic layer in pavement design.

- Instrumentation measurements indicate that geosynthetics placed at the base-subgrade interface are able to improve the performance of both the subgrade and the base layers. However, by placing an additional geogrid layer at the upper one-third of the base layer, the performance of the base layer will be further increased.
- While the geosynthetics showed appreciable benefit on reducing the permanent deformation of the subgrade in this study, it provided little effect on the resilient properties of the subgrade.
- The drainage has an important effect on the performance of pavement structures, for both the unreinforced and reinforced sections.
- For geosynthetics functioning as base reinforcement within the context of AASHTO PavementME Design, the effective resilient modulus of the base layer can be increased by thirty percent when using a single geosynthetic layer placed at the base-subgrade interface and ninety percent when using double geogrid layers. Note that these values are applicable for the case of 18 in thick base course layer used in this study built over weak subgrade soil.
- The life-cycle cost analysis (LCCA) demonstrated the potential cost savings and benefits of using geosynthetics (one layer or double layers) in pavement as compared to the unreinforced/untreated sections. However, compared to the 12-in. treated subgrade with cement stabilized base pavement section, the LCCA showed it is more cost effective to use geosynthetics to reinforce base aggregate of thickness < 12 in. (or < 15 in. of unreinforced aggregate base). However, the cost benefit becomes close for base thickness > 12 in. between using a single geosynthetic layer and a 12-in. cement/lime treated subgrade with a cement stabilized base. Moreover, the cost benefit of using double geogrid layers exceeds the cost savings of a 12-in. treated subgrade with a cement stabilized base.

RECOMMENDATIONS

Based on the results of this research study, the following recommendations are offered to DOTD engineers:

- It is recommended that DOTD pavement design engineers consider stabilization/reinforcing the base course aggregate layer with one geosynthetic layer placed at the base-subgrade interface or two geogrid layers for the design of flexible pavements built over weak subgrade soils with resilient modulus M_r < 4500 psi (or CBR value < 3). This is important especially in cases where it is difficult to stabilize/treat the soft subgrade soil with cement or lime and to create working platforms for constructing pavements and embankments on weak soils. The use of woven reinforcement geotextiles, or geogrids with a Class C nonwoven separator with elastic tensile strength at 2 percent strain, $T_{2\%} \geq 250$ lb/ft, is recommended.

- For design of geosynthetic reinforced flexbile pavements built over the weak subgrade (CBR=0.5-3) using PavementME, the α values presented in Table 26 are recommended to estimate the effective base resilient modulus input for a single geosynthetic layer or double geogrid layers.

- If only long-term benefits of geosynthetics are considered, the TBR values presented in Table 27 are recommended to estimate the extended service life of geosynthetics reinforced flexbile pavements built over the weak subgrade (for CBR=0.5-3).

- If only short-term benefits of geosynthetics are considered, the BCR factors presented in Table 28 are recommended to estimate the reduced base thickness for geosynthetics reinforced flexbile pavements built over the weak subgrade (for CBR=0.5-3).

- It is recommended to perform a comprehensive numerical parametric study to fully capture the effect of different variables and parameters on the performance of geosynthetic reinforced flexible pavements. This can be done by varying the soil properties (e.g., M_r), reinforcement configuration/properties (e.g., *location*, *J*), and pavement structures, (e.g., asphalt thickness, base thickness) in numerical simulation. Full design charts can then be developed to assist the engineers to design geosynthetic reinforced flexible pavement.

ACRONYMS, ABBREVIATIONS, AND SYMBOLS

AASHTO	American Association of State Highway and Transportation Officials
AC	asphalt concrete
ALF	accelerated loading facility
ASTM	American Standard for Testing Materials
BCR	Base Course Reduction
CBR	California bearing ratio
CV	coefficient of variation
DCP	dynamic cone penetrometer
DCPI	dynamic cone penetrometer index
DOTD	Louisiana Department of Transportation and Development
ESAL	equivalent single axel load
FHWA	Federal Highway Administration
ft.	foot (feet)
GG	Geogrid
Gg	Geogauge
HMA	hot-mix asphalt
in.	inch(es)
kip	kilo pounds
kN	kilonewton
kpa	kilopascal
ksi	kilo pounds per square inch
lb.	pound(s)
LWD	light weight deflectometer
LL	liquid limit
LTRC	Louisiana Transportation Research Center
LVDT	linear variable displacement transducer
m	meter(s)
MEPDG	mechanistic-empirical pavement design guide
mm	millimeter(s)
MPa	megapascal
NPV	Net present value
pcf	pounds per cubic feet
PG	Performance graded
PI	plasticity index
PRF	pavement research facility

psi	pounds per square inch
PSPA	portable seismic pavement analyzer
TRB	traffic benefit ratio
USCS	Unified Soil Classification System

REFERENCES

1. Tingle, J. and Jersey, S. (2005). "Cyclic Plate Load Testing of Geosynthetic-Reinforced Unbound Aggregate Roads." *Transportation Research Record: Journal of the Transportation Research Board, No. 1936*, Transportation Research Board of the National Academies, Washington, D.C., pp. 60-69.
2. Chen, Q., Abu-Farsakh, M., and Tao, M. (2009). "Laboratory evaluation of geogrid base reinforcement and corresponding instrumentation program" *Geotechnical Testing Journal*, Vol. 32, No. 6.
3. Henry, K., Clapp, J., Davids, W., Humphrey, D., Barna, L. (2009). Structural Improvements of Flexible Pavements Using Geosynthetics for Base Course Reinforcement. Report No. ERDC/CRREL TR-09-11. U.S. Army Corps of Engineers in conjunction with U.S. Department of Transportation, Pooled Fund Program, Federal Highway Administration, McLean, VA.
4. Perkins, S.W., Christopher B.R., Cuelho, E.G., Eiksund, G. R., Schwartz, C.S., and Svanø, G. (2009). "A Mechanistic-Empirical Model for Base-Reinforced Flexible Pavements," *International Journal of Pavement Engineering*, Vol. 10, No. 2, pp. 101–114.
5. Abu-Farsakh, M. and Chen, Q. (2011). "Evaluation of Geogrid Base Reinforcement in Flexible Pavement Using Cyclic Plate Load Testing." *International Journal of Pavement Engineering*, Vol. 12, pp. 275-288.
6. Jersey, S. R., Tingle, J. S., Norwood, G. J., Kwon, J., and Wayne, M. (2012). "Full-Scale Evaluation of Geogrid-Reinforced Thin Flexible Pavements." *Transportation Research Record: Journal of the Transportation Research Board, No 2310*, Transportation Research Board, National Research Council, Washington, D.C., pp. 61–71.
7. Tang, X., Stoffels, S. M., and Palomino, A. M. (2013). "Resilient and Permanent Deformation Characteristics of Unbound Pavement Layers Modified by Geogrids." *Transportation Research Record 2369*, Transportation Research Board, National Research Council, Washington, D.C.: 3–10.
8. Tanyu, B.F., Aydilek, A.H., Lau, A.W., Edil , T.B. and Benson, C.H. (2013) "Laboratory evaluation of geocell-reinforced gravel subbase over poor subgrades." Geosynthetics International Volume 20 Issue 2, pp. 47-61
9. Tang, X., Abu-Farsakh, M., Hanandeh,S., Chen, Q. (2015). "Performance of reinforced and stabilized unpaved test sections built over native soft soil under full-scale moving wheel loads," *Transportation Research Record: Journal of the Transportation Research Board, No.* 2511, Transportation Research Board, Washington, D.C., pp. 81–89.

10. Abu-Farsakh, M., Hanandeh, S., Mohammad, L., and Chen, Q. (2016). “Performance of geosynthetic reinforced/stabilized paved roads built over soft soil under cyclic plate loads.” *Geotextiles and Geomembranes*, doi:10.1016/j.geotexmem.2016.06.009.
11. Saghebfar, M., Hossain M., and Lacina, B.A. (2016). “Performance of geotextile-reinforced bases for paved roads.” *Transportation Research Record: Journal of the Transportation Research Board, No 2580*, Transportation Research Board, National Research Council, Washington, D.C., pp. 3–10.
12. Perkins, S.W. (1999). Geosynthetic Reinforcement of Flexible Pavements Laboratory Based Pavement Test Sections. Federal Highway Administration Report *FHWA/MT-99-001/8138*, Montana Department of Transportation, Helena, Montana, USA, 109
13. Al-Qadi, I.L., Dessouky, S.H., Kwon, J., and Tutumluer, E. (2008). “Geogrid in flexible pavements: validated mechanism.” *Transportation Research Record: Journal of Transportation Research Board 2045*, Transportation Research Board, National Research Council, Washington, D.C., pp. 102-109.
14. Al-Qadi, I.L., Dessouky, S., Tutumluer, E., and Kwon, J. (2011). Geogrid mechanism in low-volume flexible pavements: accelerated testing of full-scale heavily instrumented pavement sections. *International Journal of Pavement Engineering*, Vol. 12, No. 2, pp. 121-135.
15. Kwon, J., Tutumluer, E., and Konietzky, H. (2008). Aggregate base residual stresses affecting geogrid reinforced flexible pavement response. *International Journal of Pavement Engineering*, Vol. 9, No. 4, pp. 275-285.
16. Kwon, J., Tutumluer, E., and Al-Qadi, I.L. (2009). Validated Mechanistic Model for Geogrid Base Reinforced Flexible Pavements, *Journal of Transportation Engineering*, Vol. 135, No. 12, pp. 915-926.
17. Tang, X., Stoffels, S. M., and Palomino, A. M. (2015). “Mechanistic-empirical approach to characterizing permanent deformation of reinforced soft soil subgrade.” *Geotextiles and Geomembranes*, Vol. 44, No. 3, pp. 429-441.
18. Chen, Q. and Abu-Farsakh, M. (2012) Structural Contribution of Geogrid Reinforcement in Pavement. *GeoCongress 2012*.1468-1475.
19. Berg, R. R., Christopher, B.R., and Perkins, S.W. (2000). “Geosynthetic reinforcement of the aggregate base course of flexible pavement structures,” GMA White paper II, Geosynthetic material Association, Roseville, MN, USA, 130 p.
20. Perkins, S.W. and Ismeik, M. (1997). “A Synthesis and Evaluation of Geosynthetic Reinforced Base Layers in Flexible Pavements: Part I,” Geosynthetics International, Vol. 4, No. 6, pp. 549- 605.
21. Webster, S. L. (1993). “Geogrid reinforced base courses for flexible pavements for light aircraft, test section construction, behavior under traffic, laboratory tests, and design

criteria", Technical report GL-93-6, U.S. Army Corps of Engineers, Waterways Experiment Station, Vicksburg, Mississippi, USA, 86 p.
22. Haas, R., Walls, J., and Carroll, R.G. (1988). "Geogrid Reinforcement of Granular Bases in Flexible Pavements," *Transportation Research Record 1188*, pp. 19-27.
23. Barksdale, R.D., Brown, S. F., and Chan, F. (1989). "Potential benefits of geosynthetics in flexible pavement systems", National Cooperative Highway Research Program Report No. 315, Transportation Research Board, National Research Council, Washington, DC, USA, 56 p.
24. Miura, N., Sakai, A., Taesiri, Y., Yamanouchi, T., and Yasuhara, K. (1990). "Polymer grid reinforced pavement on soft clay grounds", geotextiles and geomembranes, Vol. 9, No. 1, pp. 99-123.
25. Cancelli, A., Montanelli, F., Rimoldi, P., and Zhao, A. (1996). "Full scale laboratory testing on geosynthetics reinforced paved roads", Earth reinforcement, Ochiai, H., Yasufuku, N., and Omine, K., Editors, Balkema, Proceedings of the International Symposium on Earth Reinforcement, Fukuoka, Kyushu, Japan, November, 1996, pp. 573-578.
26. Collin, J. G., Kinney, T.C., and Fu, X. (1996). "Full-scale highway load test of flexible pavement systems with geogrid reinforced base courses", Geosynthetics International, Vol. 3, No. 4, pp. 537-549.
27. Perkins, S.W. (2001). "Mechanistic-empirical modeling and design model development of geosynthetic reinforced flexible pavements", Montana Department of transportation, Helena, Montana, Report No. FHWA/MT-01-002/99160-1A.
28. Al-Qadi, I. L., Brandon, T. L., and Bhutta, S. A. (1997). "Geosynthetic stabilized flexible pavements". *Geosynthetics '97 Proceedings*, Vol. 2, edited by Paulson J. N., Long Beach, CA, USA. pp. 647-661.
29. Perkins, S.W., Ismeik, M., Fogelsong, M.L., Wang, Y., and Cuelho, E.V. (1998). "Geosynthetic-reinforced pavements: Overview and preliminary results," Proc. Of the sixth International Conference on Geosynthetics, Atlanta, GA, USA, Vol. 2, pp.951-958.
30. Halliday, A. R., and Potter, J.F. (1984). "The performance of flexible pavement constructed on a strong fabric," Transportation and Road Research Laboratory, Report 1123, Crowthorne, Berkshire, United Kingdom, 15 p.
31. Perkins, S.W. (2002). "Evaluation of geosynthetic reinforced flexible pavement systems using two pavements test facilities," Final Report, U.S. department of Transportation, Federal Highway Administration and the State of Montana Department of Transportation, FHWA/MT-02-008/20040, November.

32. Cancelli, A., and Montanelli, F., "In-ground Test for Geosynthetic Reinforced Flexible Paved Roads." *Proceedings of the Conference Geosynthetics '99*, Boston, MA, USA, April, (1999). pp. 863-878.
33. Kinney, T.C., Abbott, J., and Schuler, J. (1998). "Benefits of using geogrids for base reinforcement with regard to rutting." *Transportation Research Record: Journal of the Transportation Research Board, No. 1611*, National Research Council, pp. 86-96.
34. Al-Qadi, I.L., Morian, D.A., Stoffels, S.M., Elseifi, M., Chehab, G., and Stark, T., (2008). "Synthesis on use of geosynthetics in pavements and development of a roadmap to geosynthetically-modified pavements." Draft Report, National Cooperation Highway Research Program (NCHRP).
35. Giroud, J.P., and Han, J. (2004), "Design Method for Geogrid-Reinforced Unpaved Roads. I. Development of Design Method," *Journal of Geotechnical and Geoenvironmental Engineering*, Vol. 130, No. 8, August 2004, pp. 775-786.
36. Zornberg, J.G., Ranjiv Gupta, J.P., Luo, R., McCartney, J.S., Ferreira, J.Z., and Nogueira, C., (2008). "Validating mechanisms in geosynthetic reinforced pavements." Final Report, The University of Texas at Austin, FHWA/TX-08/0-4829-1, 268.
37. Moghaddas-Nejad, F. and Small, J.C. (1996). "Effects of Geogrid Reinforcement in Model Track Tests on Pavements," *Journal of Transportation Engineering*, Vol. 122, No. 6, pp. 468-474.
38. Brown, S.F., Jones, C.P.D., and Brodrick, B.V. (1982). "Use of non-woven fabrics in permanent road pavements," proc. of the Institute of Civil Engineers, part 2, vol. 73, pp. 541-563.
39. Al-Qadi, I. L., Brandon, T.L, Valentine, R J., Lacina, B.A., and Smith, T.E. (1994). "Laboratory Evaluation of Geosynthetic Reinforced Pavement Sections", Transportation Research Record 1439, pp. 25-31.
40. Perkins, S.W., and Edens, M.Q. (2003). "A Design Model for Geosynthetic-Reinforced Pavements." International Journal of Pavement Engineering, Vol. 4, No. 1, 37-50.
41. Webster, S.L., Grau, R.H., and Williams, R.R., *Description and Application of Dual Mass Dynamic Cone Penetrometer*. U.S. Army Engineer Waterways Experiment Station, Instruction Report, No. GL-92-3. (1992).
42. Powell, W.D., Potter, J.F., Mayhew, H.C., and Nunn, M.E., *The Structural Design of Bituminous Roads*. Transport and Road Research Laboratory (TRRL), Report LR1132, Berkshire, United Kingdom. (1984).
43. AASHTO, (2015). AASHTOWare Pavement ME Design Build 2.2 Release Notes. American Association of State Highway and Transportation Officials, Washington, DC.

44. Christopher, B.R. and Lacina, B., “Roadway Subgrade Stabilization Study”, *Proceedings of GeoAmericas (2008),* Cancun, Mexico, 2008, International Geosynthetic Society, pp. 1013–1021.
45. Christopher, B.R., Perkins, S.W., Lacina, B.A. and Marr, W.A., (2009). “Pore water pressure influence on geosynthetic stabilized subgrade performance.” *Proceedings of the Conference Geosynthetics 2009,* Salt Lake City, Utah, USA, Februray 25-27, pp. 215-221.
46. Chen, Q., and Abu-Farsakh, M., (2010). “Field rutting performance of various base/subbase materials under two types of loading.” *Transportation Research Record: Journal of the Transportation Research Board, No. 2186,* pp. 90-100.

This public document is published at a total cost of $250
42 copies of this public document were published in this first printing at a cost of $250. The total cost of all printings of this document including reprints is $250. This document was published by Louisiana Transportation Research Center to report and publish research findings as required in R.S. 48:105. This material was duplicated in accordance with standards for printing by state agencies established pursuant to R.S. 43:31. Printing of this material was purchased in accordance with the provisions of Title 43 of the Louisiana Revised Statutes.